

POLITECNICO DI TORINO

Corso di Laurea magistrale in ingegneria meccanica

Tesi di Laurea Magistrale

Dynamic delamination testing of a composite material



Relatore

prof. Giovanni Belingardi

Candidato

Andrea Ferrarese

A. A. 2019/2020

Contents

List of Figures	V
List of Tables	VII
1 Introduction	1
1.1 Preamble	1
1.2 Non-crimp fabric composites	3
1.2.1 Types of non-crimp fabric	3
1.3 Delamination in composites	5
1.3.1 Damage and failure of composites	5
1.3.2 Initiation of delamination	5
1.4 Fracture mechanics and delamination	7
1.5 Quasi-static mode I delamination testing	8
1.5.1 The double cantilever beam specimen	8
1.5.2 Standardised test methods	10
1.6 Dynamic mode I delamination testing	13
1.6.1 General overview	14
1.6.2 Closer review of selected test methods	16
1.7 Modelling delamination	20
1.7.1 The virtual crack closure technique	20
1.7.2 Cohesive zone models	21
2 Testing	23
2.1 Materials and methods	23
2.1.1 The testing apparatus	23
2.1.2 Design of the fixture	24
2.1.3 Material preparation	25
2.1.4 Specimen preparation	32
2.1.5 Testing	37
2.1.6 Post-processing and data reduction	39
2.2 Tracking crack growth with DIC and MATLAB	40
2.2.1 Motivation and principles	40
2.2.2 Implementation	41

3 Results and discussion	51
3.0.1 Initial observations	51
3.0.2 Assessing the effectiveness of the DIC-based measurements	58
3.0.3 Interlaminar fracture toughness and rate dependence	60
3.0.4 Microscope observation of the crack surfaces	61
Conclusions	69
Bibliography	71
4 Appendix	1
4.1 Crack tracking script	1
4.2 Frame processing function	10

List of Figures

1.1	Types of knitted non-crimp fabrics	4
1.2	The three crack opening modes	7
1.3	Geometry of the double cantilever beam specimen	9
1.4	Piano hinge and load block fixtures	10
1.5	Schematic of a DBC specimen under loading	11
1.6	The parameter Δ from modified beam theory	12
1.7	A simple finite element VCCT model	20
1.8	Example of ABAQUS model with VCCT	21
1.9	The cohesive zone model	21
1.10	A bilinear cohesive law	21
2.1	Schematic of the test configuration	24
2.2	Fixture assembly for the HISR machine	26
2.3	Sliding rod from the HISR machine	28
2.4	Clevis from the HISR machine	30
2.5	Adapter from the HISR machine	31
2.6	Manufacturing of the test plate	32
2.7	The specimens after waterjet cutting	33
2.8	Manufacturing of the test plate	33
2.9	The intermediate rate test setup	35
2.10	The intermediate rate test setup (details)	36
2.11	The quasi-static test setup	38
2.12	The distance between the pins monitored by DIC software GOM	39
2.13	Selection of the region of interest	43
2.14	DIC data points	43
2.15	Selected DIC data points	44
2.16	Candidate crack tip position discarded for failing the upstream check	46
2.17	Candidate crack tip position discarded for failing the whole beam check	47
2.18	Accepted candidate crack tip position	48
2.19	Simplified flow chart of the frame processing script	49
3.1	Load versus time plots for the quasi-static opening rate	52
3.2	Load versus time plots for intermediate opening rates	53
3.3	Crack length and crack velocity versus time plots for the quasi-static opening rate	54

3.4	Crack length and crack velocity versus time plots for the intermediate opening rates	55
3.5	R-curves for the quasi-static opening rate	56
3.6	R-curves for the intermediate opening rates	57
3.7	Load line opening displacement measured with an LVDT sensor and with DIC	59
3.8	Crack length obtained manually and with DIC	63
3.9	The mode I initiation and arrest interlaminar fracture toughness G_{Ic}	63
3.10	Initiation, propagation and arrest data points	64
3.11	Third degree polynomials fitted to the data points	65
3.12	The initiation interlaminar fracture toughness plotted against two rate parameters	66
3.13	30× magnification microscope images of the crack surfaces	67
3.14	Crack bridging by the polyester stitching	68

List of Tables

1.1	DCB specimen geometries encountered in literature	16
1.2	Results from literature	19
3.1	The mode I initiation and arrest interlaminar fracture toughness G_{Ic}	61

Chapter 1

Introduction

1.1 Preamble

Composite materials are a mainstay when it comes to lightweight design, both in the aerospace and automotive industries. Their strength comes from the heterogeneity of their structure, which pair together materials with diverse properties. Working with composite materials, the designer has the unprecedented ability of tailoring the physical properties of the material to his needs. On the other hand, this complexity also hinders the full realisation of composite materials' potential.

Numerical finite element simulation is a powerful tool in the engineer's toolbox to overcome this obstacle. Increasingly complex material models are being developed to better capture the behaviour of composite materials. All of this makes material testing more important than ever, because even the most advanced model is useless without properly determined material constants, and full understanding of the limits of its validity. Testing is the link between simulations and physical reality, and without it simulations remain an exercise in mathematics and programming. In the most commonly encountered composites, polymer matrix-based ones, material properties can show dependence on a number of external factors: the type of loading, temperature, moisture content, and loading rate. Investigating with properly formulated tests the effect of these external factors is paramount to develop sound material models

One of the most complex and not yet fully understood aspects of the mechanical properties of composites material are their damage and failure mechanisms. Amongst composite damage mechanisms, one of the most prevalent is delamination—the separation of layers in a laminate composite. This type of damage immediately leads to loss of stiffness in the part, and can progress to cause catastrophic failure. The resistance of a material to delamination is characterised by interlaminar fracture toughness or critical strain energy release rate G_c , a fracture mechanics concept. Indeed, linear elastic fracture mechanics have been used for decades to study delamination, as it applies well to brittle matrix composites.

By definition, delamination takes place in the inter-ply region, composed mostly of resin. As it is well-known that resins often show strain rate-dependent properties, it is legitimate to ask whether interlaminar fracture toughness is affected by a similar influence. Since the 1980s numerous test procedures have been proposed, but notably there

is no widely accepted practice—a fact underlined by the absence of any standards for delamination testing of composite above the quasi-static loading range.

The objectives of the present work were threefold:

- Assess the state-of-the-art in intermediate loading rate delamination testing of composites in the opening mode (mode I), and develop a convenient testing practice.
- Use this practice to characterise the delamination properties of a non-crimp carbon fibre fabric/epoxy composite at quasi-static to intermediate opening rates.
- Investigate the rate dependence of the aforementioned material, and determine whether further testing at high loading rate should be undertaken.

This report is structured as follows. Chapter 1 introduces concepts and notions that were taken into account when developing the test procedure, as well as a review of the literature on the subject. Chapter 2 describes in detail the experimental setup. Chapter 3 discusses the experimental results.

1.2 Non-crimp fabric composites

Non-crimp fabrics are a class of fibre reinforcing layers that were born out of the necessity of combining the advantages of unidirectional reinforcements and woven fabrics.[1, p. XVI]

Unidirectional tape reinforcements have local properties that come closest to the ideal model, due to their extremely well controlled fibre placement. Their downside is potentially complex and expensive manufacturing. On the other hand woven fabrics can be used in highly productive processes such as resin transfer moulding, and allow for large pieces of the reinforcement to be handled by automated system. However, due to the crimping of the fibres, the local properties of the materials vary significantly.

In order to understand the structure of non-crimp fabrics and their difference from traditional fabric reinforcements, a few basic textile engineering notions should be recalled. Fabrics may be manufactured using two different processes, knitting and weaving. During the weaving process, two sets of yarns are interlaced together. One set of yarns is held in tension in the direction of production of the textile constitute the *warp*, while the yarns inserted transversely make up the *weft*. Knitted fabrics, on the other hand, are produced by connecting loops of a single yarn. A *wale* is a column of knitted loops in the direction of fabric production, a *course* is a row of knitted loops, width-wise across the fabric.[2]

Non-crimp fabrics can be defined as “drawn parallel oriented layers of reinforcing threads or tows, which are positioned by means of an additional fixation material” [1, p. 3]. The role of keeping the fibres positioned correctly is delegated to an auxiliary, dedicated structure, allowing the structural fibres to remain close to their ideal placement. In general, this can be done by knitting with secondary fibres (the *yarn*) or bonding. Generally speaking knitted non-crimp fabrics may be thought of reinforcing fibre tows inserted in a knit fabric consisting of the secondary threads.

1.2.1 Types of non-crimp fabric

Non-crimp fabric can classified in a number of ways:

- 2D or 3D textiles, depending on whether the architecture of the fabric extends in two or three directions.
- Uniaxial, biaxial or multiaxial, depending on the number of orientations the main (structural) warp and weft fibres present.
- A further, more articulated categorisation is based on the production process.

A quick overview of the most commonly encountered forms of woven non-crimp fabrics follows.

Warp-knitted non-crimp fabrics

A warp-knitted fabric is produced with loops that were formed in the direction of production of the textile.[1, p. 5] A row of compound needles knits simultaneously across the whole width of the textile, creating an entire course. Warp-knitted non-crimp fabrics are also known as *stitch-bonded*. The reinforcing weft can be inserted in coursewise or

non-coursewise fashion. In the former case, the yarn loops around every reinforcing weft thread (figure 1.1a). The stitch length is determined by the thickness of the tows of reinforcing fibres. Naturally this requires precise placement of the reinforcing fibres, and therefore results in more complex production machines.

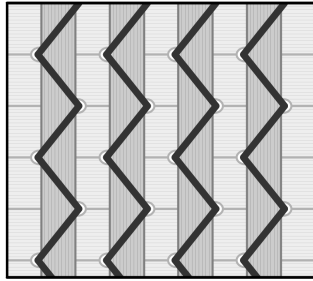
In contrast, with non-coursewise reinforcing weft insertion, the stitch length is decided independently from the thickness of the reinforcing weft (figure 1.1b). As a consequence the knitting loops pierces the weft, potentially causing damage to the fibres. However, as it can be imagined, this simplifies production and lowers costs. Uniaxial and biaxial warp-knitted non-crimp fabrics can be produced both with coursewise or non-coursewise weft insertion. Multiaxial NCFs are most commonly produced via warp-knitting with non-coursewise weft insertion.[1, p. 14]

Weft-knitted non-crimp fabrics

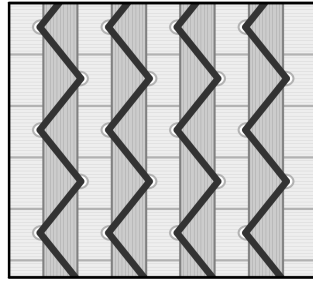
A weft-knit fabric is produced with loops that were formed in perpendicular direction to that of production of the textile.[1, p. 22] A needle adds one loop to the course at a time. The reinforcement weft insertion is always coursewise, as it passes through the knit loops (figure 1.1c).

Tape-weave non-crimp fabrics

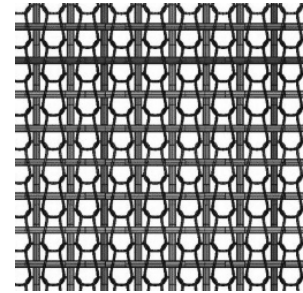
Tape-weave non-crimp fabrics are produced on a loom similarly to conventional woven fabrics, but using widely spread fibre tows that resemble tapes. This reduces the undulation and crimping effect in the fabric.



(a) Warp-knitted, coursewise weft insertion



(b) Warp-knitted, non-coursewise weft insertion



(c) Weft-knitted non-crimp fabric¹

Figure 1.1: Types of knitted non-crimp fabrics

¹Adapted from M. Q. Pham *et al.*. Numerical modelling of the mechanical behaviour of biaxial weft-knitted fabrics on different length scales. *Materials*. 12(22):3693, 2019; Creative Commons Attribution (CC BY) license (<http://creativecommons.org/licenses/by/4.0/>)

1.3 Delamination in composites

1.3.1 Damage and failure of composites

By definition, the structure of composite materials is heterogeneous. This results in an equally heterogeneous variety of damage mechanisms, often interacting with each other in complex ways. The damage mechanism may involve one of the material's components, more than one, or the interface between two. Considering long-fibre-reinforced laminated composites, the main macroscopic damage mechanisms are:

- Fibre breakage: cracking and failure of the reinforcement fibres
- Fibre buckling: compressive load instability of the fibres
- Debonding: a failure of the matrix–fibre interface
- Intralaminar fracture or matrix cracking: cracks, initially microscopic, growing in the matrix
- Interlaminar fracture or delamination: a crack growing in the interface between two laminas

Several factors make *Interlaminar fracture* or *delamination* a particularly insidious damage mechanism. It can initiate at load levels far below those that would cause failure, and it may be difficult to detect, since it can occur well below the surface of the composite. It causes a loss of stiffness—which depending on the application might be enough to put a component out of service—as well as a reduction in mechanical strength. Finally, its growth under load may ultimately result in catastrophic failure. Coupled with matrix cracking, in some lay-ups delamination may cause complete failure without breaking a single reinforcement fibre.[3]

The underlying causes of delamination can be found in the structure of laminated composites themselves. The fibres, which bear most of the load due to their high modulus relative to the matrix, cannot provide much reinforcing effect in the through-the-thickness direction. In-between the plies the matrix bears all the load; there are simply no fibres to resist delamination in the direction normal to the plies. Hence delamination is governed mostly by the properties of the matrix.[4]

Interlaminar fracture is often studied using fracture mechanics.[5] A delamination crack in a brittle polymeric matrix is a textbook case of application of linear elastic fracture mechanics.

1.3.2 Initiation of delamination

The onset of delamination can have many originating causes, and take place at any moment of the component's life, even before being put into service. They can be summarised in:[6, p. 30–37]

- **Manufacturing and environmental conditions.** The manufacturing process of composite materials normally involves at least one heating and cooling cycle, which may leave residual stresses and in turn trigger delamination. In composites, these

stresses can arise not only because of the common causes (external constraints or thermal gradients) but also because the heterogeneity of the material extends to its thermal properties. As it happens, the coefficient of thermal expansion of a composite lamina is different in the direction of the fibres (where it is fibre-dominated) and in the transverse direction (where the matrix properties dominate). The fibres themselves may have different thermal properties in the longitudinal and transverse direction, as is the case with carbon fibres.[7, p. 81]

- **Geometric factors.** The main geometric singularities which may favour delamination onset are tapered sections, bonded skin-stringer interfaces, and free edges. A number of design guidelines exist to increase the delamination resistance of free edges. These include edge capping, dropping the critical ply before the edge, and interleaving extra plies at the free edge.[8]
- **Machining operations.** Machining operations may cause small delaminations in composite laminates, especially if the workpiece is not properly supported. Delamination is nearly always present in drilling: the two main mechanisms are *peel up*, the peeling of the topmost layers at the periphery of the drill bit, and *push out*, due to the thrust force applied to the last, uncut, plies.[9]
- **Low-velocity impacts.** Damage from low- to medium-velocity impacts with foreign objects is a major preoccupation in the composite industry for aerospace. This is mainly because unlike in the case of high-velocity impact, damage may be sub-surface only and nearly impossible to detect with visual inspection, but evolve to critical conditions during the operating life of the component. Typical scenarios take place during manufacturing or maintenance (tool drops), or during service life (impact with runway debris). The damage mechanism is understood to involve micro-cracking of the matrix following the impact, creating stress concentration in the interlaminar region, and conditions favourable to the the onset of delamination.[10]

In stress analysis, there exist numerous criteria for the initiation of delamination. One of the most noted is the quadratic stress criterion by Brewer and Lagace in 1988. Only the stresses out of the plane of the lamina are included, since they are the only ones that can induce delamination:[11]

$$\left(\frac{\bar{\sigma}_{zz}}{Z_{int\ t}}\right)^2 + \left(\frac{\bar{\sigma}'_{zz}}{Z_{int\ c}}\right)^2 + \left(\frac{\bar{\tau}_{xz}}{S_{xz}}\right)^2 + \left(\frac{\bar{\tau}_{yz}}{S_{yz}}\right)^2 \geq 1 \quad (1)$$

Where $Z_{int\ t}$ is the interlaminar tensile strength, $Z_{int\ c}$ is the interlaminar compressive strength, S_{xz} the interlaminar shear strength, S_{xz} the through-the-thickness shear strength, and S_{yz} the transverse shear strength.

Equally old and equally noted is the criterion by Ye:[12]

$$\begin{aligned} \bar{\sigma}_{zz} \geq 0 & \quad \left(\frac{\bar{\sigma}_{zz}}{Z_{int\ t}}\right)^2 + \left(\frac{\bar{\tau}_{xz}}{S_{xz}}\right)^2 + \left(\frac{\bar{\tau}_{yz}}{S_{yz}}\right)^2 \geq 1 \\ \bar{\sigma}_{zz} \leq 0 & \quad \left(\frac{\bar{\tau}_{xz}}{S_{xz}}\right)^2 + \left(\frac{\bar{\tau}_{yz}}{S_{yz}}\right)^2 \geq 1 \end{aligned} \quad (2)$$

1.4 Fracture mechanics and delamination

It is possible to identify three elementary crack opening modes (figure 1.2). *Mode I* is an opening mode, with displacements normal both to the crack front and the crack surfaces, and symmetrical with respect to the crack surface. *Mode II* and *mode III* are shear modes, characterised by separation antisymmetric with respect to the original crack surface. In mode II the displacements are parallel to the crack surface and normal to the crack front, while in mode III the displacements parallel both to the crack surface and to the crack front. In the context of delamination, the three modes correspond to *interlaminar tension*, *interlaminar sliding shear* and *interlaminar scissoring shear*.

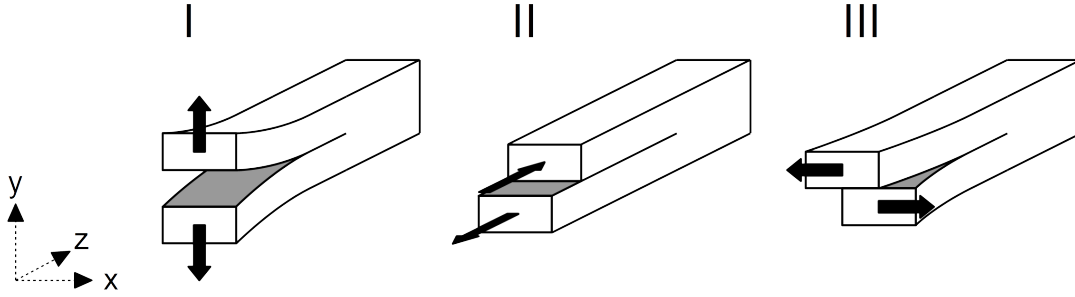


Figure 1.2: The three crack opening modes

The resistance of a material to delamination is quantified by interlaminar fracture toughness G_c . This is none other than strain energy release rate, a well-known linear elastic fracture mechanics.

The energy balance for a plate containing a crack and under remote load can be written as:[13]

$$U_{tot} = U^* + \Pi \quad (3)$$

Where U_{tot} is the total energy in the system, U is the potential energy stored in the system, and Π is the energy absorbed to form the crack surface. The (3) can be differentiated with respect to crack area A .

$$\frac{\partial U_{tot}}{\partial A} = \frac{\partial U^*}{\partial A} + \frac{\partial \Pi}{\partial A} \quad (4)$$

The *strain energy release rate* is then defined as:

$$G = -\frac{\partial U^*}{\partial A} \quad (5)$$

The critical condition for crack growth is reached when the potential energy released matches the energy required for crack growth, i.e. $\frac{\partial U_{tot}}{\partial A} = 0$. A *critical* value of strain energy release rate corresponding to this condition can therefore be identified:

$$G_c = -\frac{\partial U^*}{\partial A} = \frac{\partial \Pi}{\partial A} \quad (6)$$

Comparing the energy release rate to its critical value gives a criterion for crack growth:

$$G \geq G_c \quad (7)$$

Now, the potential energy U^* consists of the strain energy U , diminished the work done by external forces W .

$$U^* = U - W \quad (8)$$

In a displacement-controlled system, the work term vanishes. On the other hand, in a load-controlled system it is equal to:

$$W = Pd\delta \quad (9)$$

Where P is the external load and $d\delta$ is the increment in crack opening displacement. Meanwhile, the change in strain energy is:

$$U = \frac{P\delta}{2} \quad (10)$$

Therefore, under these conditions it can be written that:

$$U^* = -U \quad (11)$$

Finally, if the width of the plate b is constant, this is equivalent to differentiating with respect to crack length a . Using (10), G becomes:

$$G = -\frac{\partial U^*}{\partial A} = \frac{1}{b} \frac{\partial U}{\partial a} = \frac{P}{2b} \frac{\partial \delta}{\partial a} \quad (12)$$

For a linear elastic body, the (12) can also be expressed in terms of *compliance* $C = P/\delta$. In load-controlled conditions, this results in the following expression, known as Irwin-Kies equation:[14]

$$G = \frac{P^2}{2b} \frac{\partial C}{\partial a} \quad (13)$$

This equation stands as the theoretical basis of all delamination tests.

1.5 Quasi-static mode I delamination testing

The aim of delamination testing of composites is determining the material's interlaminar fracture toughness G_c .

Quasi-static mode I delamination testing of unidirectional long-fibre-reinforced polymer matrix composites is well-established, and is covered by ASTM standard D5528 (introduced in 1994, and updated in 2001 and 2013) as well as by ISO 15024:2001.[15][16] Even when reviewing the literature for dynamic of tests, it is useful to begin from the quasi-static standards, as many authors used them as the starting point to build their own dynamic test procedures.

1.5.1 The double cantilever beam specimen

The specimen typically used in mode I delamination tests is the so-called double cantilever beam, or *DCB*, specimen (figure 1.3). It consists of a prismatic, constant width and thickness composite beam, with fibres oriented along the main dimension. A pre-existing

mid-plane interlaminar crack at one end of the specimen splits it in two arms, which can be likened to beams cantilevered in the remaining part of the specimen. Point loads are applied to the extremities of the arms, in a direction normal to the specimen's midplane, so that the two structures are subject to bending. When critical strain energy release rate is reached, the crack starts propagating.

The advantages of using this configuration to test long-fibre-reinforced composites are apparent. Firstly, the specimen is simply a rectangular coupon cut out of a laminate. Secondly, the initial interlaminar crack can be obtained without the need for machining or fatigue precracking operations, simply by interposing a thin non-adhesive insert between the two midplane plies during the lay-up process. For epoxy matrix composites, a PTFE (such as Teflon™) film is used, as recommended by both ASTM and ISO, where curing temperatures allow.

Film thickness is not inconsequential. Formation of a resin pocket at the end of the film is inevitable, and it might influence significantly the initiation value of interlaminar fracture toughness. On the other hand, extremely thin films are difficult to manipulate during manufacturing. ISO and ASTM suggest a 13 μm maximum thickness. At and below this value, round-robin tests showed that the measured initiation interlaminar fracture toughness values for carbon fibre/epoxy composites plateaus, meaning the toughening effect of the resin pocket becomes negligible.[17]

The sides of the specimen are painted white in order to provide high contrast and facilitate crack tip cracking. To determine crack tip length, usually a scale is marked by

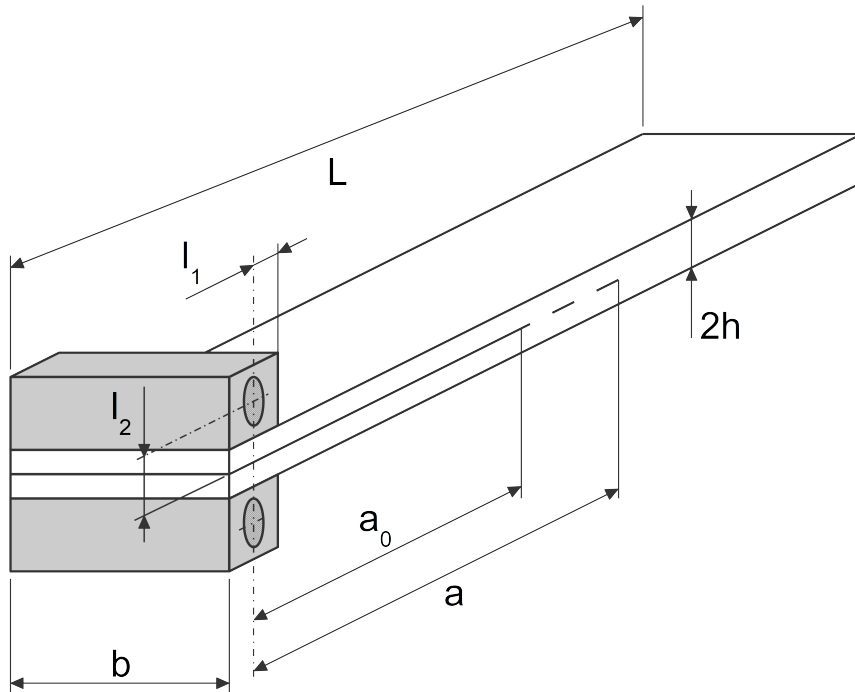


Figure 1.3: Geometry of the double cantilever beam specimen

hand at 1 mm intervals in black over the white paint.

Types of fixtures

In order to properly perform the test, the specimen needs to be loaded along a invariant direction throughout the test. This require the specimen-machine joint to have a rotational degree of freedom. To this end, two different type of fixtures are used: piano hinges and load blocks. Both are attached to the specimen's upper and lower surfaces, normally by bonding—or more rarely, when the bonding agent proves too weak, by threaded fasteners. It should be noted that the thick metal fixtures will inevitably produce an undesired stiffening effect on the thin specimen's bending behaviour.

The first type of fixture, piano hinges, is best suited to testing machines equipped with grips. One hinge-half is bonded to the specimen, while the other is gripped and pulled by the machine. Besides being an inexpensive, readily available piece of hardware, piano hinges have the advantage of reducing the stiffening of the specimen's arms by placing the loading point at one extremity of the fixture. To make the most of this, piano hinges are nearly always bonded with the hinge oriented towards the crack tip.

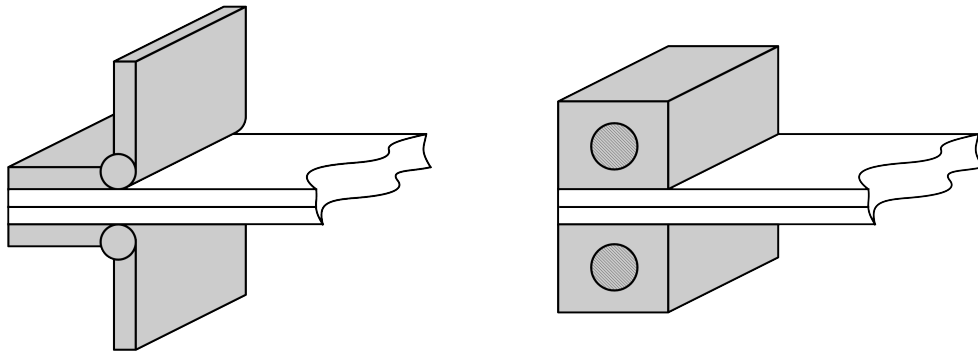


Figure 1.4: Left, piano hinges; right, load blocks

Loading blocks, on the other hand, must be purpose-designed and fabricated. They usually consist of simple machined metal prisms with a through hole for a pin, used to connect the block to the testing machine. In dynamic testing loading block design is usually more studied, removing as much material as possible with the aim of reducing the mass of the fixture. Besides being more complex, multi-piece ordeals, loading blocks have the disadvantage over piano hinges of producing a greater stiffening effect on the specimen, since oftentimes the pin is located at the centre of the block. As will be described later, this effect is accounted for in ASTM and ISO quasi-static testing standards by use of a stiffening correction term applied to the reduction formula.

1.5.2 Standardised test methods

The most significant standardised mode I delamination test methods come from the ASTM and ISO organizations. Those are the standard ASTM D5528-13 (introduced in 1997, revised in 2001 and in 2013) and ISO 15024:2001 (introduced in 2001). The

two are very similar, nearly interchangeable in some respects. Both make use of a DCB specimen, and leave to the researcher the choice of either piano hinges or loading blocks.

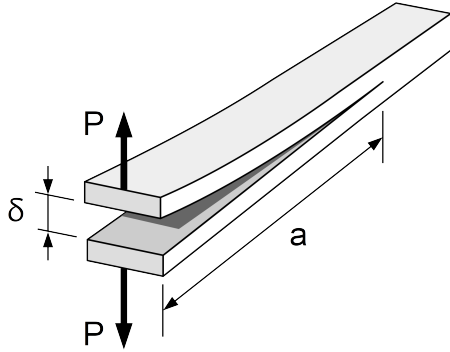


Figure 1.5: Schematic of a DCB specimen under loading, showing the quantities that need to be recorded during the test.

Test procedure and measurements

The test itself consists of two loading-unloading cycles. The prescribed crosshead rate (i.e. the load line opening rate) is constant and between 1 and 5 mm/min, and the unloading rate upwardly limited to 25 mm/min. The initial loading serves to generate a clean precrack, and is continued until the crack extends 3 to 5 mm away from the insert. The following reloading takes place at the same opening rate, and is continued until the crack has propagated 50 mm away from the precrack. The quantities recorded during the test are three (figure 1.5): load P , the corresponding load line displacement δ and crack length a . Load is measured with a load cell. Crack tip length is monitored optically using a traveling microscope; for this measurement, a resolution of at least 0.5 mm is advised.

Interpretation of results

After having obtained the load-displacement curve, it is necessary to identify which point corresponds to the initiation critical energy release rate value. Both standards propose three criteria.

- **Deviation from linearity.** According to this criterion, the initiation of crack growth coincides with the deviation from linearity of the load-opening displacement curve. Studies using radiography determined that this point is the closest to actual onset of crack propagation in the centre of the specimen.[18, p. 69] The downside of this method is reproducibility, especially considering the experimental nature of the data and that the lack of a standard definition of what constitutes a deviation from linearity.
- **5% offset or maximum load.** In response to the shortcomings of the previous criterion, a method was developed involving secants with a stipulated increase in compliance, akin to that used in standard ASTM E399 for determination of K_{Ic} in metals.[18, p. 69] According to this criterion, a line is traced from the origin of the load-opening displacement curve with a slope 5% lower than that of the linear portion of the curve. If the intersection point of the line with the curve occurs before the absolute maximum in the curve, the initiation G_{Ic} is the one calculated at the intersection point. Otherwise, the initiation G_{Ic} is the one corresponding to the maximum point in the curve.

- **Visual observation.** The initiation G_{Ic} is taken when propagation of the crack is visually observed on the side of the specimen. This criterion has the advantage of giving a result consistent with the subsequent propagation values, which can only be obtained by tracking the crack on the side of the specimen.[18, p. 69]

Data reduction methods

The ASTM standard proposes the three methods for data reduction and G_{Ic} calculation, while the ISO one only mentions two of them.

- **Modified beam theory.** Assuming that the two specimen arms behave like cantilever beams, and following Euler-Bernoulli beam theory, the strain energy release rate can be calculated as:

$$G_I = \frac{3P\delta}{ba} \quad (14)$$

This method was found to overestimate G_I , because the beam is not perfectly clamped at its end, and some rotation might occur. As initially proposed by Hashemi *et al.*, and reprised both by ASTM and ISO standards, this can be accounted for considering a longer delamination length:

$$a' = a + \Delta \quad (15)$$

The parameter Δ (figure 1.6) is the intercept with the abscissa axis of a least squares plot of the cube root of experimentally determined specimen compliance, $C^{1/3}$, as a function of crack length a . Compliance is defined as the ratio of load line displacement and measured load. The expression for G_I therefore becomes:

$$G_I = \frac{3P\delta}{2b(a + \Delta)} \quad (16)$$

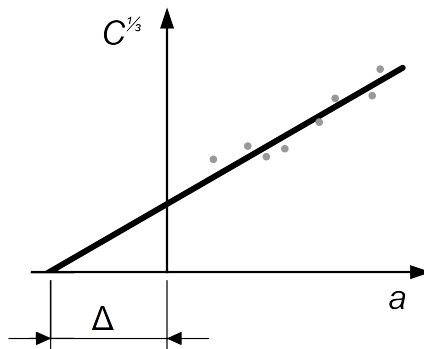


Figure 1.6: Obtaining the parameter Δ for modified beam theory

- **Compliance calibration method.** This empirical method was originally proposed by Berry, and sanctioned by ASTM. The premise is that compliance of the double

cantilever beam may be expressed as an exponential function of crack length a : [19]

$$C = \frac{a^n}{H} \quad (17)$$

H and n are parameters determined from a least squares fit of experimental results. In particular, n is the slope of a double logarithmic plot of the compliance (computed as the ratio of measured loads and displacements) as a function of a . Substitution (17) in the Irwin-Kies equation (13) returns an expression of G_I which is independent from H :

$$G_I = \frac{nP\delta}{2ba} \quad (18)$$

- **Modified compliance calibration method.** A further evolution of the empirical compliance-based method, it is proposed in different forms by both ASTM (19a) and ISO (19b):

$$G_I = \frac{3P^2C^{2/3}}{2A_1bh} \quad (19a)$$

$$G_I = \frac{3A_2P^2(wC)^{2/3}}{2(2h)b} \quad (19b)$$

The standards leave the choice of the reduction method free, but ASTM D5228 remarks that MBT method yields the most conservative results.

Correction factors

The large displacements encountered during the test cause a shortening in the moment arm of the applied force and non-negligible rotation of the load blocks. These effect are accounted for applying a correction factor F to all G_{Ic} values, irregardless of the type of fixture used:

$$F = 1 - \frac{3}{10} \left(\frac{\delta}{a}\right)^2 - \frac{2}{3} \left(\frac{\delta l_1}{a^2}\right) \quad (20)$$

Load blocks bonded to the specimen cause a stiffening of the specimen arms. This is corrected with a second factor N :

$$N = 1 - \left(\frac{l_2}{a}\right)^3 - \frac{9}{8} \left[1 - \left(\frac{l_2}{a}\right)^2\right] \frac{\delta l_1}{a^2} - \frac{9}{35} \left(\frac{\delta}{a}\right)^2 \quad (21)$$

Where l_1 is the distance between the axis of the pin and the midplane of the specimen, and l_2 is the distance between the axis of the pin and the edge of the load block (see also figure 1.3).

1.6 Dynamic mode I delamination testing

In the last three and a half decades a dazzling array of diverse test methods for dynamic mode I delamination have been proposed. Still, manly due to the issues that arise with

higher opening rates, there is no standardised or generally accepted test method. Although double cantilever beam specimens are the most commonly used, the discussion remains open not just the test method, but even on specimen geometry. Some of the most commonly encountered difficulties are:[20]

- At high crack opening rates it is problematic to perform pure mode I tests, due to undesired asymmetry in the opening of the specimen's arms, mostly due to dynamic effects. What happens is that the bending is limited to one of the specimen arms, while the other remains straight, and the specimen rotates. The loading is then not pure mode I anymore, but rather mixed mode I/II.[14]
- The definition of interlaminar fracture toughness is energetic, meaning kinetic energy and friction should to be taken into account, increasingly so with rising testing velocity.
- Strain rate cannot properly be defined, due to the singularity in the stress field at crack tip. An appropriate representative parameter to has to be found in its place. A number of different one have been proposed, generally based either on crack velocity (the time derivative of crack length a) or on opening rate (the time derivative of load line displacement δ).

1.6.1 General overview

The inexperienced researcher entering the field of dynamic mode I delamination testing can count on a precious recent review articles to guide him in his readings. It is sufficient to note the ones by Brunner *et al.* (2008), who put together a status report on of testing for opening modes I, II and I/II, including high-rate testing; by May (2016), who reviewed nearly all the possible test methods and measurement techniques for high-rate mode I testing; and finally by Tabiei *et al.* (2018), who recently not only reviewed the test procedures but also the nowadays omnipresent simulation techniques, ad also summed up some of the findings.[21][14][22]

One aspect that becomes a source of issues passing from quasi-static to dynamic delamination testing is tracking and measuring the crack length a throughout the test.[14] Optical tracking methods are the most commonplace, and switch from traveling microscope to high-speed imaging for rising rates. The other method that has found practical application is the electrical one, using conductive paint grids or delamination gauges.[14]

DCB specimen tests

The double cantilever beam specimen remains a favourite. The most straightforward test configurations involves conventional screw-driven or servo-hydraulic test machines, which have been used to reach opening rates of up to 670 mm/s.[14]

One way to reach higher opening rates on conventional setups is to implement some kind of lost-motion device, to ensure the machine has the time to accelerate to desired velocity before engaging the specimen. With such a device, Blackman *et al.* achieved opening rates of 15,000 mm/s.[23] However the vibrations and resonances caused by any kind of mechanism interposed between the machine's crosshead and the specimen

may lead to noisy load recordings. Dampers used to limit such effects may conversely introduce compliance, and lead to discrepancies between the displacement measured by the machine and that experienced by the specimen.[23] Alternatively drop weight towers have also been used, but a distinct downside of setup is non-constant test velocity.[14]

While conventionally-loaded DCB specimens are perfectly suited to quasi-static testing, one issue that may sometimes arise during high loading rate testing is the already mentioned asymmetrical opening of the two arms. An example is what was experienced by de Verdiere *et al.* using a drop tower setup.[24]

Through the years different researchers tried to address this issue. Hug *et al.* developed a complex device to convert the vertical motion of a testing machine crossbar into horizontal, symmetrical opening of the specimen's arms. The highest opening rate reached was 1,600 mm/s; above that threshold, inertia effects due to the considerable mass of the device led again to asymmetrical opening.[20]

An entire class of tests aiming to enforce perfectly symmetrical opening are the wedge-loaded DCB methods. These techniques involve driving a wedge between the DCB arms instead of pulling them apart. Kusaka *et al.* in 1998 used one such geometry, christened *wedge-insert fracture (WIF)*, on a split Hopkinson bar.[25] The impacting bar of the Hopkinson setup drove the wedge between the arms of the specimen, which was carried by the receiving bar. Similar arrangements continue to be used, e.g. by Isakov *et al.* in 2019, who inverted the configuration making the wedge fixed and having the impacting bar hit the specimen.[26] Wedge-loading setups have also been used on servo-hydraulic testing machines and drop towers. The obvious downside of all wedge setups is that some energy is being dissipated by friction instead of being used to propagate the crack; an amount that is hard to estimate, due to the difficulties in measuring the friction coefficient for composites in dynamic conditions.[14]

Lately Liu *et al.* have developed a novel specially-developed electromagnetic dual Hopkinson bars, that pull apart a DCB specimen in perfectly symmetrical fashion. Opening rates of up to 25,000 mm/s were achieved.[27]

Other tests

Some authors have proposed modified double cantilever beam specimens. Recalling that the Irwin-Kies equation (13) is the basis of data reduction in DCB tests; if, by tailoring the geometry of the specimen $\partial C/\partial a$ could be made constant, tracking crack length becomes unnecessary and fracture toughness can be determined by monitoring the load P alone. This can be achieved using height- or thickness-tapered DCB specimen, a geometry that has been accepted in standards for testing of adhesives such as ISO 25217:2009.[28]

Other geometries encountered in literature are the compact tension, compact compression, and small-edge notch bending specimens. All of them, while well-suited to testing of metals, have a major drawback when applied to delamination of composite laminates: their major dimension is transverse to the crack, i.e. to the plane of the laminas. This requires extremely thick laminates—with lay-ups sometimes numbering over a hundred plies—which are both very problematic to manufacture and are very far from the geometry of actual composite components.[14]

Reference	Fixture type	$L \times b \times 2h$ [mm]	a_0 [mm]
Smiley and Pipes[4]	Hinges	$250 \times 25 \times \text{n. a.}$	50
Blackman <i>et al.</i> [23]	Load blocks	n. a.	35
Zabala <i>et al.</i> [29]	Inverted hinges	$200 \times 22 \times 3.7$	55
De Verdiere <i>et al.</i> [24]	Load blocks	$200 \times 20 \times 4.1$	40

Table 1.1: DCB specimen geometries encountered in literature

1.6.2 Closer review of test methods similar to the one used in this work

What follow is a more detailed review of the papers that, because of the similarity in the material tested, in the machine employed or the measurement techniques, were considered closely when developing the experimental procedure used in the present work

Specimen and hinge geometries

An overview of specimen geometries and hinge types encountered is given in table 1.1.

Test procedure

Smiley and Pipes in their seminal work on dynamic delamination testing used an hydraulic test frame. They only considered initiation G_{Ic} values, and every specimen was reloaded multiple times, obtaining multiple data points.[4]

Blackman *et al.* used an hydraulic test frame fitted with a special lost motion device, a slide-catch mechanism with an internal elastomeric damper—for all intent and purpose identical to the mechanism described in section 2.1.1. The purpose of this apparatus was making sure that the had accelerated to the desired velocity before beginning to deform the specimen.[23]

De Verdiere *et al.* made use of a drop tower and a sliding rail-pin fixture, to constrain all of the specimen's degree of freedom different from the vertical opening of the two arms. Due to the type of test machine used, the test was continued up to failure of the specimen.[24]

Crack length measurement

As they were not interested in crack propagation but in initiation values only, Smiley and Pipes only needed the known crack length at the beginning each specimen loading/unloading cycle.

Since then, optical measurement has become the favoured method for cracking track length. Blackman *et al.* used high-speed photography, and projected the images to determine crack length and opening displacement. De Verdiere *et al.* as well as Zabala *et al.* made use of post-processing digital image correlation scripts, whose working principle was not specified. Given the sides of the specimens were marked with 1 mm intervals,

it is safe to assume that some form of digital image correlation tracking the opening of these markings was used.

In recent years use of high-speed photography coupled with increasingly sophisticated digital image correlation for analysis of the captured frames is becoming more and more popular. Isakov *et al.* for example developed an Octave algorithm which worked by fitting the shape of deformed Euler beams to the profile of the specimen, photographed in stark high-contrast black and white.[26]

Data reduction methods

Smiley and Pipes used a beam theory approach to calculate G_{Ic} , and included a second subtractive term, the kinetic energy contribution at the onset of crack propagation:

$$G_{Ic} = \frac{3A_1 P^2 a^2}{2b} - \frac{33 \rho h \dot{\delta}^2}{280} \quad (22)$$

The constant $A_1 = C/a^3$ was obtained as the intercept of a linear fit of specimen compliance plotted logarithmically against crack length:

$$\log(C) = 3 \log(a) + \log(A_1)$$

Blackman *et al.* used a form of corrected modified beam theory. Dependence from the load P was removed using the expression of compliance for an Euler-Bernoulli beam, since measurements at higher rates of test were overly noisy and unusable. The formulation was purely quasi-static; nevertheless, the kinetic energy term was evaluated and found to reduce G_{Ic} values by about 8%.

$$G_{Ic} = \frac{3}{16} \frac{F}{N^2} \frac{\delta^2 h^3 E_{11}}{(a + \Delta h)^4} \quad (23)$$

De Verdier *et al.* started from beam theory and also removed dependence from load measurements. All dynamic effects were neglected, and all correction factors were omitted:

$$G_{Ic} = \frac{3}{16} \frac{\delta^2 h^3 E_{11}}{a^4} \quad (24)$$

Studying rate dependence

The purpose of dynamic delamination testing is most often to establish whether this damaging mechanism is strain rate-dependent or not. As noted before, since delamination is being studied with an elastic model, the crack tip corresponds to a singularity in the stress and strain fields. It is therefore not possible to exactly define strain and strain rate in that position. In order to investigate the effect of strain rate on material behaviour, a separate representative parameter has therefore to be found. A number of different ones have been proposed through the years.

Smiley and Pipes, as well as Thorsson *et al.* who followed their approach, used *crack tip opening rate* \dot{y}_{CT} . This is the time derivative of opening displacement, calculated

at an arbitrarily small distance ϵ from the crack tip—e.g. the thickness of two plies in Smiley and Pipes’ work.[4][30]

$$\dot{y}_{CT} = \frac{3\dot{\delta}\epsilon^2}{2a^2}, \quad \epsilon \ll a \quad (25)$$

Blackman *et al.* chose simply *displacement rate* $\dot{\delta}$, the time derivative of load line displacement δ .

$$\dot{d} = \frac{d(d)}{d(t)} \quad (26)$$

Kusaka *et al.*, Sun and Han,[31] Hug *et al.*, as well as Liu *et al.*, instead favoured *loading rate* \dot{G}_{Ic} , the time derivative of the strain energy release rate. For a DCB specimen, it can be estimated as:[25]

$$\dot{G}_{Ic} = \dot{G}_{Ic} \frac{2\dot{\delta}}{\delta} \quad (27)$$

De Verdier *et al.* chose *crack velocity* \dot{a} , which was determined from the successive positions of the crack tip.

Zabala *et al.* found that a function of $\ln(\delta)$ and $\dot{\delta}$ was a good fit for the experimentally measured crack length, and used the time derivative of this expression, christened *crack rate* \dot{a} , as an indicator of strain rate.

Results from literature

Nearly all authors found that higher opening rates have either no or a negative effect on the fracture toughness of carbon fibre and epoxy composites.

Table 1.2 gives a selection of results from studies on rate dependency of interlaminar fracture toughness of the aforementioned materials. There are only a handful of papers reporting mode I fracture toughness values mildly rising with opening rates, all of them very early works such as the one by Aliyu and Daniel from 1985.[32]

Reference	Fabric type	Displacement rate $\dot{\delta}$ [m/s]	Rate parameter [m/s]	Fracture toughness G_{Ic} [kJ/m ²]	Effect of higher rates on G_{Ic}
Smiley and Pipes[4]	Uniaxial	4.2×10^{-6} to 6.7×10^{-1}	Opening rate $1 \times 10^{-10} < \dot{y} < 1 \times 10^{-6}$	0.17 to 0.04	G_{Ic} starts decreasing for $\dot{y} > 2 \times 10^{-8}$
Blackman <i>et al.</i> [23]	Uniaxial	3.33×10^{-5} to 1.5×10^1	Displacement rate $3.33 \times 10^{-5} < \dot{\delta} < 1.5 \times 10^1$	0.3	None
Zabala <i>et al.</i> [29]	Uniaxial	8.3×10^{-5} to 1.9×10^1	Crack rate $2 \times 10^{-5} < \dot{a} < 0.9 \times 10^{-1}$	0.8 to 0.4	G_{Ic} decreases 24% going from quasi-static to dynamic
de Verdiere <i>et al.</i> [24]	Biaxial non-crimp	—	Crack velocity $0.1 < \dot{a} < 13$	0.3 to 0.6	G_{Ic} slightly increases for $\dot{a} > 0.6$ m/s

Table 1.2: Results from literature, tests conducted on carbon fibre and epoxy composites.

1.7 Modelling delamination

The two most used numerical modelling techniques for delamination in composites are virtual crack closure technique and cohesive zone models. Both make use in some form of interlaminar fracture toughness G_c .

1.7.1 The virtual crack closure technique

The virtual crack closure technique (VCCT) was originally proposed by Rybicki and Kanninen in a paper that dates back to 1977.[33, p. 4] Its foundations lie in Irwin's crack closure integral, according to which the energy necessary to extend a crack by a length Δa is the work needed to virtually close it to its previous length a . [34, p. 558] The strain energy can be computed via Clapeyron's theorem, which states that the work done by forces is equal to half the product of the final value of said forces by the displacements of their points of application. [35, p. 136]

A simple two-dimensional finite element crack propagation problem is illustrated in figure 1.7. Rybicki and Kanninen introduced the assumption of self-similar crack propagation: a crack extension by a small distance Δa does not alter significantly the crack tip. [33, p. 5] What this implies is that once the crack tip will progress from node b to node c , the displacement at current crack tip node b will be the same that can now be observed between nodes a' and a'' . It is then possible to calculate the strain energy release rate for the crack extension from node b to node c : [22]

$$G_I = \frac{1}{2\Delta a} N_b v_b \quad (28)$$

Similar formulations can be written for G_{II} and G_{III} .

The criterion for crack propagation is then the usual:

$$f = \frac{G_{equiv}}{G_{equiv c}} \geq 1.0 \quad (29)$$

In the traditional implementation of VCCT, the crack has to be already present in the model. In the example illustrated in figure 1.8 a DCB specimen is modelled in Abaqus/-CAE. The upper and lower arms of the DCB specimen are two separate entities. A surface-to-surface contact interaction between the adjoining surfaces (in magenta) is limited to the subset of nodes representing the non-cracked part of the specimen (in yellow). When condition equation (29) is met, the interaction that holds together the two nodes at the crack tip is released. [36] This is known as *node release method*, and is currently implemented in major finite element software such as Abaqus, Ansys and Nastran.

The classical virtual crack closure technique has several limitations: [22]

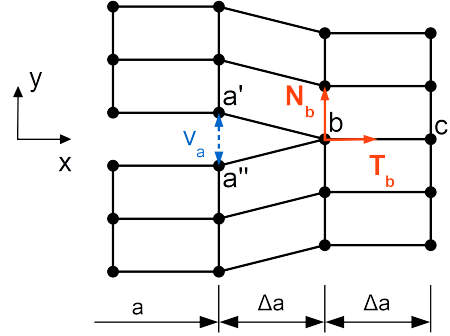


Figure 1.7: A simple finite element VCCT model

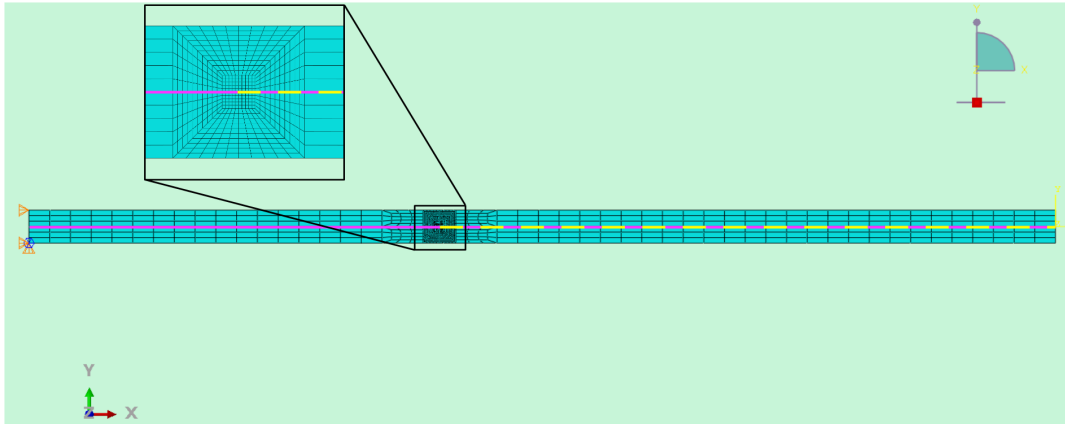


Figure 1.8: Example of a DCB specimen modelled in ABAQUS with VCCT to simulate the crack

- It cannot model crack initiation, unless paired with a separate crack initiation criterion such as equation (1) and equation (2).
- As it depends on a pre-existing cracks, it cannot model crack migration to other planes of propagation.
- Naturally, being based on classic linear elastic fracture mechanics, it has the same limitation in its validity: fracture process zone of a size negligible compared to that of the whole problem, i.e. brittle crack propagation.

1.7.2 Cohesive zone models

This method hypothesises the existence a process zone ahead of the crack tip, held together by tractions—that is, the cohesive zone (figure 1.9).[37, p. 55]

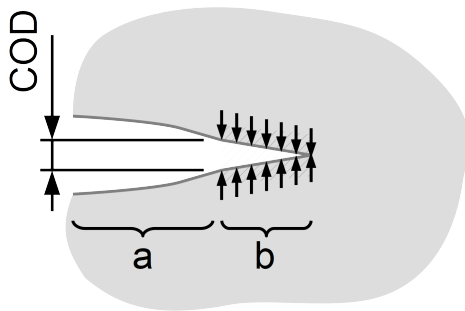


Figure 1.9: The cohesive zone ahead of the crack tip. a , fully opened crack; b , cohesive zone with tractions on the faces; COD , crack tip opening displacement.

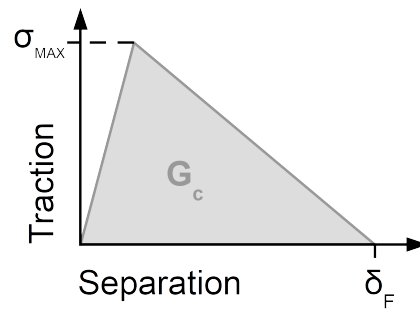


Figure 1.10: A bilinear cohesive law. σ_{MAX} , maximum stress; δ_F , separation at fracture.

In this zone the material behaves according to a traction-separation law, a constitutive relationship relating the tractions and crack opening displacement. In the most straightforward implementation of a traction-separation law, depicted in figure 1.10, the material behaves in linear elastic fashion until traction reaches its mechanical strength, and then starts degrading. The area under the traction-separation curve corresponds to the energy absorbed during crack propagation, and corresponds exactly to the critical strain energy release rate. For example, considering mode I crack opening:

$$G_{Ic} = \int_0^{\delta_F} \sigma d\delta \quad (30)$$

Thus one of the parameters used to determine can be the fracture toughness, determined for example with a DCB test.

The most common implementation of CZM in finite element models is with interface elements, which follow the chosen cohesive law but have no other properties. These elements are interposed between the regular 2D solid, 3D solid or shell elements representing the plies, and usually have zero thickness or a small finite thickness (in which case they are intended to stand for the inter-ply resin layer).[37, p. 58]

Unlike VCCT, cohesive zone models can successfully capture the initiation of delamination without the need for additional criteria. A potential downside, the fact that interface elements need to be placed beforehand in the model along the predicted likely crack propagation paths, is inconsequential in the case of delamination, which can only take place at the interface between plies.

A method for determining a material's cohesive law can be deduced from equation (30):[38]

$$\sigma = \frac{\partial G_{Ic}}{\partial \delta} \quad (31)$$

Equation (31) is the core of the so-called *direct method* to determine a cohesive law.

Chapter 2

Testing

An in-depth literature review helped identifying beforehand some issues frequently encountered in dynamic mode I delamination testing by researcher testing similar materials on similar machines. The necessary measures could be taken to avoid them before testing a single specimen. Those issues, already mentioned in the introductory chapter, are:

- Asymmetrical specimen arm opening.
- Defective crack length measurement methods.
- Unusable load (and sometimes even opening displacement) measurements when recorded with traditional sensors.

The first issue was addressed with careful fixture design; the second with a novel DIC-based crack tracking method. The third one was tackled by devising a test configuration and data reduction process based solely on measurements obtained via imaging and direct image correlation. A schematic of this is visible in figure 2.1. Two cameras, 1 and 2, recorded images that was processed to obtain crack length a and load line displacement δ respectively. Thanks to a reworked data reduction formula, no other measurements were needed to be recorded during the test. The load P measured by the load cell on-board the machine was used only as a secondary, qualitative check.

2.1 Materials and methods

2.1.1 The testing apparatus

Medium-rate as well as quasi-static tests were conducted on hydraulic test machines. Medium-rate tests were performed on the High Intermediate Strain Rate (HISR) hydraulic frame, visible in figure 2.9 and figure 2.10a. It is a custom test machine built in-house at the University of Waterloo,[39] capable of displacement rates up to 1,300 mm/s. Like most machines, it consists of two vertical columns, a fixed crosshead carrying the upper fixture, and an hydraulic cylinder which moves the lower, mobile, fixture.

The HISR frame employs a lost-motion device to make sure the hydraulic piston has time to accelerate and achieve the desired test velocity. Refer to figure 2.2 for a cutaway

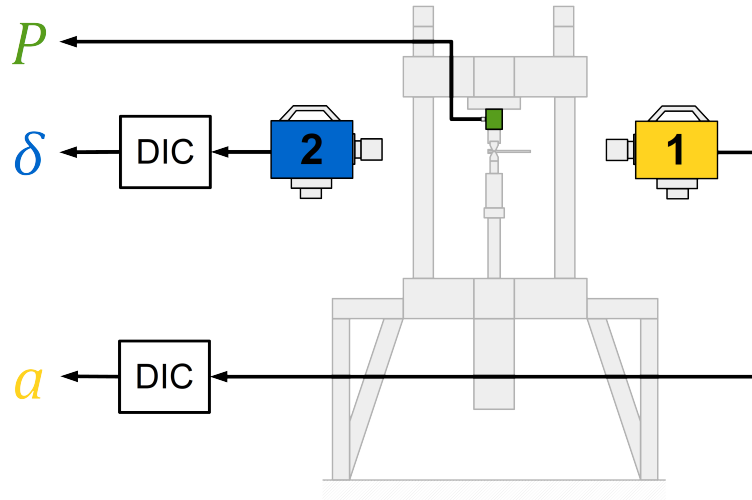


Figure 2.1: Schematic of the test configuration

drawing of (the redesigned version of) this apparatus. In particular the hydraulic cylinder piston is not directly connected to the fixture and thus to the specimen, but instead to a hollow cylindrical catch (numbered 10 in figure 2.2). A rod (11 in figure 2.2), to which the lower fixture (6 in figure 2.2) is actually attached, slides inside this catch and provides a few tens of millimetres of free travel to the hydraulic piston. This allows the piston to accelerate and reach the desired test velocity before engaging the specimen. Friction between the sliding parts is reduced using a brass bushing as mating surface as well as by lubricating the sliding rod. A rubber pad between catch and the bottom of the rod helps smoothing the mechanism's engagement. This setup is not uncommon, refer for example to the one used by Blackman *et al.* already mentioned in section 1.6.2.

Quasi-static tests were carried out on the Small hydraulic frame (figure 2.11), another machine custom built in-house at the University of Waterloo. Its construction is similar to that of the HISR, but on a smaller scale and designed for quasi-static tests only.

2.1.2 Design of the fixture

The HISR machine was originally intended to carry out very different tests on metals—and therefore sustain loads several orders of magnitude higher. A fixture had to be developed and manufactured to carry out the test. Since all mass attached to the specimen translates in dynamic effects during testing, which might adversely affect the results, it was decided to redesign all the unnecessarily robust (and thus heavy) parts downstream of the load cell and upstream of the catch sleeve. The existing parts were so heavy that a DCB specimen was opened by their static weight alone during a test fit. From the literature review, it had been learned that maximum loads during testing could be expected not to exceed 200 N. To make it usable for future testing of tougher material fixture was designed to comfortably carry a load ten times that.

The design brief was thus:

- Ability to bear a 2000 N load without significant deformation.
- Mass as low as possible.
- Simplicity in design and production, making use of hardware parts if possible.
- M16 male threaded ends to connect to the HISR machine. This ruled out immediately a pure piano hinge setup.

The fixture devised for this series of experiments is a novel hybrid of a piano hinge and load block designs, intended to combine the advantages of the two fixture designs: ease of mounting and dismounting of the load blocks, and the reduced stiffening effect on the specimen, low weight and large use of hardware of the piano hinges.

An assembly drawing is visible in figure 2.2, while the finished parts can be seen in figure 2.8b, and finally in action in figure 2.10b. Machined clevises (figure 2.4), as in a load block configuration, work in conjunction with standard 3/16 in diameter dowel pins and piano hinge-halves purchased from a hardware supplier. Upper and lower clevises are interchangeable. The material selected was 6061-T6 aluminium alloy.

The new rod (figure 2.3), also in the same material, had its free travel length reduced, is hollow, and has a reduced height lower retaining ring. The clevises are located via a prismatic mating surface machined at the top of the rod, and a screw with washer. A shoulder screw is used, to avoid damaging the soft aluminium with the threads if unwanted sliding between the parts occurs. An Helicoil threaded insert ensures safe and wear-free coupling between the parts, even with repeated use. As a result, the mass of the rod went from 457.1 to 89.3 grams.

The upper clevis is connected to the existing load cell via an adapter (figure 2.5), machined out of steel since mass is not a concern for the upper, fixed part of the testing rig. All of the new parts were produced in-house by the University of Waterloo Engineering Machine Shop.

The selected piano hinges had 1 in long knuckles, as wide as the specimens. The thickest ones available in this size (0.075 in thick sheet metal) were preferred, maximizing stiffness with little drawback in terms of mass. They were cut into pieces using a band saw, deburred, and their bottom side was sanded with 180-grit sandpaper to flatten and roughen the surface that was to be bonded. A vertical line corresponding to the centreline of the pin and the initial load line was measured and marked on each hinge. To ensure repeatability of the bonding process, the area where the adhesive would be applied was also marked on the bottom of every hinge.

2.1.3 Material preparation

The laminated plates were produced and supplied by the Fraunhofer Project Centre for Composites Research¹ using a high-pressure resin transfer moulding process based around a KraussMaffei HP-RTM line and a 2,500 ton Dieffenbacher hydraulic press (figure 2.6a).

¹Based in London, Ontario, Fraunhofer Project Centre for Composites Research is a joint venture between Western University (London, Ontario) and the Fraunhofer Institute of Chemical Technology (Pfinztal, Germany).

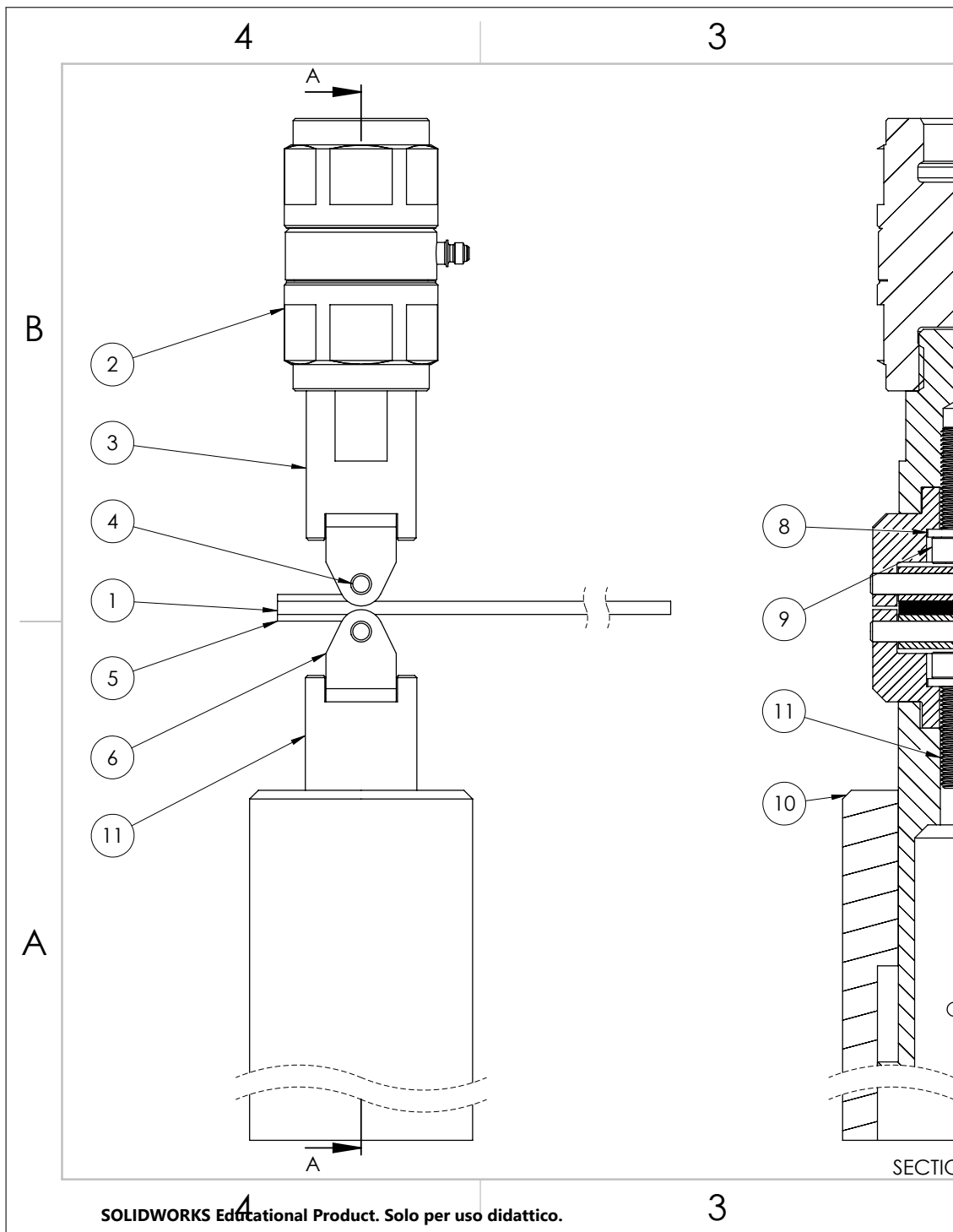
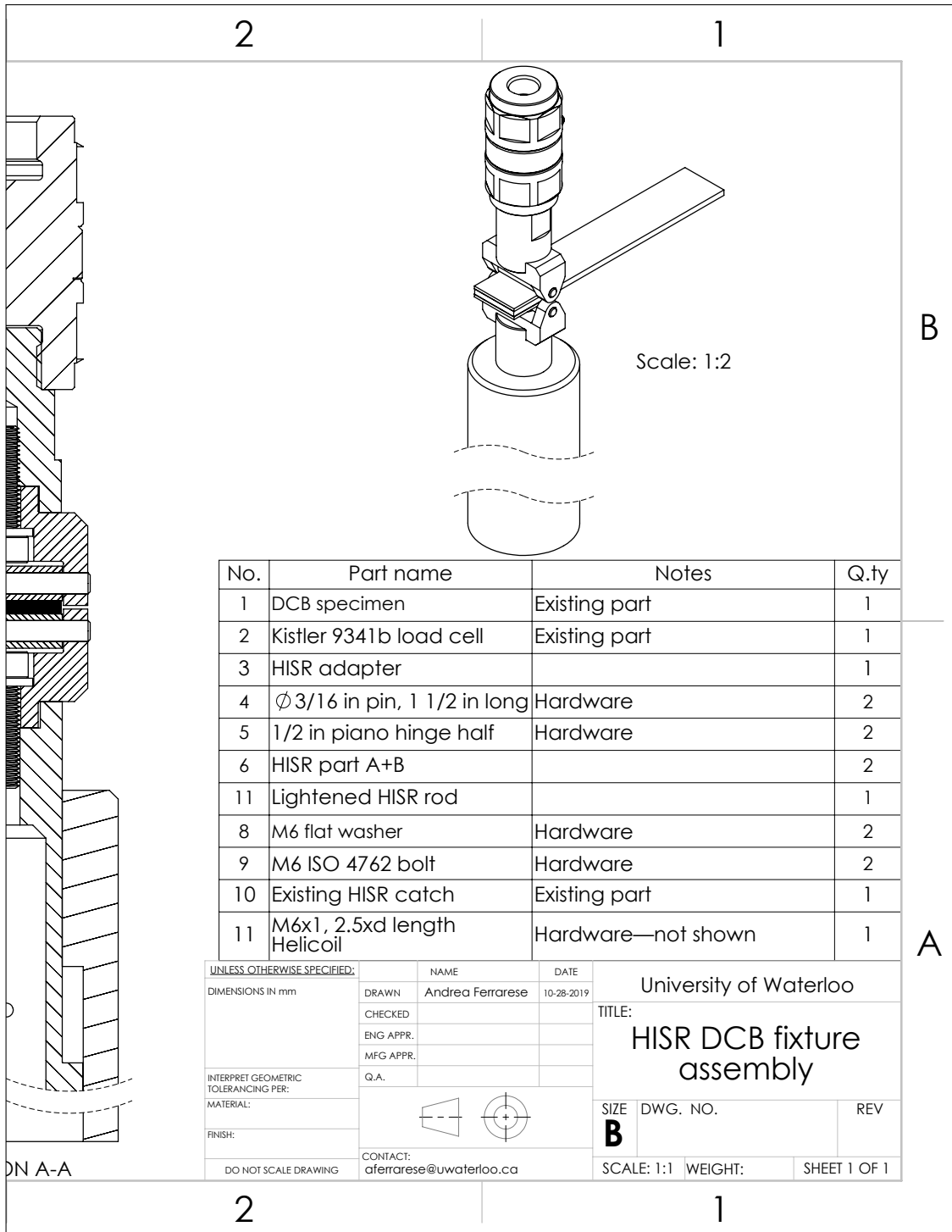


Figure 2.2: The redesigned fixture assembly for the HISR machine



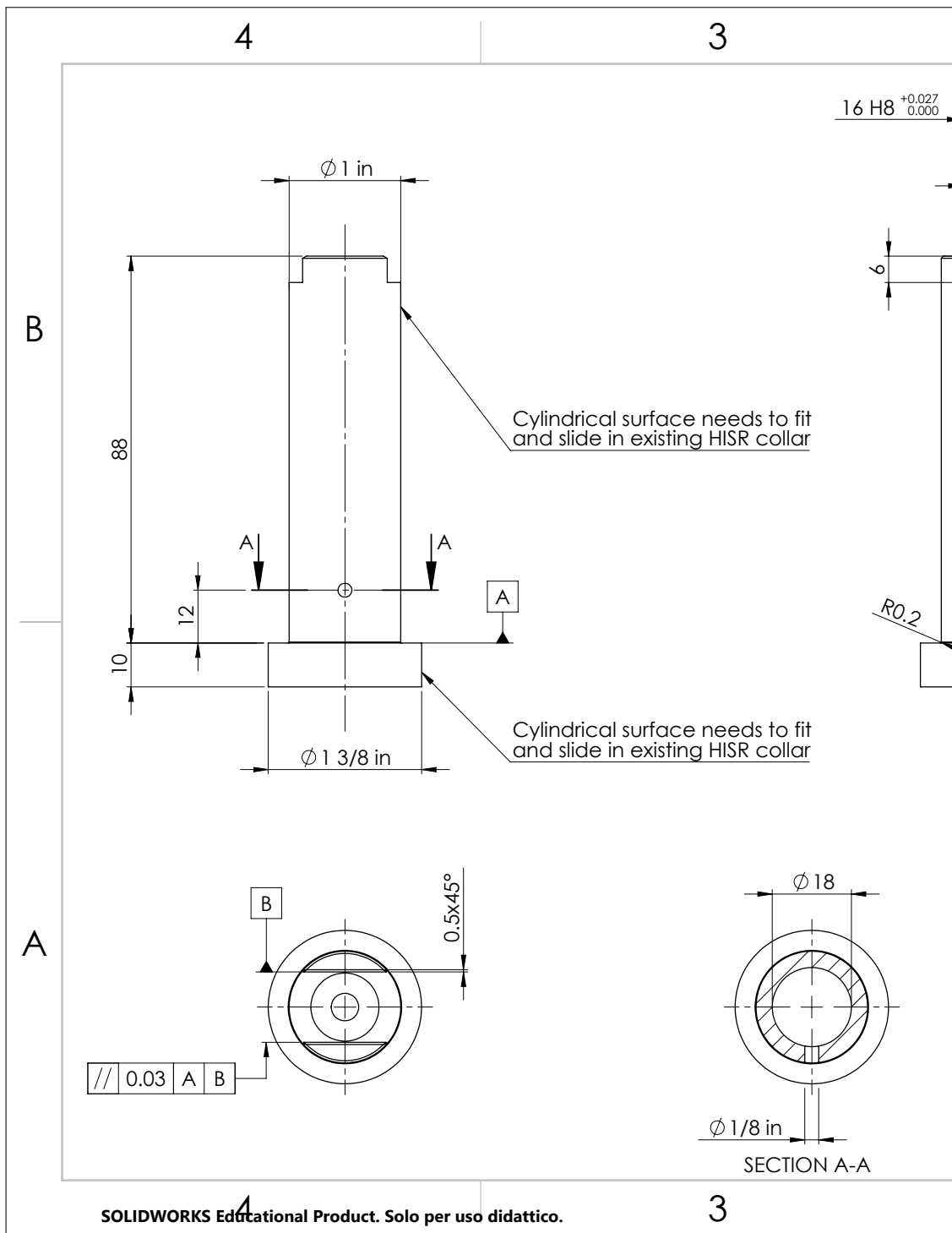
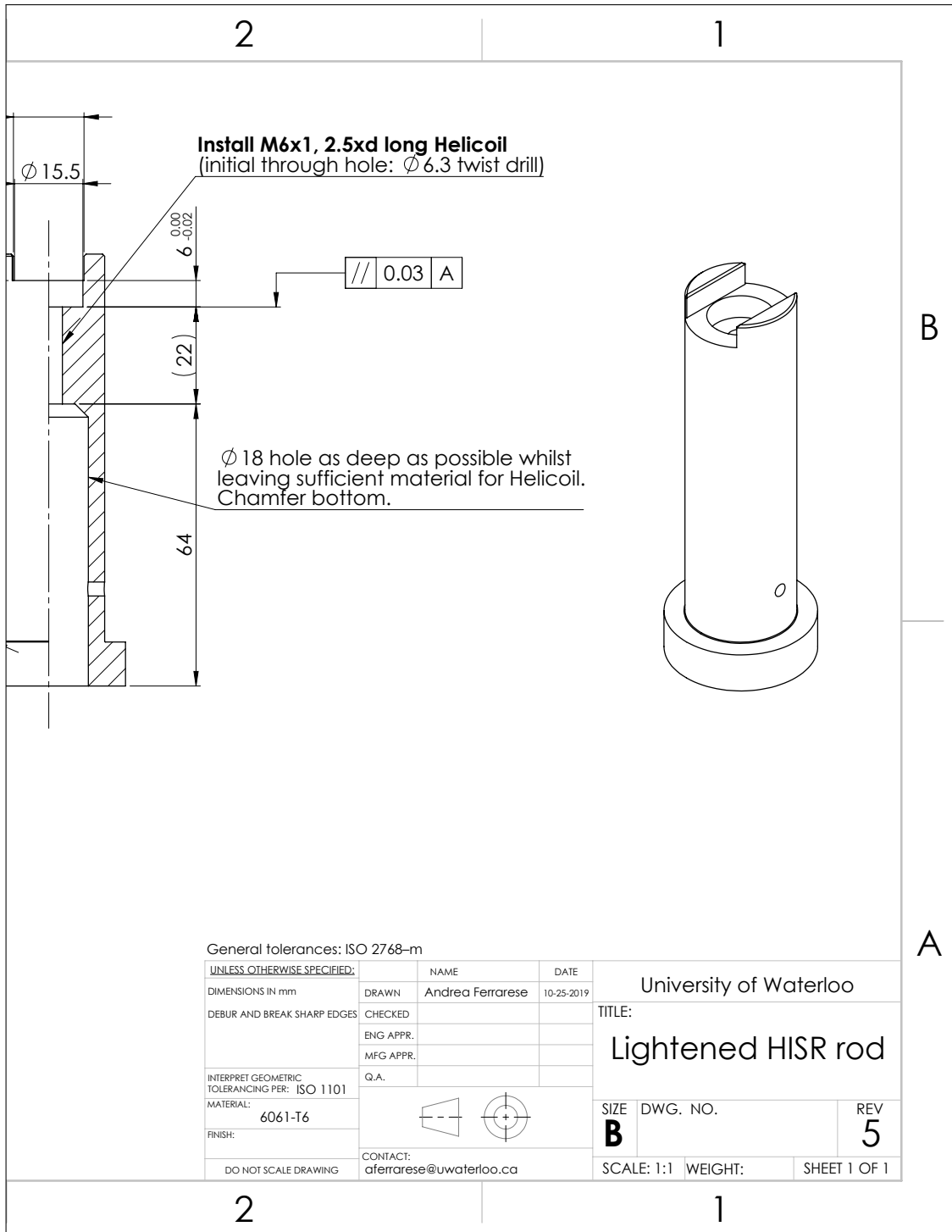


Figure 2.3: The sliding rod from the redesigned fixture assembly for the HISR machine



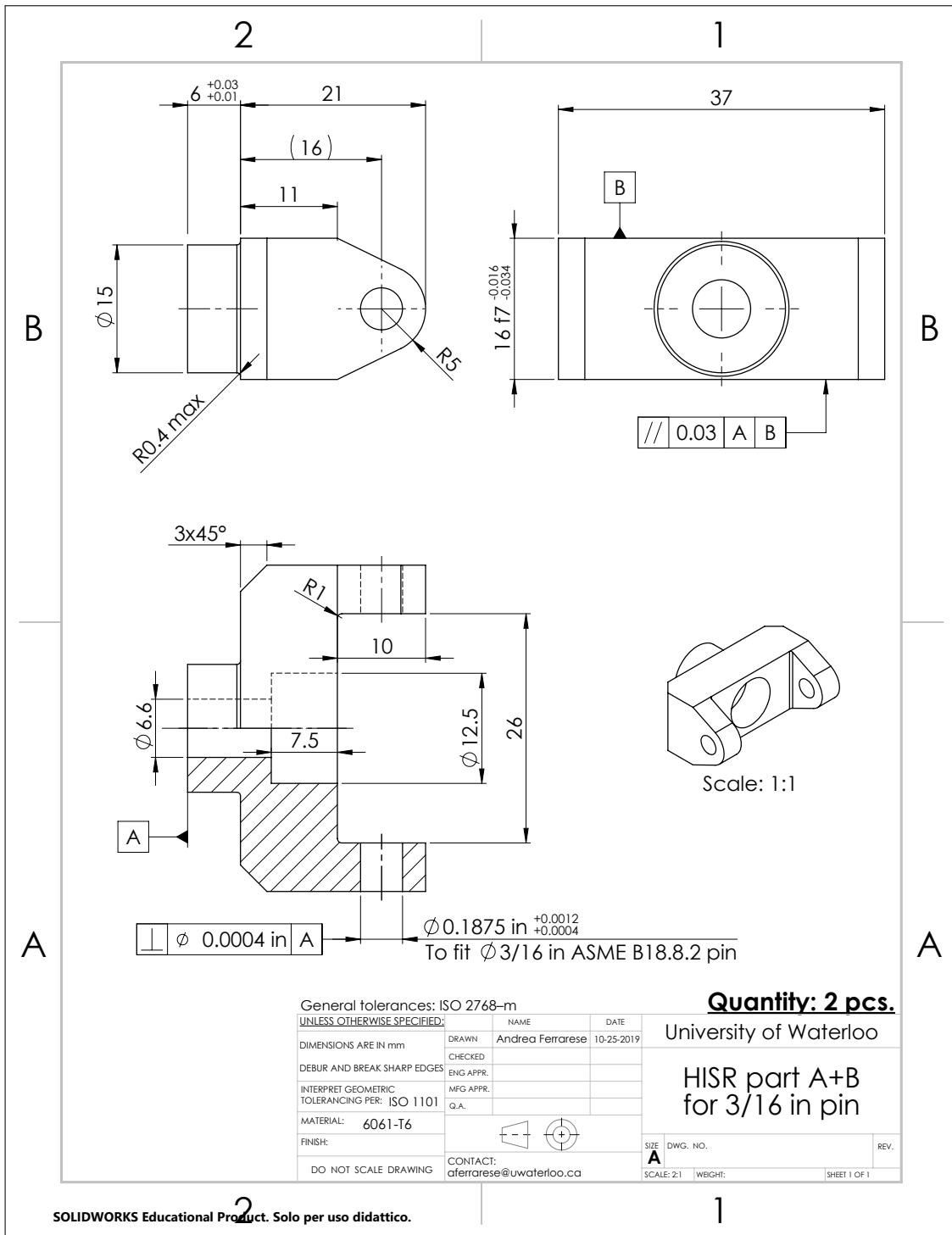


Figure 2.4: The clevis from the redesigned fixture assembly for the HISR machine

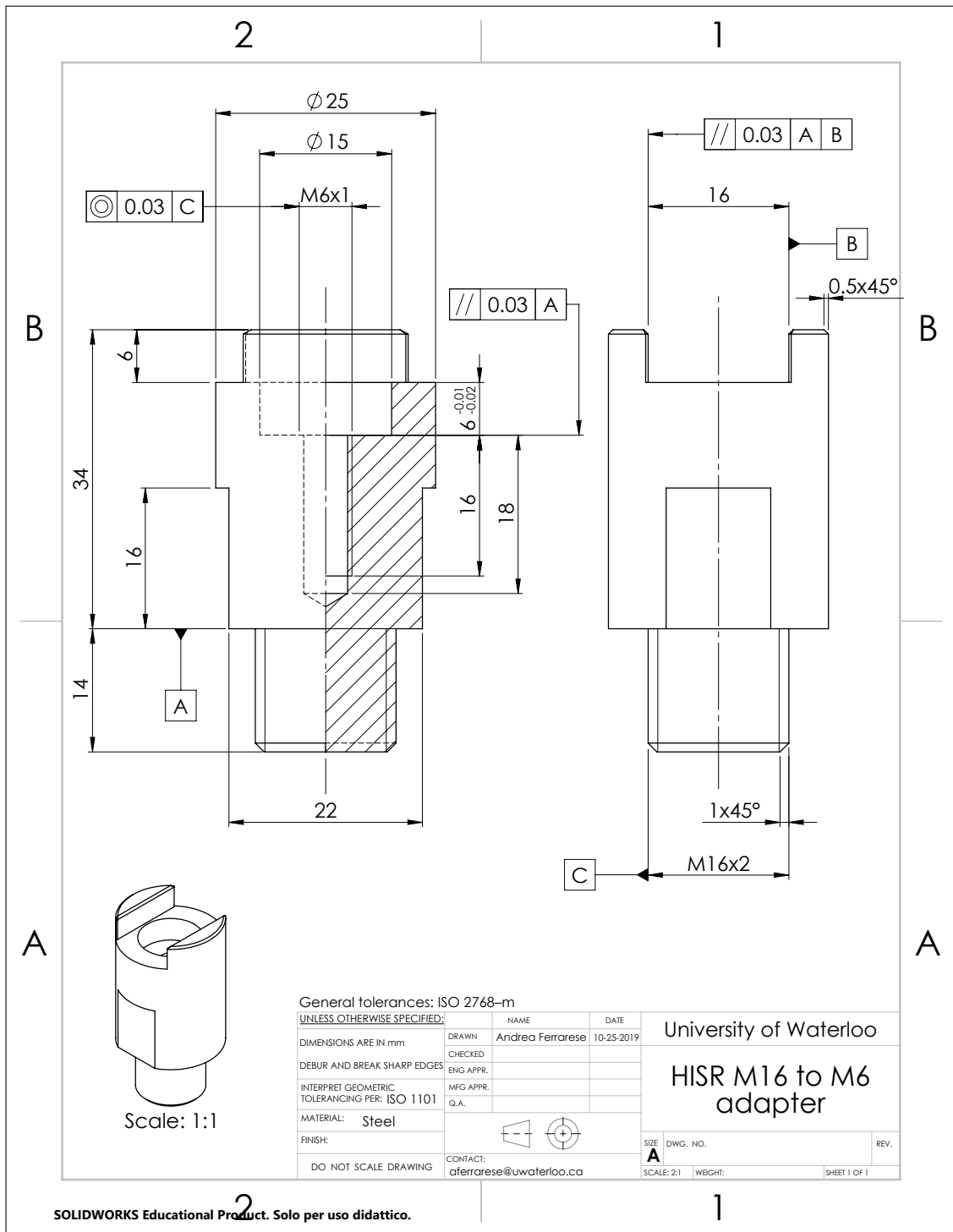


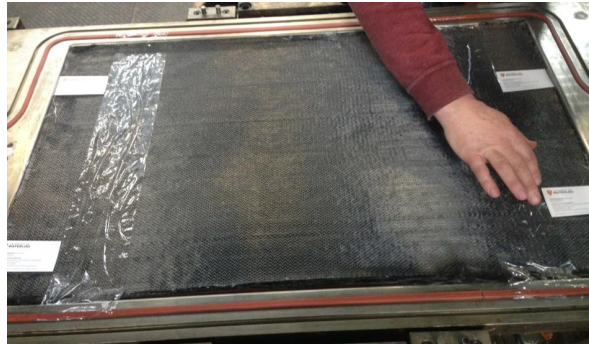
Figure 2.5: The M16 to M6 adapter from the redesigned fixture assembly for the HISR machine

The fibre came in the shape of 300 g/m^2 , unidirectional, bindered carbon fibre non-crimp fabric. In particular, the fabric was warp-knitted with polyester fibres, and auxiliary glass fibres yarns in a 90° direction. The mould was rectangular, its inner area measuring 900 mm by 550 mm . It featured a central injection point with a distribution channel along the minor dimension of the rectangle, and full fibre clamping around the edge. The layup was $[0_8]$.

Two 100 mm wide strips of $13 \mu\text{m}$ thick Teflon™ were placed sandwiched between the two middle plies, at “business card distance” from the two ends of the mould (figure 2.6b). The fibre volume fraction of the cured product was determined to be 53% and the density 1.456 g/cm^3 .



(a) The Dieffenbacher press at Fraunhofer Project Centre



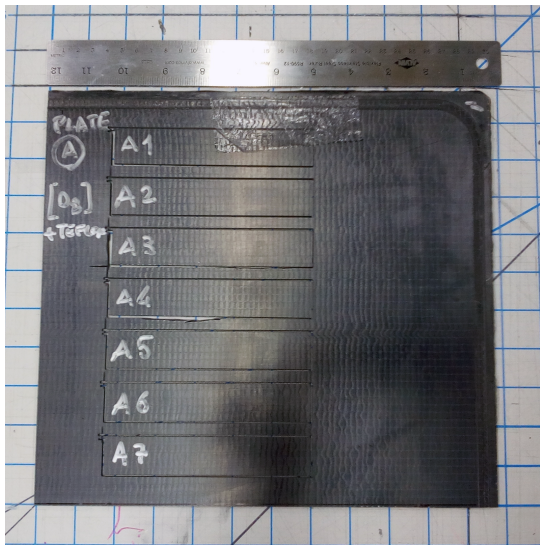
(b) Layup: placing the Teflon™ at “business card distance” from the two ends of the plies

Figure 2.6: Manufacturing of the test plate (credit: Gleb Meirson at FPC)

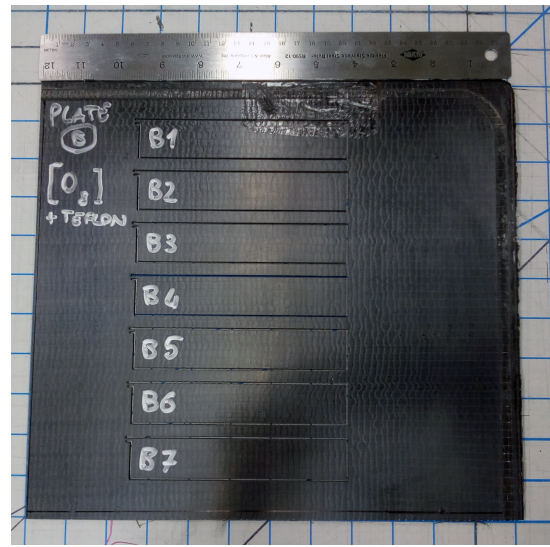
2.1.4 Specimen preparation

Specimen preparation was carried out in the laboratories of the University of Waterloo. All 14 specimens were cut from a single laminated plate using a water jet cutting machine and garnet abrasive, to nominal dimensions of 135 by 25 millimetres. Specimen dimensions were measured and recorded following ISO 15024:2001 practice. Length and width measurements were taken with a Vernier calliper. Three width measurements were taken for each specimen, respectively close to two ends and in the middle. They were then averaged, to obtain the value used in calculations. Specimen thickness was measured using a micrometre, at the same three locations described for width measurements plus two additional ones at each side of the middle point, in order to check for transverse warpage. These five values were also averaged out.

The bonding areas on the specimen was roughened with 600-grit sandpaper to increase bonding surface and promote adhesion. Prior to bonding, surfaces on both the specimen and hinge were thoroughly cleaned and degreased using acetone. Preliminary tests showed conventional two-part epoxy room temperature cure adhesive was not strong enough to bond the hinges to the specimen. Instead Loctite 480 adhesive was used, an impact- and



(a) Plate A



(b) Plate B

Figure 2.7: The specimens still attached to the plates after waterjet cutting



(a) A specimen during the hinge bonding procedure



(b) Test fitting of the fixture components and a specimen off the machine

Figure 2.8: Specimen preparation

peel-resistant, one-component, instant-curing ethyl cyanoacrylate resin. During the process the specimen was clamped down to a working surface, and the hinges were carefully aligned with the specimen itself and with each other using aluminium blocks. Hinges were bonded one side at a time. Bonding pressure was applied using standard 1 in wide paper binder clips.

Both sides of the specimens where crack propagation would take place were painted white, to provide high contrast with the darker background and aid with visual tracking of the crack. Two coats of a high coverage primer-type spray paint were applied within few minutes of each other. Care was taken that the painting process would always take place the same amount of time before the test, to ensure the paint layer had consistent mechanical properties across all specimens. Overly wet paint is ductile enough to mask crack propagation with its own plastic deformation, while overly dry paint is so brittle as to fracture ahead of the actual crack tip. From previous experience, a two- to three-hour drying time was found to be the best compromise. Finally, a speckle pattern for the DIC method was then overlaid on the white surface with black spray paint.

Rather than marking 1 mm notches on the side of the specimen as done traditionally in this sort of tests, graduated paper scales with a resolution of 0.5 mm were applied to the specimen upper or lower surfaces. They provided a very convenient way of tracking crack growth along the curved specimen arms, as well as a reference for calibration of the DIC software, all without interfering with the speckle pattern on the specimen side and removing the uncertainties deriving from a hand-drawn scale. A similar solution was used by Murray *et al.*[40]

Configuration for intermediate rate tests

The HISR test machine is equipped with a Kistler 9341B quartz load cell sandwiched between the upper crosshead and the upper fixture, which measured the load P . The machine does not output the displacement of the lower fixture, relying solely on external imaging and DIC to track it.

Images of the test were captured using a brace of Photron Fastcam SA-5 high-speed cameras (figure 2.9b and 2.10a). They were equipped with AF Micro-Nikkor 60 mm 1:2.8 D optics, and set to their maximum resolution of 1024×1024 pixels. For the 20 mm/s rate tests the images were captured with a frequency of 1,000 fps, resulting in 2,700 frames recorded per test. For the 1300 mm/s rate tests, the frequency of capture was 7,000 fps—the maximum frame rate for the selected resolution, resulting in 700 frames recorded per test.

The test machine, load cell and cameras were operated together and produced synchronised outputs.

Configuration for quasi-static tests

The small frame hydraulic test machine (figure 2.11a) outputs both load and displacement time histories, the latter measured by an LVDT sensor. Both measurements were recorded with a frequency of 900 Hz, and downsampled during post-processing in MATLAB to match the camera frame rate.

Images of the test were captured using a pair of Nikon 3200 DSLR cameras, which recorded video at 30 fps (effectively 29.97 fps) and a resolution of 1080p. Camera 1, used



(a) Overview of the HISR test room

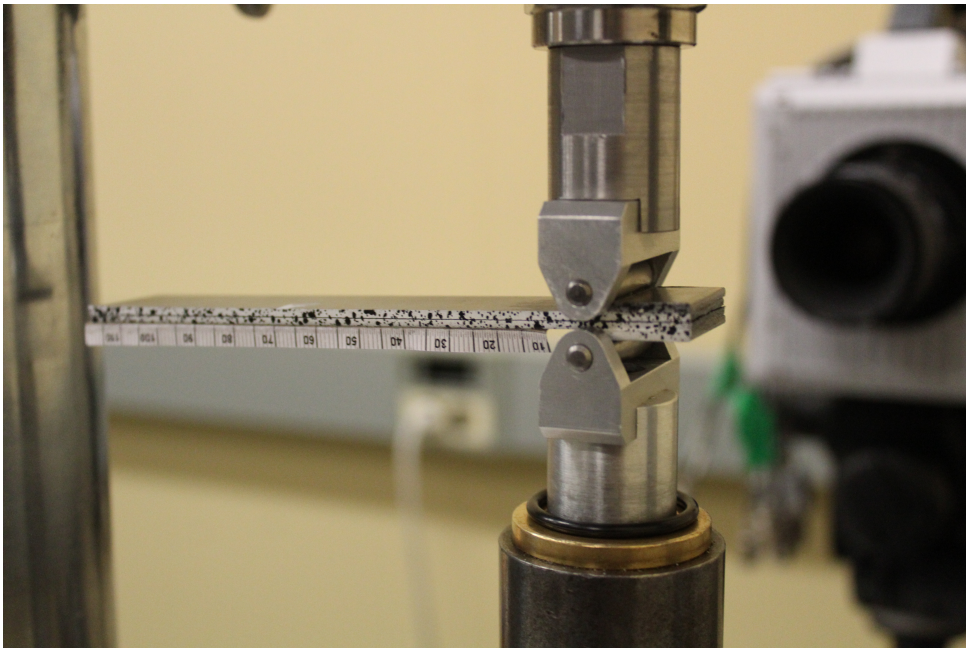


(b) The high-speed cameras were placed on the two sides of the specimen; two LED light fixtures were used to obtain high-contrast imagery.

Figure 2.9: The intermediate rate test setup



(a) Left, camera 2; right, camera 1



(b) The specimen on its shackles

Figure 2.10: The intermediate rate test setup (details)

to imaging the crack propagation, was equipped with a Sigma 105 mm 1:2.8 Macro DG OS HSM optic; Camera 2, used for tracking the opening of the specimen arms, with a Kenko N-AF 2× Teleplus Pro 300 and a Nikon DX AF-S Nikkor 18-55 mm 1:3.5-5.6G optic. The frames were extracted from the video using open-source video processing software VirtualDub, and they were cropped to the area of interest in order to reduce their bulk with Adobe Photoshop CS5.

Contrary to the dynamic tests, the cameras were not synchronised with the testing machine. An expedient was used to determine which frames were relevant. A blue LED, visible in the background of the frame, was wired in such a way that it lighted up only while the test was running (figure 2.11b). Frames where the LED was completely unlit were discarded.

Load line displacement δ

Load line opening displacement δ was obtained by means direct image correlation, specifically using commercial DIC and measurement software GOM Correlate from GOM GmbH. In both dynamic and quasi-static tests, a pattern was traced on the heads of the pins used to secure the specimen to the fixture. Two point instances were tracked by the software throughout the frames (figure 2.12); the change in distance between them is the load line displacement. In order to calibrate the DIC software, a small 15 mm scale was applied to the fixture surface facing Camera 2.

An issue that was encountered is that during the extremely rapid unstable crack propagation some of the frames might be out of focus. Correlation would then be lost, resulting in missing data for one or two frames. A cycle was implemented in the MATLAB data import script to automatically find and fill these gaps in the data series using simple linear interpolation.

The displacement was differentiated numerically using the central finite difference formula to evaluate line opening velocity $\dot{\delta}$.

Crack length a

Tracking of the crack length was automated exploiting direct image correlation and a MATLAB script. The principles and implementation of this script are examined in detail in section 2.2.

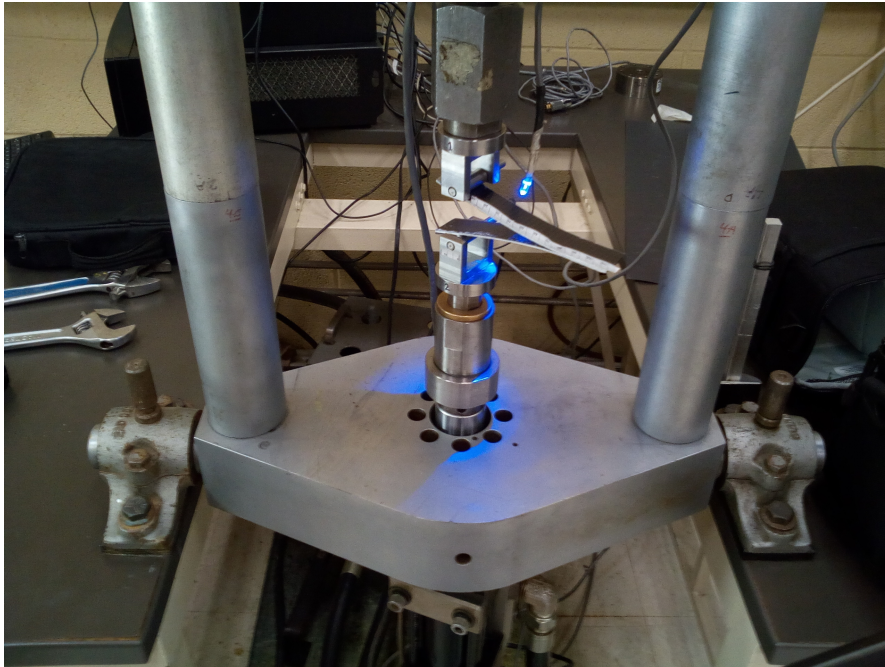
2.1.5 Testing

The tests were performed in displacement control, imposing monotonically increasing load line displacement δ . Ten specimens were tested at intermediate opening rates on the HISR frame: five at an opening rate of 20 mm/s and five at 1300 mm/s. Four specimens were tested on the small hydraulic frame machine at an opening rate of 5 mm/min. All tests were performed at room temperature. The test rates were chosen as the upper and lower limit of the range permitted by the HISR frame.

Due to the nature of the intermediate opening rate testing, the tests were continued until the specimen failed. Quasi-static tests were instead halted after the crack had propagated around 50 mm beyond the tip of the precrack, according to the ISO standard (section 1.5.2).



(a) Overview of the Small hydraulic frame setup. The compactness of the DSLR cameras allowed them to be placed side by side.



(b) A quasi-static test underway

Figure 2.11: The quasi-static test setup

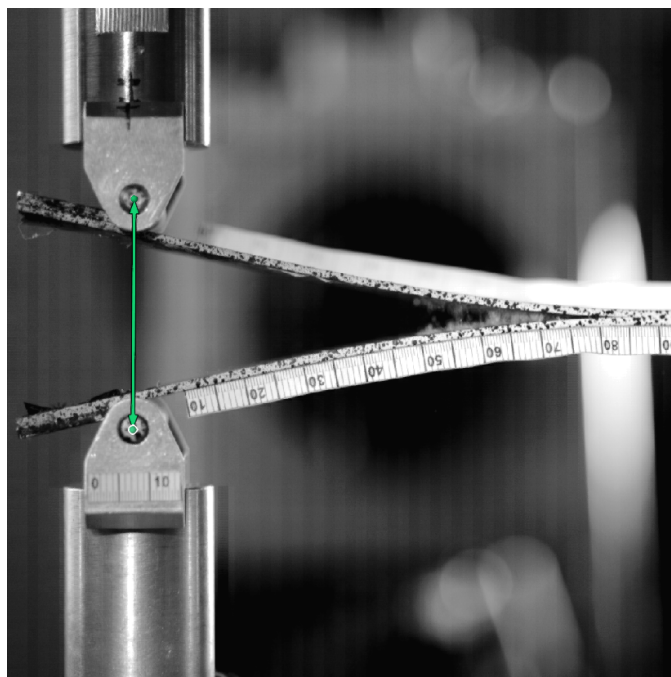


Figure 2.12: A frame from camera 2, with the distance between the pins monitored by DIC software GOM

2.1.6 Post-processing and data reduction

All data was imported and processed using a MATLAB script. Data reduction was performed using a modified beam theory method from the ISO 15024:2001 standard (section 1.5.2, equation (16)), reworked to remove dependence from the load recordings similarly to what was done by [24] (equation (24)).section 2.1.5

$$G_{Ic} = \frac{3}{16} \frac{\delta^2 h^3 E_{11}}{(a + \Delta)^4} \quad (32)$$

2.2 Tracking crack growth with DIC and MATLAB

The objective of crack growth tracking is determining the value of crack length a in mm, for every frame captured. In this work, this was done using direct image correlation and a MATLAB post-processing script to analyse the high-speed imagery of the specimens captured during the tests. The integral MATLAB crack tracking script and the frame processing function it uses are included in the Appendix.

2.2.1 Motivation and principles

The conventional method for observing crack growth is with a traveling microscope at low rate, or analysing frame by frame the captured images at higher rates. This process is clearly heavily dependent on the sensitivity of the operator, and hence scarcely repeatable. It is especially inadequate for monitoring unstable crack growth, where the crack suddenly extends by several millimetres over the span of 2–3 frames. Such an event is easily detected examining the load cell output, as it is marked by a vertical drop in the measured load.

What can be observed in the corresponding captured images following such a propagation, is that the opening of the specimen arms takes place over a large number—often tens—of frames. Simply observing where the crack tip (apparently) is in a frame therefore leads to delayed recording of such events in the crack length plot, which will end up not matching the load plot. The correct method instead involves looking for changes of the pattern sprayed on the side of the specimen, which will dilate in the direction normal to the crack propagation as the specimen splits in two. Thus, rather than examining a single frame at a time, what should be done is a *comparison* of two adjacent frames. Such a task is evidently tedious and repetitive for a human operator, and as often happens is better left to a machine.

As it happens, comparing successive frame pixel by pixel is precisely the operating principle of direct image correlation software. Some of these applications output a parameter, *sigma*, which measures the correlation (or rather, loss of correlation) between two consecutive frames. By comparing a colour map of this parameter with the crack tip position, located with the method described before, it is possible to identify which value of this parameter corresponds to the crack tip, and set a threshold. For reference some color maps of *sigma* overlaid to the corresponding frame are visible in figures 2.17, 2.17 and 2.18. It is then just a matter of implementing a script that searches automatically for the crack tip position, and calculates crack length using a reference point.

This technique was originally proposed in a 2018 conference paper by Murray *et al.*[40] Murray *et al.* conducted a parametric study on the effect of the DIC software settings (subset size and subset spacing) on the results. Their findings were helpful in reducing the time needed to tune those parameters. However, no information was given on the working principle of their post-processing script; a new one was therefore developed from scratch. As proof of concept, Murray *et al.* applied their technique to mode I and mode II quasi-static as well as fatigue delamination tests.

To the best knowledge of the author, the present work is the first application of this technique to intermediate rate delamination testing.

2.2.2 Implementation

Commercial direct image correlation software VIC-2D 6 from Correlated Solutions, Inc. was used to process the crack tracing images from camera 1. This software was chosen for the ease and freedom of manipulation of its results. Due to the nature of the problem, which involves tracking displacement of points of a planar surface which stays perpendicular to the camera, two-dimensional DIC and imaging from a single camera were sufficient.

The crack tracking proper is carried out by an automated script developed from scratch using MATLAB, which processes the raw data generated by VIC-2D 6.

In the following the image processing procedure and the workings of this script are briefly described.

Generating the data in VIC-2D 6

To begin the frame processing all the frames captured by camera 1 during one test run have to be imported in VIC-2D 6. Since the desired output is in millimetres, not pixels, it is necessary establish a physical scale for the measurements through a calibration process. To do this, the user chooses one of the frames as calibration image, and selects a selects two points corresponding to known locations on the scale applied to the specimen, which is visible in the frames. He then inputs the linear distance between them. The software can generate a pixel-to-millimetres conversion factor.

To limit processing time and the volume of data generated, it is then necessary to limit the portion of the frame that the software processes to a smaller area around the specimen. After this step it is possible to run the correlation analysis.

During this process the software creates a rectangular array of subsets inside the area of interest. Subsets are square portions of the picture, spaced by the same distance (the step size) both in vertical and horizontal directions. The software subsequently attempts to track each of the subsets in the following frames. Naturally the subsets outside of the speckled part of the image are immediately lost after the first frame. In this case the *sigma* parameter is then set to -1 , making it easy to discard those data points devoid of information during post processing. The parameters used were a subset size of 21 pixels, and subset spacing of 1 pixel. Since the expected deformation is very large, it is necessary to enable incremental correlation: each frame is compared with the previous one instead than with the reference one. The arrangement of 1-pixel spaced dots superimposed to the image in figure 3.14 is a visual representation of the array of subsets created by VIC-2D 6.

The output of VIC-2D can be exported in MATLAB format, for further and more flexible post-processing. A *.m* file is then created for every frame, containing the exported variables. Each of them is an array, each entry corresponding to a subsets. Eight variables are provided in every frame, namely x and y , the initial position in pixels of the subset within the image, u and v , the x- and y-displacement in pixels of the subsets in the n -th frame, x_c , y_c , u_c and v_c are the position and displacement converted to mm through the calibration process. Finally *sigma* is a correlation parameter between the current n -th frame and the frame $n - 1$. This is the parameter can be exploited to track the crack growth: an extension of the crack between two frames corresponds to a lack of correlation between them, and an increase in *sigma*.

After careful examination of crack propagation frames and several test runs, the *sigma* threshold value was set at 0.01 pixels—incidentally, the same value used by [40] Murray *et al.* in their study.

The MATLAB script

The MATLAB script used to post-process this data processes automatically every frame captured for the chosen specimen. Fundamentally, the script works by running a search for subsets with a value of the *sigma* correlation parameter higher than a preset threshold value. This search is limited to the area in the vicinity of the previous crack tip, where crack propagation will occur. The new crack tip position is the point that fulfils the condition on *sigma* and is further away—“downstream”—from the previous crack tip. The script is able to process both “left handed” and “right handed” specimen images.

Due to the variability in the captured images (i.e. different specimen positioning in the frame) user input is required in two instances while running the script. This is handled through a graphical interface and exploiting MATLAB’s image processing toolbox.

The first user contribution helps reducing the points over which the search is performed, with great advantages in decreasing both processing time and the number of false positives. If the script has been run before on the selected specimen’s data, the user is asked whether to discard or reuse the existing saved calibration file. In the former case, the first deformation image is loaded and displayed.² Next, the user is prompted to select the area of possible crack propagation by drawing a rectangle that encompasses the midplane of the specimen (figure 2.13).

This *region of interest* (ROI) is used to create a cropping template which discards all data from outlying points. The template will be applied to the data from every frame loaded in the subsequent search. This is visually displayed to the user by overlaying a cloud of points on the deformation image, each of them representing the original position of a subset. Points within the cropping template are displayed in red, the others in gray (figure 3.14).

As an additional check on the region of interest selection, the data points taken in consideration in the subsequent analysis are again overlaid over the first and tenth to last deformation images. If the analysis has been run before, the previously determined successive positions of the crack tip are plotted as white circles (figure 2.15). Some of them may lie outside of the actual beam, as correlation of the corresponding subset might have been completely lost in an earlier frame, due to the large deformation in the curved specimen arms. This is inconsequential, as the only points that matter to the search are the ones which the crack has not yet reached.

The second user contribution is needed to calibrate the crack length calculation. The user is asked to draw a line secant to the beam in correspondence of the 110 mm marking on the graduated scale. The script then searches and stores the coordinates of the data point P closest to the midpoint of this segment. Its position in the reference frame of the specimen is known: it is located at midplane and has a known 110 mm linear distance

²It should be noted that the all deformation images displayed by the script and shown on these page are solely a visual aid for the user, as MATLAB processes numerical data exported from VIC-2D 6, not images.

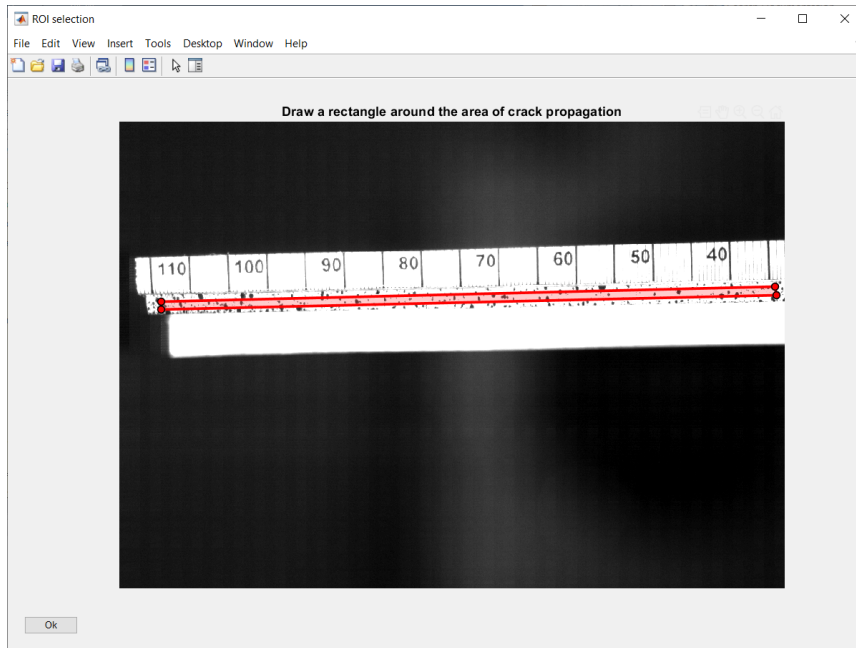


Figure 2.13: The user selects the region of interest.

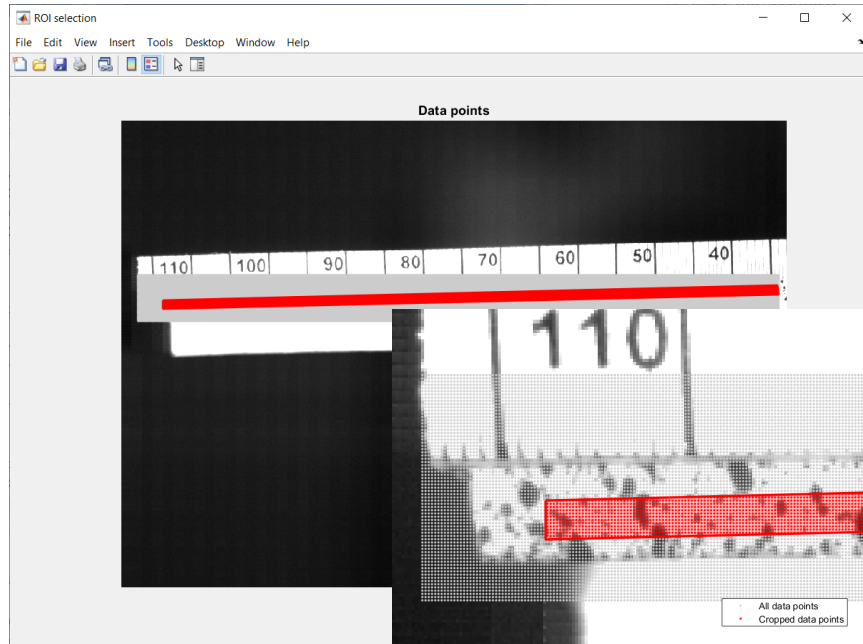


Figure 2.14: All the data points plotted in gray, and the selected ones in red. The individual data points are visible in the magnification at the bottom right.

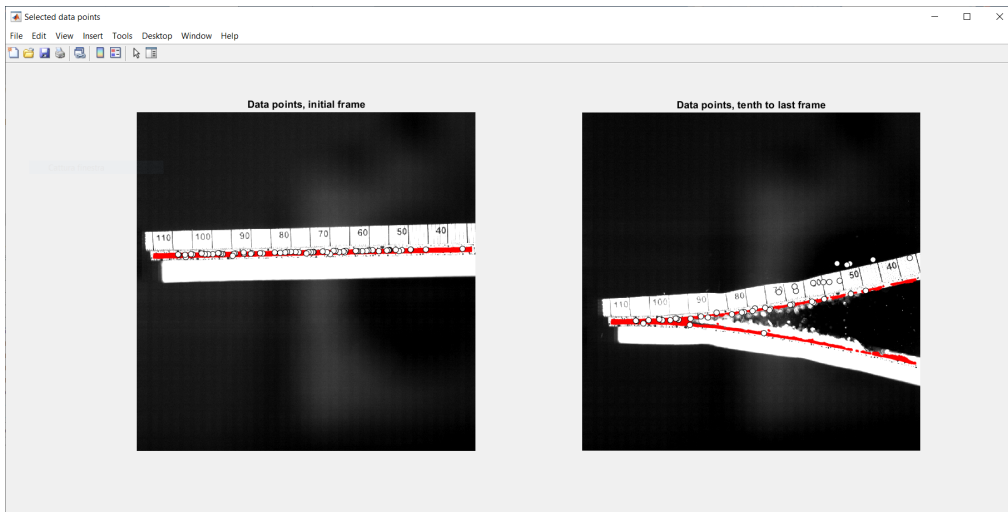


Figure 2.15: The selected data points in the first and tenth to last frame

from the load line. The crack length when the crack tip is located at data point C will then be computed simply as:

$$a = 110 \text{ mm} - \|C - P\|; \quad (33)$$

The script is the ready to run the frame processing function, looping over the frames. This function receives in input the specimen number, all the information necessary to load the data files and a number of options. Its output is the structure `crack`, inside which the index and the usual eight variables for the data point corresponding to the crack tip are stored for every frame.

Now, if the crack has grown from the previous frame to the current one, the current crack tip is the point that meets the following two criteria:

- It is the data point closest to free end of the beam whose correlation parameter is above the threshold. The first data point to meet the condition is the candidate as new crack tip. This is very easily implemented in the MATLAB code:

```

1      \% Find the crack tip and store properties
2      crack_tip_candidate = ...
        find(S.NaN_crop2.sigma>=0.01,1,'first');
```

- The points beyond it must have a high value of the correlation parameter σ as well, since the beam is split in half and bent.

This second feature is used to implement a useful check for false positive values. In fact, two checks are implemented in the code:

Check upstream of the crack tip candidate

A check is performed on a “tail” of 5×50 points upstream of the candidate crack position: a certain fraction of them must have a value of σ over the threshold, like the crack tip point itself. For close crack jumps (less than 40 px, or roughly 3.5 mm long), 40% of the points in this tail must have a σ over the threshold; for long crack jumps, 90% of the points must meet that condition. An example of a false positive crack tip candidate value identified and discarded through this check is shown in figure 2.16.

Check on the whole beam

Sometimes it might happen that, due to oscillations of the beam and subsequently overall worse correlation, the value of the correlation parameter might rise all over the beam. This is a rare albeit dangerous source of false positives, as the crack tip might erroneously skip far ahead of the actual one, compromising the rest of the analysis. For this reason an additional check is performed. If more than 0.4% of the data points to the intact part of the beam (downstream of the crack tip) are over the σ threshold, the new crack value is discarded. An example of a false positive crack tip candidate value identified and discarded through this check is shown in figure 2.17.

If the crack tip candidate point passes both checks, like the one in figure 2.18, the data of is stored in the `crack_tip` structure which will be the output of the frame processing

function. As an average the script discovered 39 crack propagation points and discarded 110 false positives for each specimen.

Irregardless of whether the crack tip candidate point is accepted or discarded, pictures like those in figures 2.17, 2.17 and 2.18 are generated and stored in separate folders, ready to be checked by the user.

Once it has run through all frames for a specimen, the frame processing script returns the data structure `crack` with all the parameters relative to the successive crack tip positions. The main script then calculates the crack length, using an implementation of equation (33), and `aves` is in a `.m` file ready to be loaded in MATLAB for data reduction.

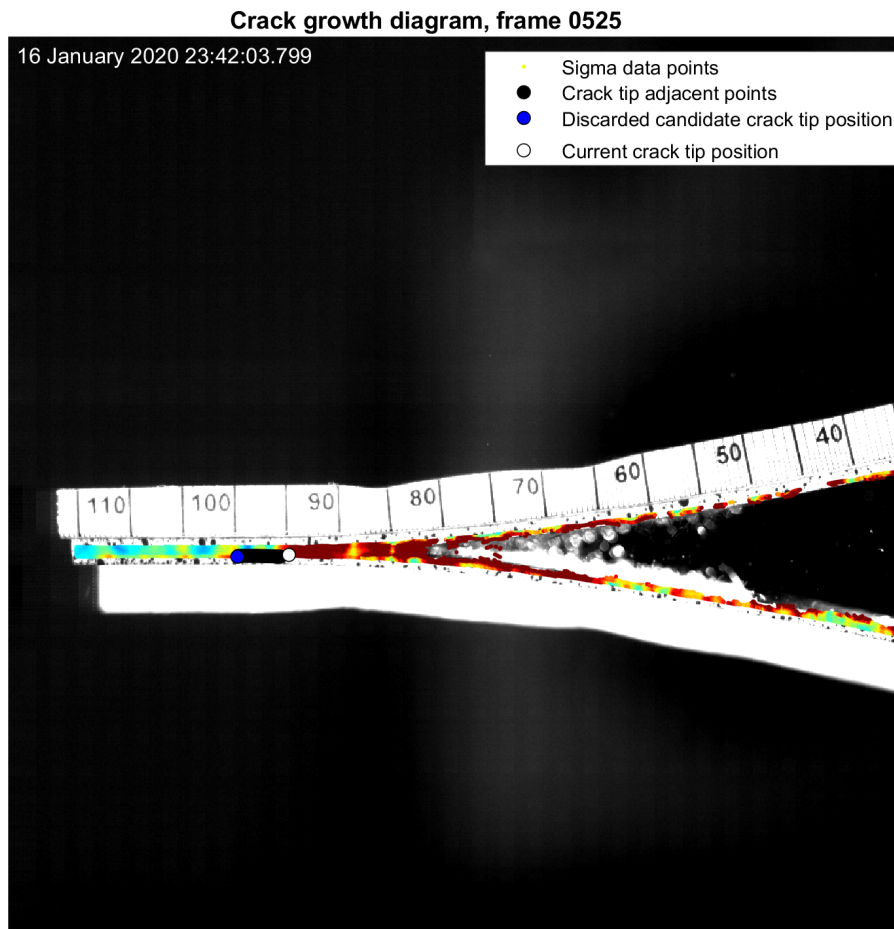


Figure 2.16: A candidate crack tip position discarded because it failed the check on the “tail” of points upstream of the crack tip candidate. The colour map is for *sigma*, with the threshold value 0.01 px being bright red. (Specimen 10, frame 525)

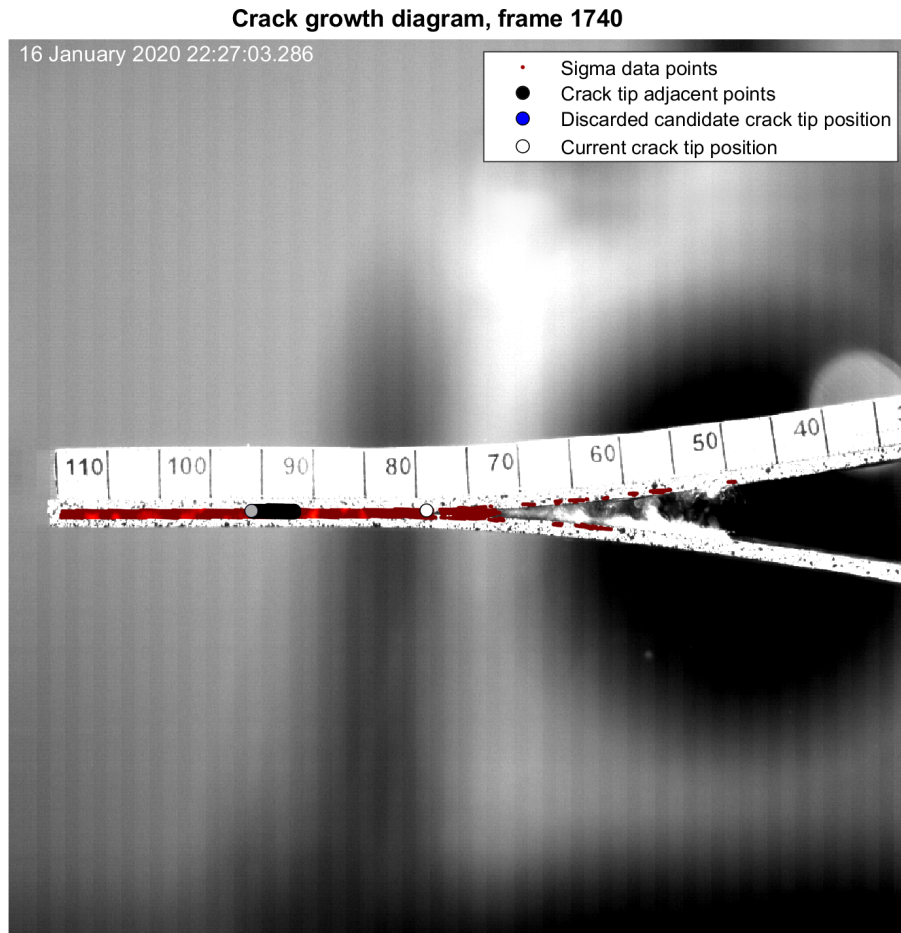


Figure 2.17: A candidate crack tip position discarded because it failed the whole beam check. The colour map is for σ , with the threshold value 0.01 px being bright red. (Specimen 2, frame 1740)

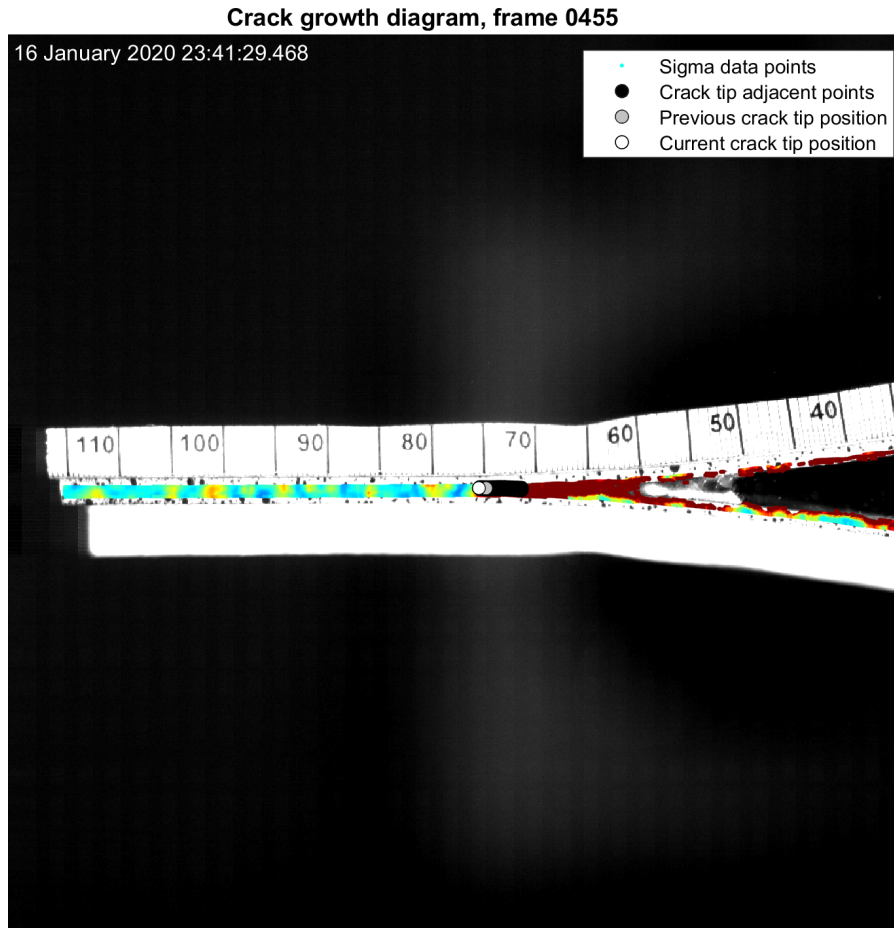


Figure 2.18: A candidate crack tip position that passed both checks and was accepted. The colour map is for *sigma*, with the threshold value 0.01 px being bright red. (Specimen 10, frame 455)

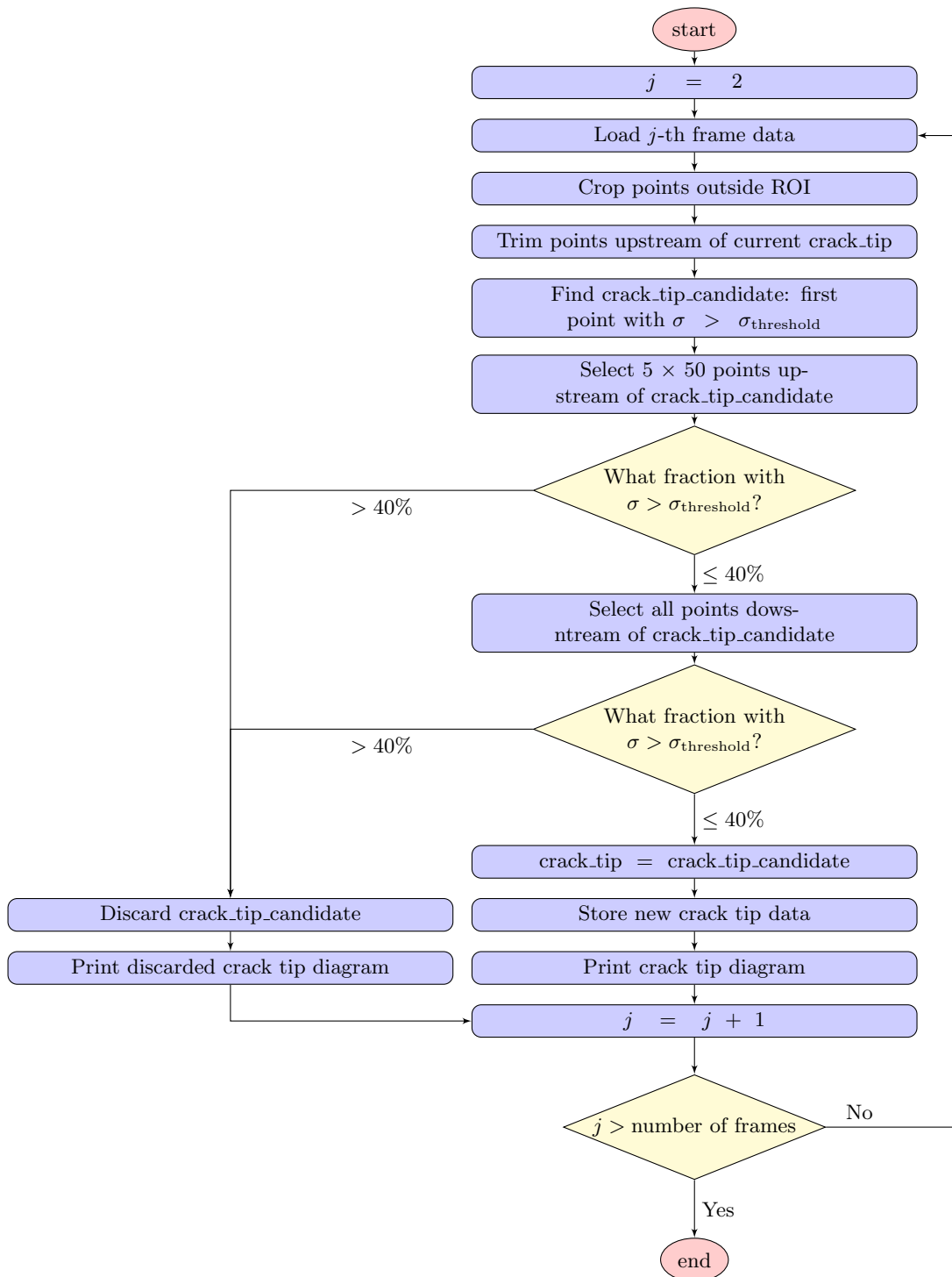


Figure 2.19: Simplified flow chart of the frame processing script

Chapter 3

Results and discussion

3.0.1 Initial observations

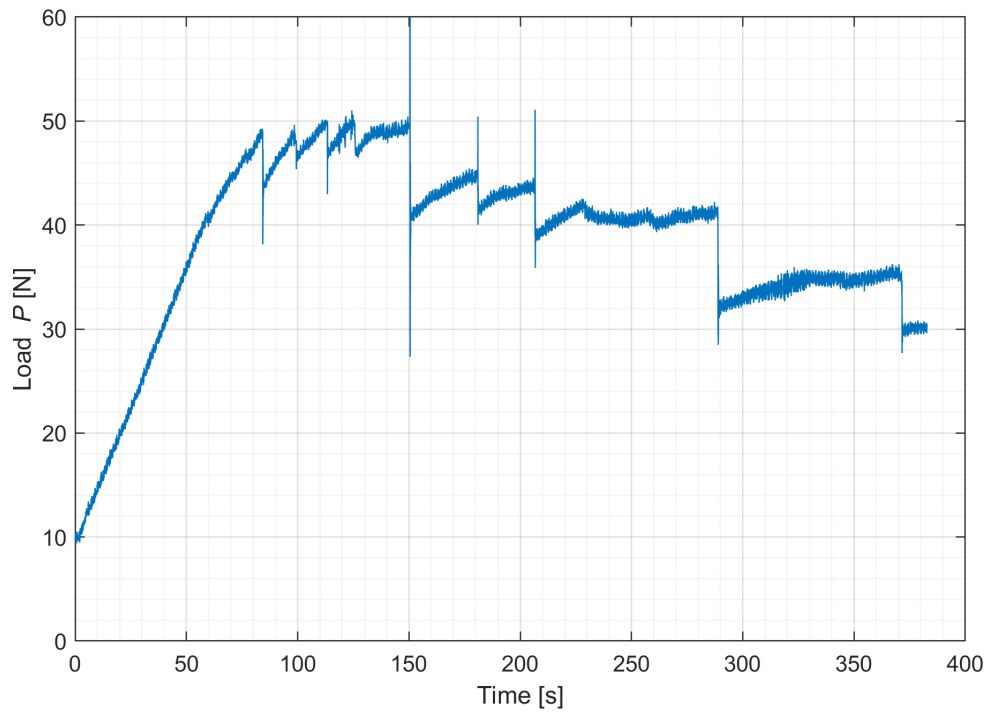
An initial analysis of the camera images shows that all tests were performed satisfactorily. The specimen arms always opened in the desired symmetrical fashion, even in the high-intermediate rate tests. In all instances the crack progressed in the interlaminar region at the specimen's midplane, and never migrated to other planes of propagation.

Representative unprocessed load and time signals for each of the three opening rates are shown in figure 3.2. With the exception of the quasi-static case, where it was omitted due to the data logging methodology, a phase of non-linear loading can be observed at the beginning of the curve. This is due to the inevitable internal friction in the slide-catch mechanism of the testing machine. Such an effect does not, however, influence test results, as friction forces disappears as soon as the catch engages. This engagement takes place smoothly in both the quasi-static and low-intermediate rate tests, while it causes heavy oscillations in the high-intermediate rate tests (figure 3.2b). Following this first phase the two specimen arms start opening along the pre-existing crack, resulting in a linear load trace.

Consistently stable crack propagation was never observed. At all rates of loading the crack propagation progressed unstably followed by periods of arrest, the so-called "stick-slip" behaviour. The unstable crack propagation is recorded in the load signal as vertical drops. Between successive crack jumps two different behaviours are possible: linear or sub-linear load growth. The former indicates a stationary crack, the latter a short period of stable crack propagation or of minor crack jumps.

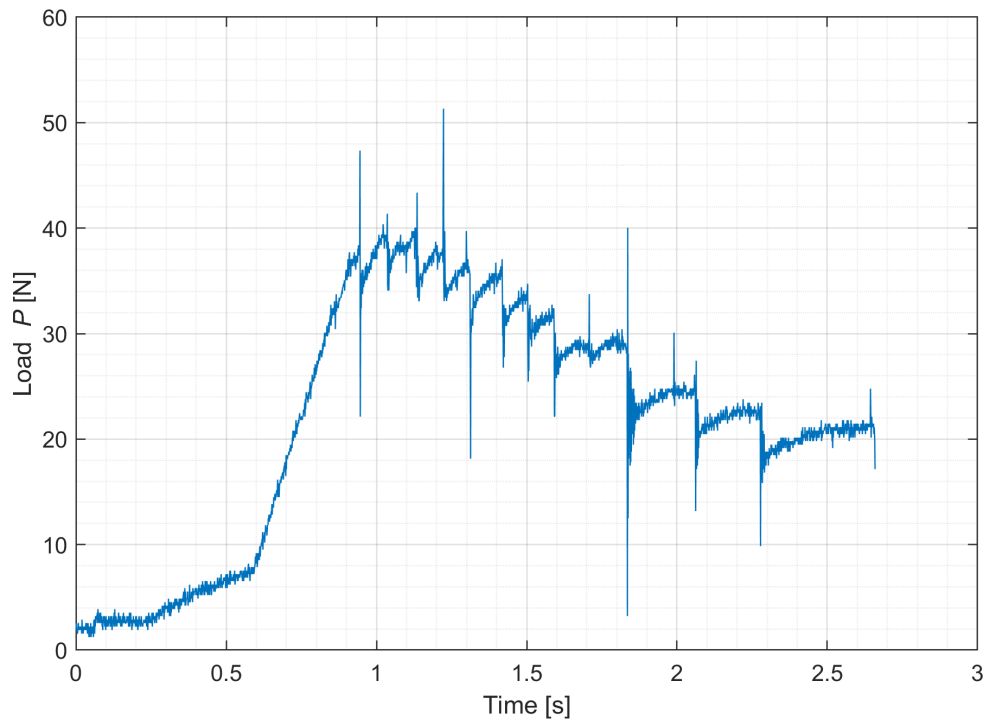
Examining the plots for the single opening rates, at 5 mm/min (figure 3.1a) some high-frequency noise is observed throughout the signal, as well as ample, immediately damped oscillations where unstable crack propagation takes place. The maximum load reached was around 50 N.

Increased noise can be noted at 20 mm/s (figure 3.2a), but the signal is quite similar overall. The maximum load reached is lower, at around 40 N, but this stems from the longer initial delamination in the specimens used for those tests—a consequence of the manufacturing process.

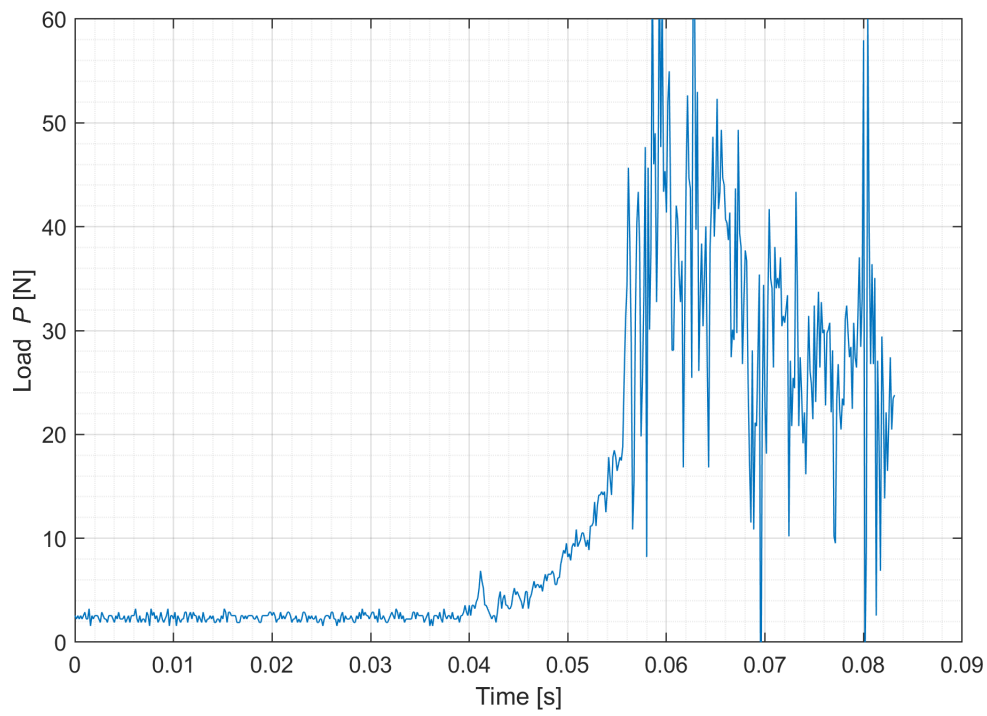


(a) 5 mm/min (specimen 11)

Figure 3.1: Load versus time plot representative of the quasi-static opening rate

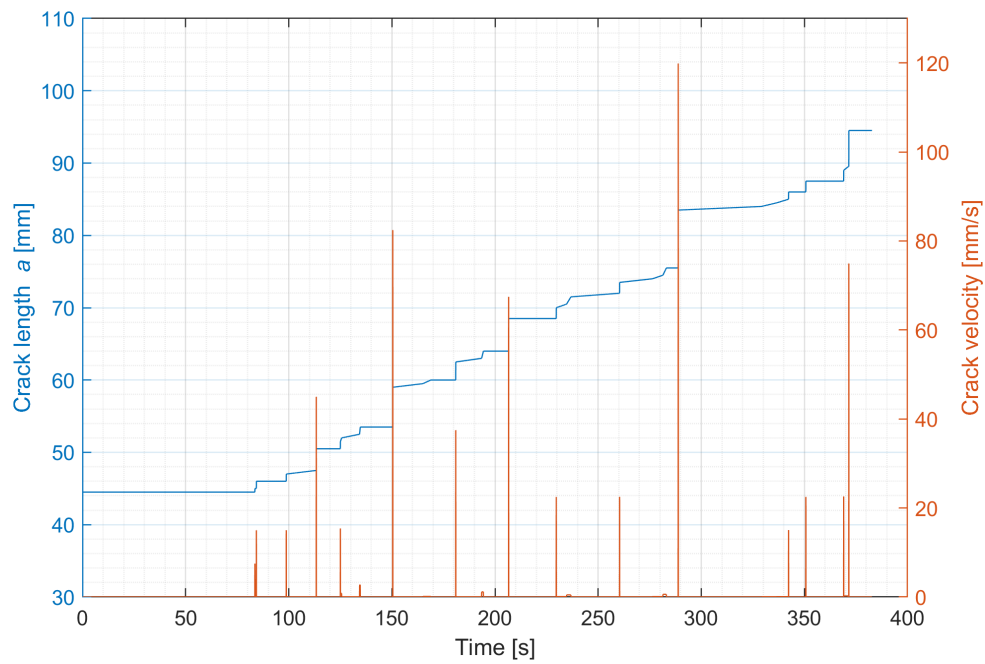


(a) 20 mm/s (specimen 1)



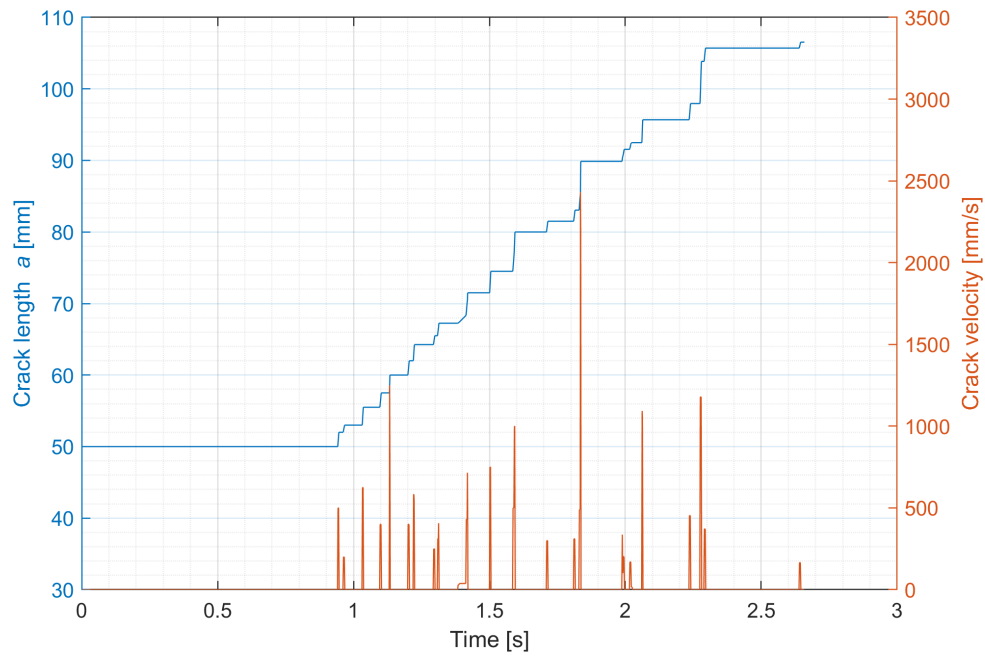
(b) 1300 mm/s (specimen 10)

Figure 3.2: Load versus time plots representative of the intermediate opening rates

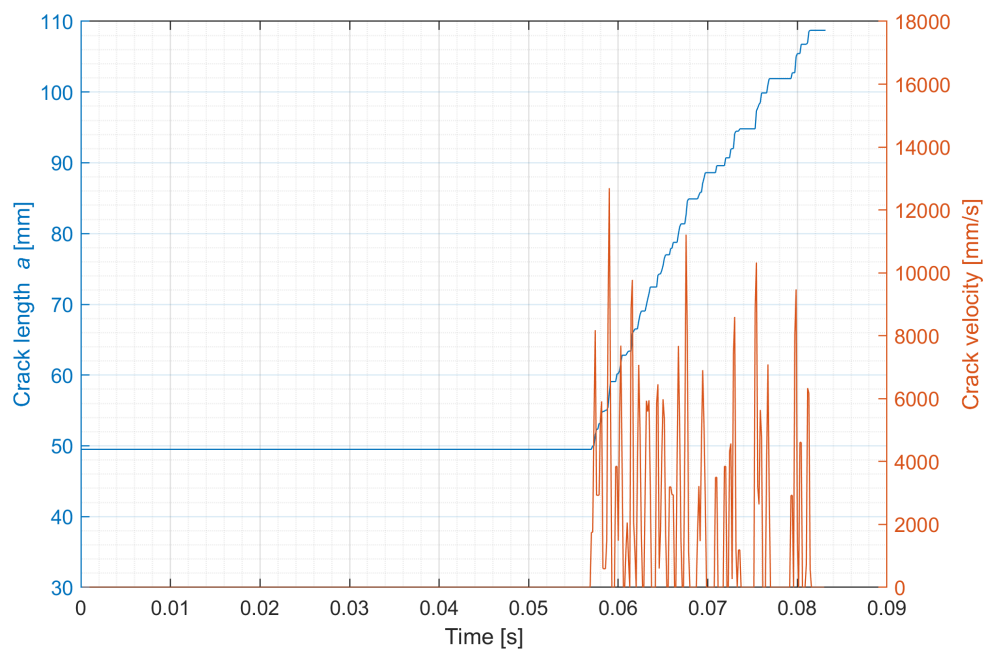


(a) 5 mm/min (specimen 11)

Figure 3.3: Crack length versus time and crack velocity versus time plots representative of the quasi-static opening rate



(a) 20 mm/s (specimen 1)



(b) 1300 mm/s (specimen 10)

Figure 3.4: Crack length versus time and crack velocity versus time plots representative of the intermediate opening rates

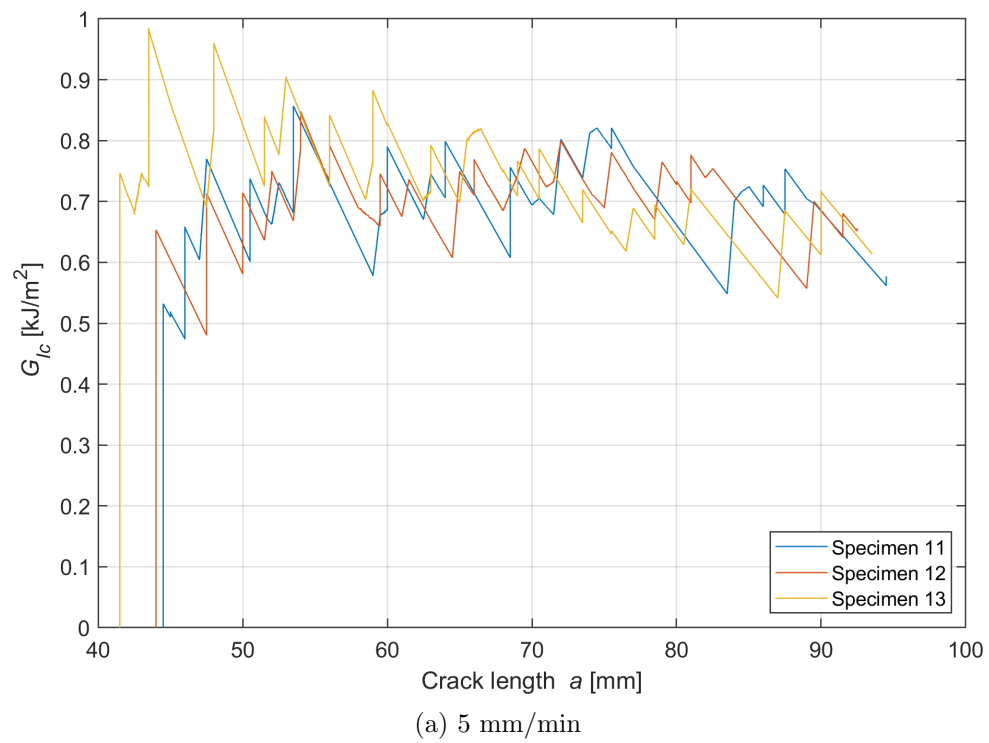
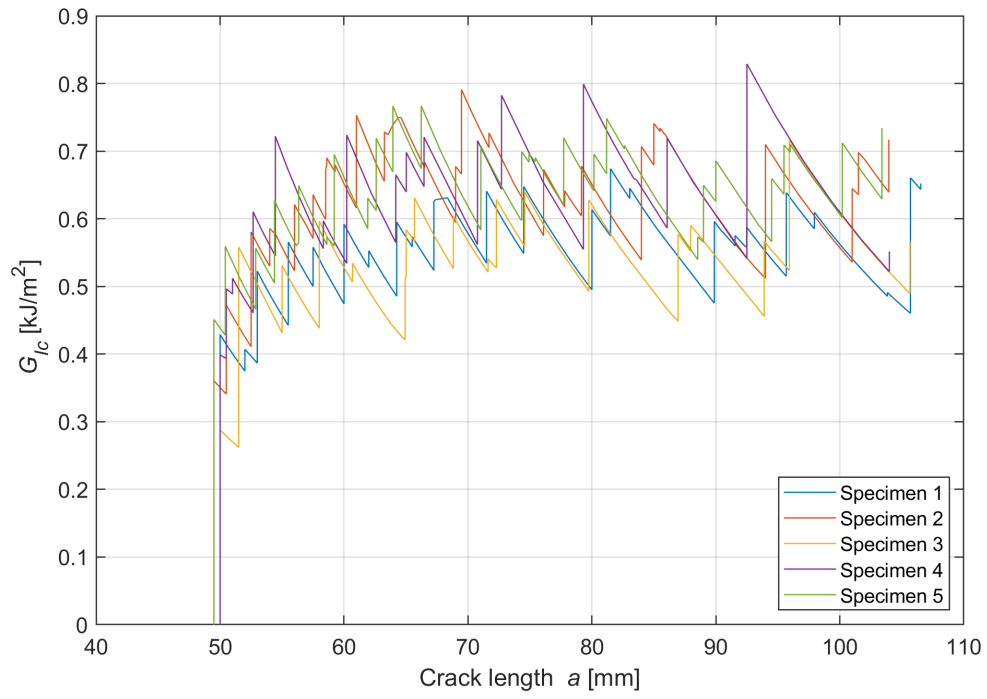
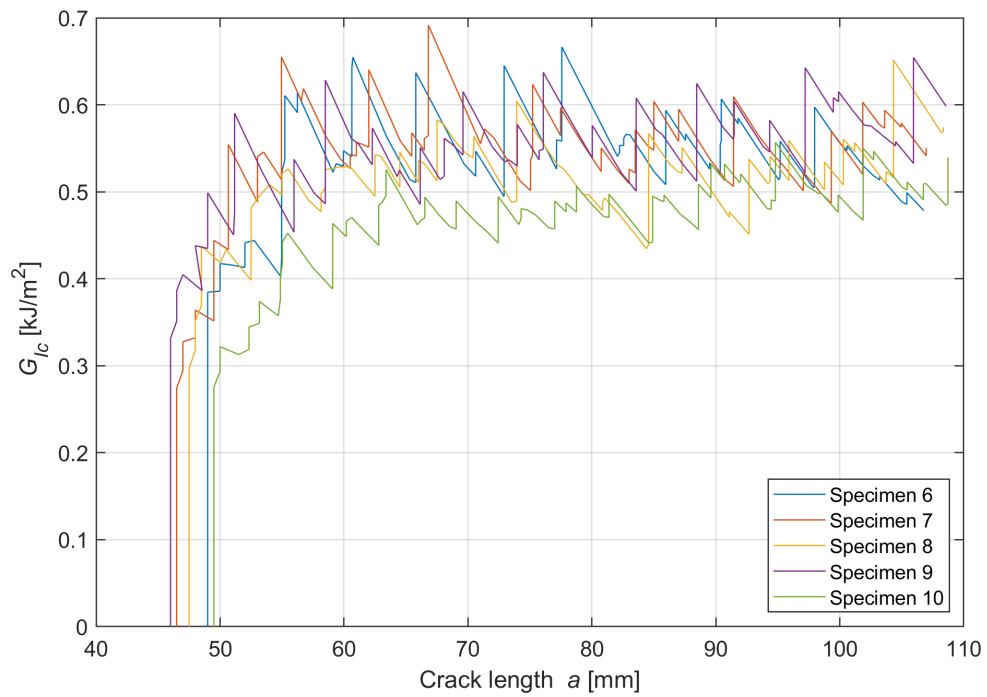


Figure 3.5: R-curves for the quasi-static opening rate



(a) 20 mm/s



(b) 1300 mm/s

Figure 3.6: R-curves for the intermediate opening rates

The 5 mm/min and 20 mm/s load time histories are wholly usable in the data reduction process to obtain G_{Ic} , only requiring some filtering to remove high-frequency noise and oscillations caused by unstable crack propagation.

The same cannot be said for the 1300 mm/s load time history (figure 3.2b). It is plain to see that the noise level is overwhelming and the signal's information content is lost. Ample oscillations initiate as soon as the slide-collar mechanism engages. It is impossible to distinguish what is actual load and what is a result of dynamic effects. As a result, the load signal is useless to the end of data reduction. This was expected from comparable experiments encountered in the literature review, such as the one from Blackman *et al.*. Consequently, data reduction formula equation (32) was used, requiring only the crack length and not the load. Furthermore, consistency within the measurements dictated that the crack initiation criterion used be the visual observation one (see section 1.5.2).

Representative crack length versus time and crack velocity versus time signals are shown in figure 3.4. The stair-like crack length diagrams confirm the unstable stick-slip crack propagation mechanism already deduced from visual observation of the test and from load measurements. A notable observation is that increasing the opening displacement rate the crack jumps become shorter and shorter: the steps in the higher rate crack length diagrams are more numerous and shallower, and the crack velocity diagram is less discrete and more continuous. This effect, as was also observed by Blackman *et al.*, might lead to a false impression of crack propagation that becomes more stable as the rate increases.[23]

3.0.2 Assessing the effectiveness of the DIC-based measurements

Load line displacement δ

Compared to more traditional measurement via transducers such as LVDTs or encoders, the DIC-based method (section 2.1.4) has three distinct advantages.

First, the measurement obtained is exactly the displacement experienced by the specimen. Traditional sensors need to be placed on the machine or along the fixture. Taking the quantity they measure as related to the specimen equates to assuming that all the interposed mechanical components to be infinitely stiff and with no play between them. An example of the consequences of this is visible in figure 3.7a. There is a notable discrepancy between the displacement measured by the machine's LVDT transducer and with DIC. Observing the camera imagery, this is quickly ascribed to the excessive play between the pin and the clevis—which, in the case of the quasi-static tests, was not purpose-designed for this type of specimen. This phenomenon was obviously impossible for the machine-mounted LVDT to detect.

The second advantage is obviously being a non-contact measurement, further reducing the chances of interference.

The third one is cost and flexibility: for quasi-static tests, all the equipment that is needed is a simple DSLR camera, a camera stand and a image processing software, which can be freeware or developed using MATLAB or Octave. Even more expensive high-frame rate equipment, can be quickly moved from one to the other and quickly repurposed for different measurements. By changing the post-processing software, the same model of camera provided both displacement and crack length measurements, which

would normally require completely different sensors.

As a testament to the reliability of the DIC based measurement, in figure 3.7b some oscillations generated by the machine were picked up by both methods. Accuracy can be improved using higher definition imaging or a longer scale for calibrating the DIC software.

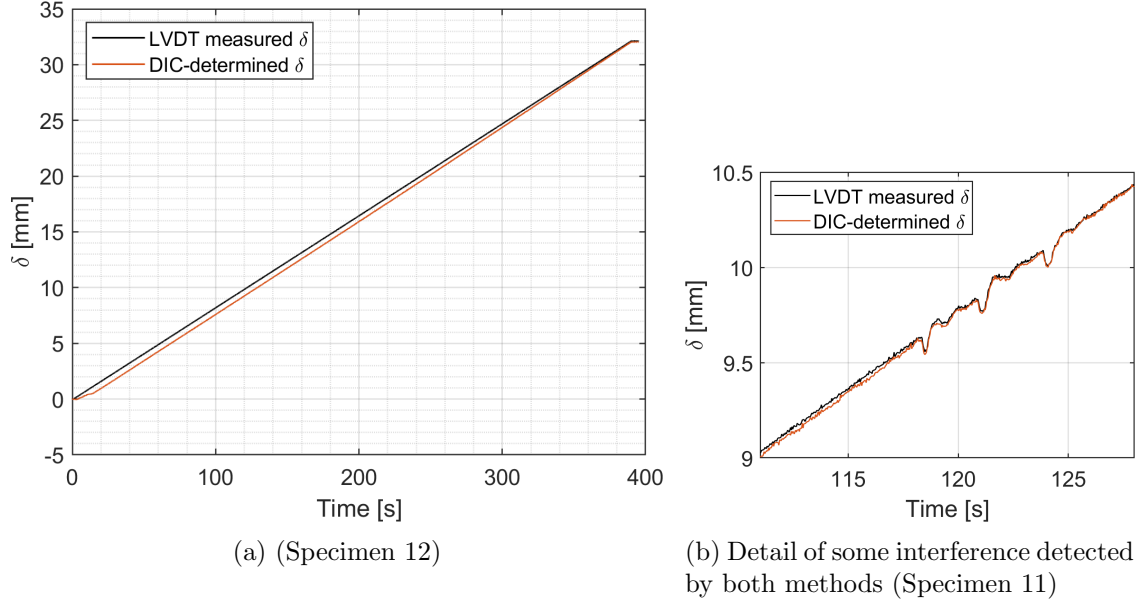


Figure 3.7: Comparison of load line opening displacement measured with the testing machine's built-in LVDT sensor and with DIC

Crack length a

The crack tracking script provided satisfactory results—extremely close in accuracy to the laborious manually-obtained measurements, and what is more important perfectly repeatable. Figure 3.8 compares the time history determined by hand, comparing frame by frame, with the output of the script for specimen 10. Nearly all the crack propagation events were correctly identified, and nowhere the crack lengths differed more than the 0.5 mm required resolution.

A no immediately obvious advantage of the method used is that it operates in the frame of reference of the specimen. The crack length is calculated as the distance between two points that belong to the specimen itself—a reference point selected via user intervention and the automatically pinpointed crack tip. Therefore this system automatically corrects for rotations or vibrations of the specimen.

The method used is also, in the opinion of the author, superior to other DIC-based ones that track series of dots or marking on the specimen, as encountered in some works mentioned in the literature review. This is because there is no need for an operator to trace by hand precisely spaced markings on the specimen, but instead a random pattern is sprayed on the specimen's side and a computer takes on the task of extracting a precisely spaced grid from it.

The main downside to this procedure is its being incremental—if one false positive crack tip position escapes detection by the in-built checks, it will invalidate the rest of the results. This issue has been addressed by saving and storing easy to analyse images of every crack tip position, even of the discarded ones, that can be rapidly checked after having run the script

3.0.3 Interlaminar fracture toughness and rate dependence

Interlaminar fracture toughness is plotted against crack length separately for each rate of testing in figure 3.6. The trend for all specimens is interlaminar fracture toughness that is increasing from its initial values with the progression of the crack—i.e., they exhibit a crack propagation resistance curve, or R-curve. This is a desirable result, indicative of the fact that there is no toughening effect due to resin pockets at the edge of the Teflon™ insert.[15]

Because of the unstable crack propagation, not one but several crack initiation points were obtained—one after each crack arrest. Data points were then classified as initiation, propagation or arrest value using a MATLAB algorithm; an example is shown in figure 3.10. Both the initiation and arrest interlaminar fracture toughness values follow a similar trend, so the following observations apply to both. The initiation and arrest data points are reported separately in figure 3.11a and in figure 3.11b. Third-order polynomial curves were fitted to the data. Such curves visibly shift to lower toughness values as the test rate rises, which would suggest a rate effect on the interlaminar fracture toughness. Due the high dispersion there is no clear separation between the data at the tree opening rates. The 95% confidence bound of the lowest rate (5 mm/min) test results even partially overlap the curve of the higher rate tests (1300 mm/s).

Some interesting observations can be made looking at the effect of increased opening rates on these curves. First, the curves become flatter. Second, the spread of the results reduces. This is linked to what was already observed in section 3.0.1: as the opening rate rises, not only the crack jumps become shorter, but they also become more consistent in their amplitude. As a consequence the data points condense towards the median curve.

Figure 3.9 and table 3.1 display some “hard numbers” for the initiation interlaminar fracture toughness over the entire curve. The coefficient of variation is very high, between 18% and 15%, and it decreases with growing test rates. This is, however, typical of composite materials—coefficient of variation up to 13% were obtained in round robin testing and are reported in the ASTM D5528 standard.[15] It should be pointed out that in figure 3.9 the error bars for the 50 mm/min and 1300 are not overlapping, further evidence of rate effect.

A major teaching that can be had from this data is that the value of interlaminar fracture toughness determined with quasi-static tests cannot safely be applied to dynamic loading conditions. This testing campaign was, therefore, not mere intellectual exercise but an actual necessity. To be on the safe side, it is advisable to use the less dispersed, lower value of G_{Ic} obtained from the 1,300 mm/s intermediate test in simulation a design.

Two rate parameters found in literature were to the initiation values of interlaminar fracture toughness, load line displacement rate (equation (26)) and loading rate (equation (27)). Both parameters are closely related, as they involve the time derivative of the load line opening displacement. The result is reported in figure 3.12, together with

Load line opening rate	Average G_{Ic}	Standard deviation	CV %
5 mm/min	0.82562 kJ/m ²	0.1469 kJ/m ²	17.8
20 mm/s	0.62995 kJ/m ²	0.097548 kJ/m ²	15.6
1300 mm/s	0.53439 kJ/m ²	0.079182 kJ/m ²	14.8

Table 3.1: The mode I initiation interlaminar fracture toughness G_{Ic} determined with the tests

their mean values and bounds inside which fall 90% of the data. Three clouds of results form for the three opening rates, with the lower intermediate being very close to the quasi static results—this being a semi-logarithmic plot. The loading rates reached are consistent with similar tests found in literature—for example Hugh *et al.* also reached 10²kJ/(m² s) with an opening displacement rate of 1,600 mm/s.[20]

3.0.4 Microscope observation of the crack surfaces

Post-mortem images of the crack surfaces were taken with a Keyence VHX-S550 digital optical microscope at 30× magnification. Two specimens were sampled for each testing rate, and both their upper and lower crack faces were imaged. The glossy surface visible to the left is the pre-crack, where the Teflon™ sheet was positioned; to the right is the crack face. The images confirm that propagation took place exclusively in the interlaminar region. What is visible, as evidenced by the visible traces of the stitching, is the very interface between the plies, just as they were juxtaposed during lay-up. The carbon fibres are left neat, and show little evidence of fibre breakage. Most of the fibres stayed attached to the ply they belonged to; for contrast, a bunch of fibres that remained attached to the opposing ply are visible on the lower edge of specimen 10. On the contrary, nearly every polyester stitch was broken.

At this level of magnification there are no visible differences that might hint at a change in the mechanism of crack propagation for different opening rates. There is also no apparent sign left by the stages of unstable crack propagation and arrest.

The observation of the broken and pulled-out stitching filaments suggests an explanation to the trend observed in the interlaminar fracture toughness and smoother crack propagation for higher rates. The polyester yarns may have had a toughening effect, by placing themselves across the progressively opening crack—the so-called *crack bridging* phenomenon—and favouring longer, unpredictably long crack arrests. More evidence can be deduced from the images of the quasi-static tests (figure 3.14), where this bridging is obvious. The polyester fibers can be seen giving way, and the specimen arms changing shape when released from their resistance. This effect seems to be negatively affected by the rising rate of testing, up to the point where at high rate it becomes negligible and the only the actual properties of the matrix are left.

Two more factors can be identified from the microscope imagery, that may have contributed to the variability of the material’s behaviour and therefore to the high spread in

the test results:

- The direction of the fibres varies within each specimen due to the plies having shifted around during the high-pressure resin transfer moulding process. This is macroscopically visible as wavy patterns in the composite plate.
- The patterns of the polyester stitches of the two plies at the midplane interface are naturally not aligned in the same way in every specimen.

Both these factors are a by-product of the production process itself. This all goes to say that the spread observed in the test result is effectively a characteristic of the tested material, and should therefore be taken into account during simulation or the the design process.

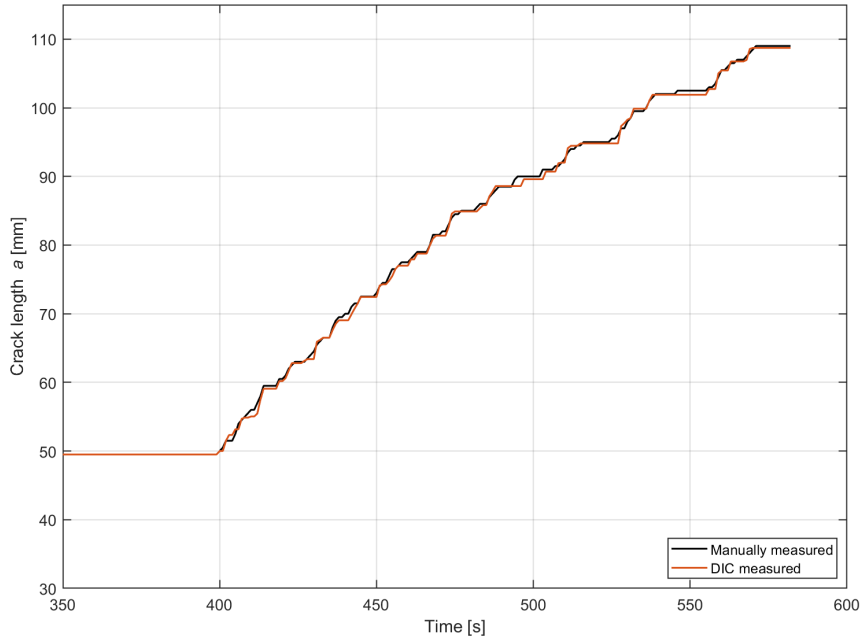


Figure 3.8: Comparison of the crack length obtained manually and with DIC and the MATLAB script (Specimen 10)

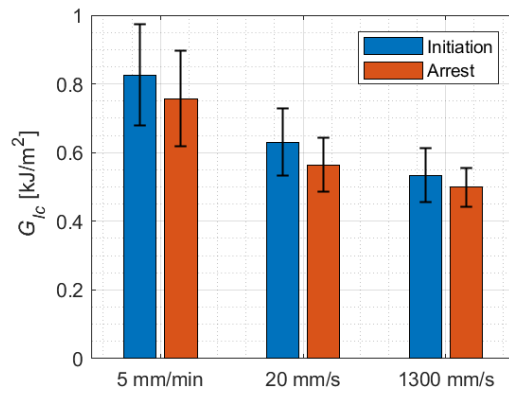


Figure 3.9: The mode I initiation and arrest interlaminar fracture toughness G_{Ic} determined with the tests

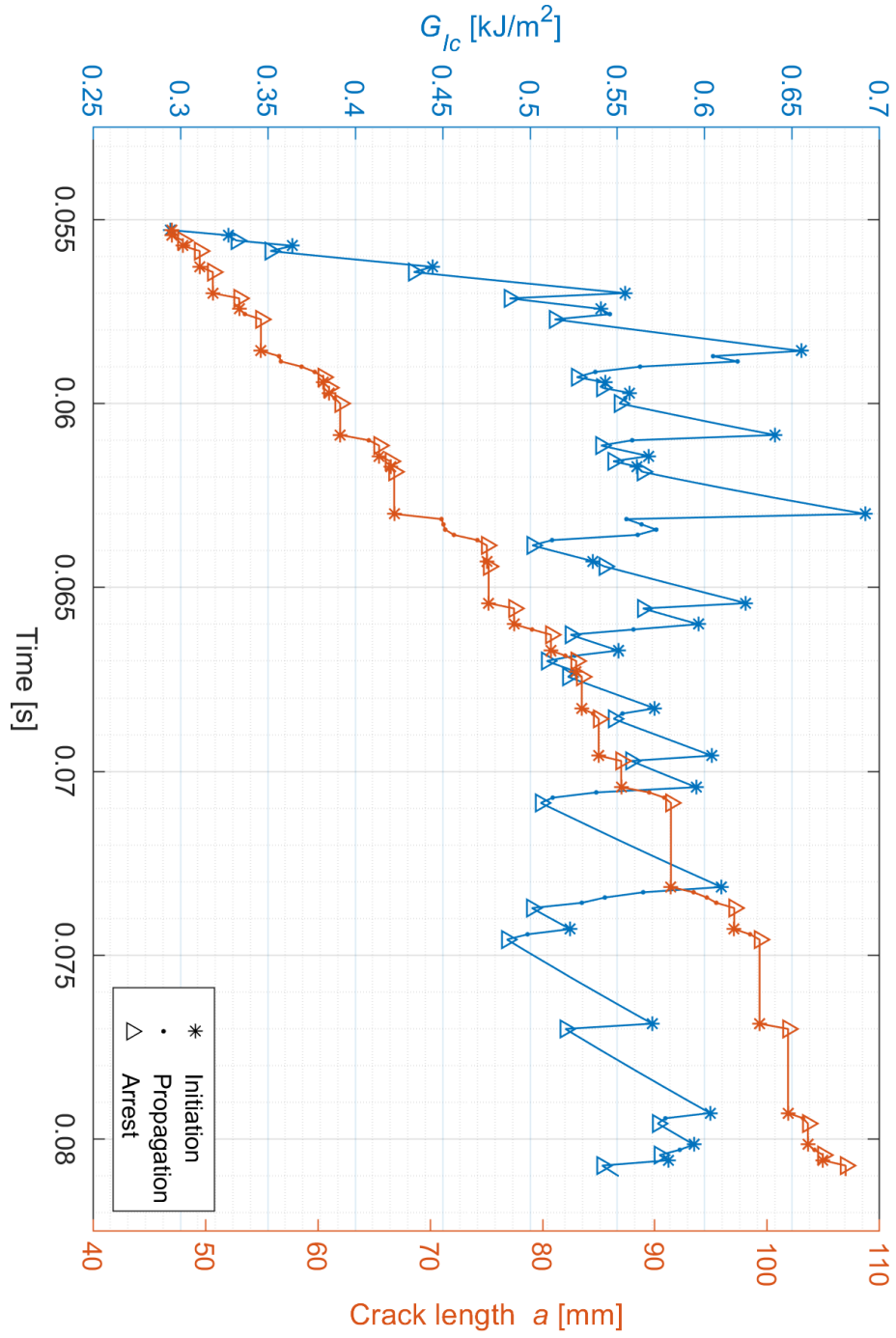
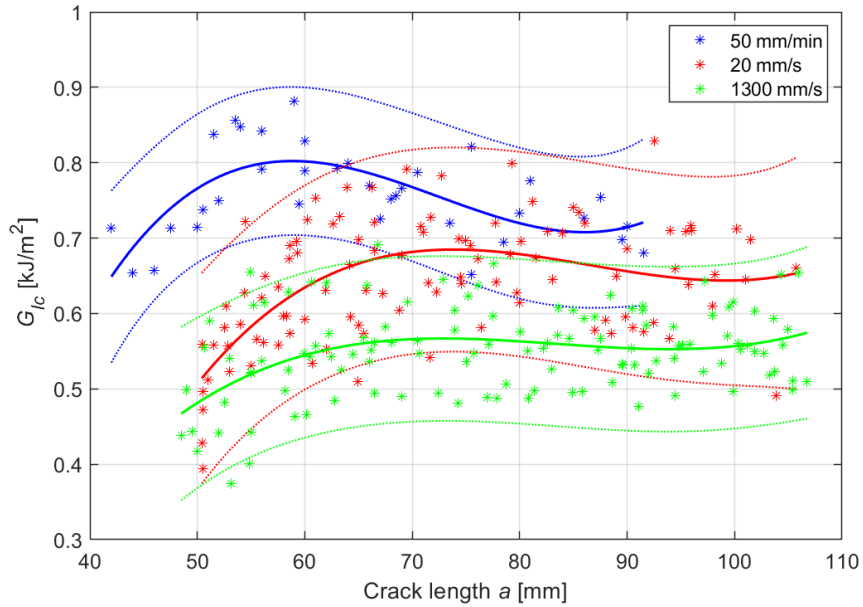
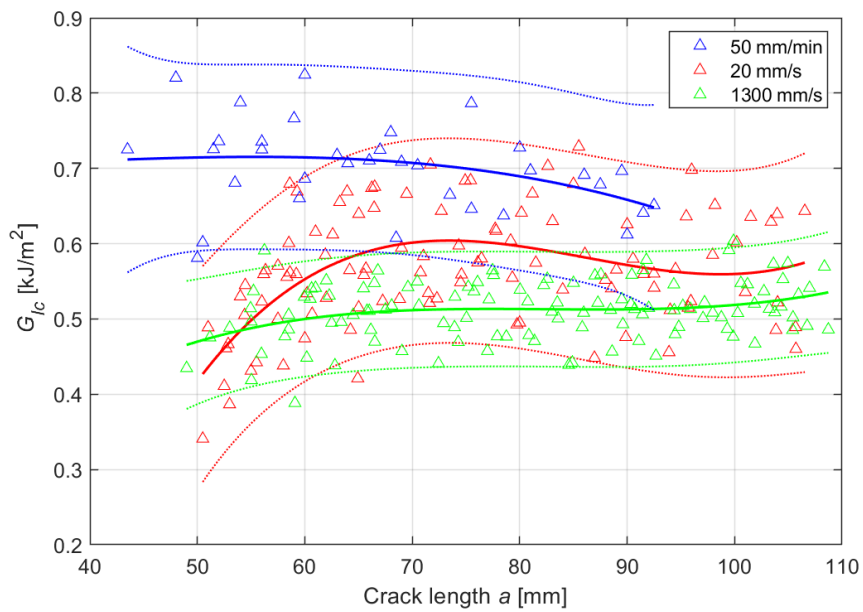


Figure 3.10: Classification of the data points as initiation, propagation or arrest values (Specimen 7)



(a) Initiation values



(b) Arrest values

Figure 3.11: Third degree polynomials fitted to the data points from the R-curves (continuous lines), with 95% prediction bounds (dashed lines)

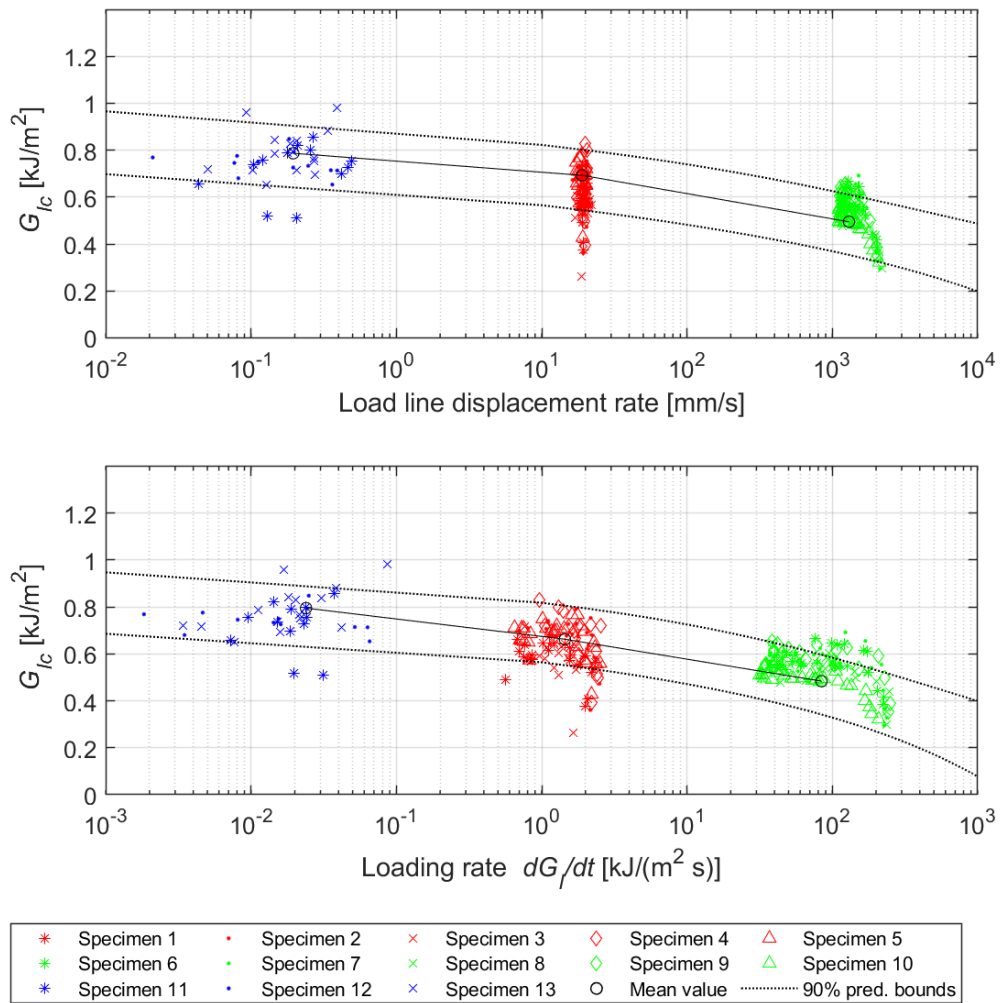


Figure 3.12: The initiation interlaminar fracture toughness values plotted against two rate parameters found in literature

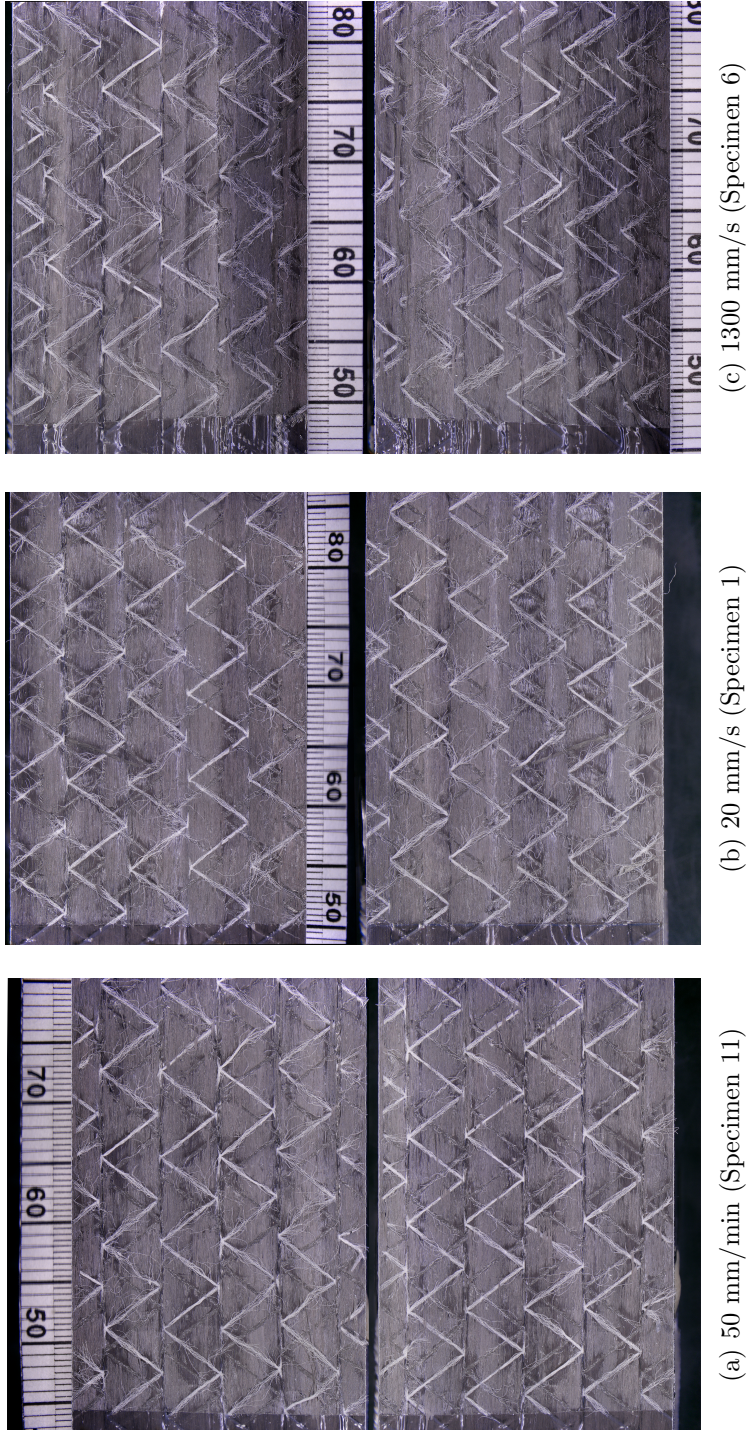
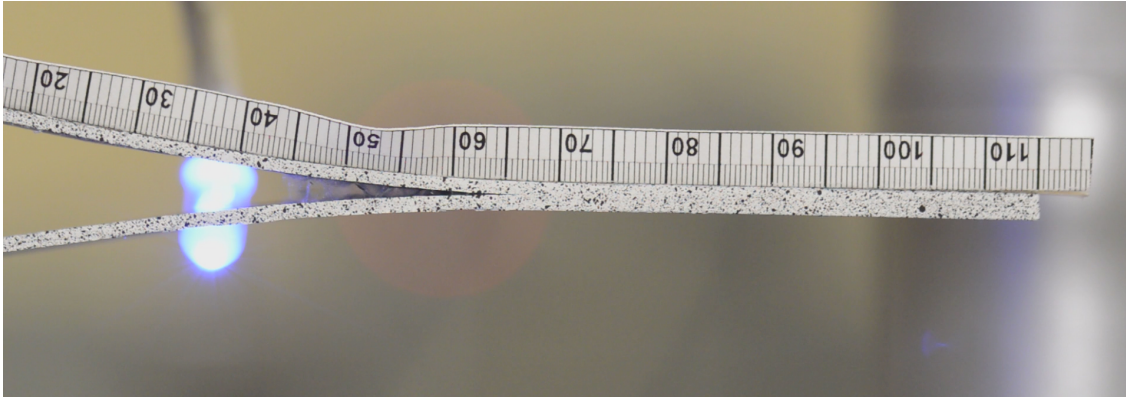
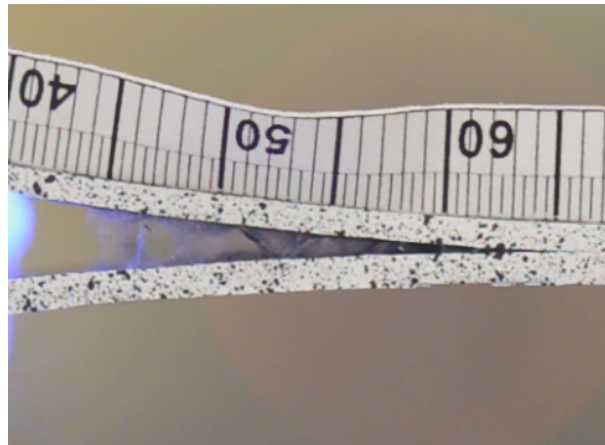


Figure 3.13: 30× magnification microscope images of the crack surfaces



(a) Specimen 12, frame 6754



(b) A magnification of the crack tip area from the picture above

Figure 3.14: Crack bridging by the polyester stitching clearly visible in a quasi-static test.

Conclusions

A testing methodology was developed for determining the mode I interlaminar fracture toughness of long-unidirectional fibre composite materials at intermediate rates of load line opening, combining the quasi-static ISO standard and existing procedures found in literature. The methodology involves exclusively measurements obtained via digital imaging and direct image correlation. Tests were carried out on two test frames, one for quasi-static and one for intermediate opening rates.

A unique lightweight fixture—combining features from the two types traditionally used, piano hinges and load blocks—was designed and manufactured for this purpose. The testing apparatus performed well, and none of the undesired dynamic effects described by some authors were experienced.

A novel method proposed by [40] was used for what is still arguably the most delicate and error-prone measurement in delamination tests, crack growth tracking. High-speed imaging, direct image correlation and a MATLAB post-processing script replaced the traditional manual frame-by-frame analysis. The new method proved successful, yielding measurements just as accurate as the old one and perfectly repeatable.

The delamination behaviour of a non-crimp carbon fibre fabric and epoxy composite was characterised using this setup. The material was tested at one quasi-static and two intermediate opening rates—50 mm/min, 20 mm/s and 1,300 mm/s respectively. Crack propagation was found to follow a brittle and unstable mechanism at all three rates, with a marked tendency for shorter, more frequent crack jumps as the opening rate rose.

Both the initiation and the arrest value of interlaminar fracture toughness followed the same trend. The results were highly dispersed at quasi-static rate, a consequence of the inconsistency in the length of crack jumps. This behaviour has been attributed to the very nature of the composite material, and to the strain-rate dependent bridging effect given by the stitching of the non-crimp fabric. Interlaminar fracture toughness values tended to condensate closer to the median values in intermediate rate tests, yielding better results. The initiation interlaminar fracture toughness values determined were 0.826 ± 0.147 kJ/m² at 50 mm/min, 0.630 ± 0.098 kJ/m² at 20 mm/s and 0.534 ± 0.0792 kJ/m² at 1,300 mm/s.

The initiation G_{Ic} values were analysed using rate parameters found in literature. Although the results form a dispersed cloud, there is an undeniable trends towards reduction of the interlaminar fracture toughness, both going from quasi-static to the lower intermediate rate of test and from the lower intermediate to the higher intermediate rate.

These findings warrant further testing of rate effect on the delamination behaviour of this material. Tests should be conducted at high rates of opening displacement, on a

purpose-developed symmetrical Hopkinson pressure bar rig. Future research could also continue to make use of the now proven and convenient test procedure, investigating the effect of specimen thickness and of varying lay-ups on the delamination properties.

Bibliography

- [1] S. Sridharan. *Delamination behaviour of composites*. Woodhead Publishing, 2008.
- [2] ISO 4921:2000. Knitting — Basic concepts — Vocabulary. Standard, International Organization for Standardization, Geneva, CH, 2000.
- [3] M. Wisnom. The role of delamination in failure of fibre-reinforced composites. *Philosophical transactions. Series A, Mathematical, physical, and engineering sciences*, 370:1850–70, 04 2012.
- [4] A. Smiley and Byron Pipes. Rate effects on Mode I interlaminar fracture toughness in composite materials. *Journal of Composite Materials*, 21:670–687, 07 1987.
- [5] B.F. Sørensen. Modeling damage, fatigue and failure of composite materials. chapter Delamination fractures in composite materials. Woodhead Publishing, 2016.
- [6] A. Riccio. Delamination in the context of composite structural design. In Srinivasan Sridharan, editor, *Delamination Behaviour of Composites*, Woodhead Publishing Series in Composites Science and Engineering, page 28–64. Woodhead Publishing, 2008.
- [7] E.J. Barbero. *Introduction to composite materials design, second edition*. Composite Materials. Taylor & Francis, 2010.
- [8] Wen Chan. Design approaches for edge delamination resistance in laminated composites. *Journal of Composites Technology and Research; (United States)*, 13, 01 1991.
- [9] DeFu Liu, YongJun Tang, and W.L. Cong. A review of mechanical drilling for composite laminates. *Composite Structures*, 94(4):1265–1279, 2012.
- [10] Review of delamination predictive methods for low speed impact of composite laminates. *Composite Structures*, 66(1):677 – 683, 2004. Twelfth International Conference on Composite Structures.
- [11] John C. Brewer and Paul A. Lagace. Quadratic stress criterion for initiation of delamination. *Journal of Composite Materials*, 22(12):1141–1155, 1988.
- [12] Lin Ye. Role of matrix resin in delamination onset and growth in composite laminates. *Composites Science and Technology*, 33(4):257–277, 1988.
- [13] Dietmar Gross and Thomas Seelig. *Fracture mechanics*. Mechanical engineering series. Springer, 01 2006.
- [14] Michael May. Measuring the rate-dependent mode I fracture toughness of composites – a review. *Composites Part A Applied Science and Manufacturing*, 81:1–12, 02 2016.
- [15] ASTM D5528 - 13. Standard test method for mode I interlaminar fracture toughness of unidirectional fiber-reinforced polymer matrix composites. Standard, ASTM International, West Conshohocken, PA, USA, 2013.

-
- [16] ISO 15024:2001. Fibre-reinforced plastic composites — determination of mode I interlaminar fracture toughness, GIC, for unidirectionally reinforced materials. Standard, International Organization for Standardization, Geneva, CH, 2001.
- [17] P. Davies, C. Moulin, H.H. Kausch, and M. Fischer. Measurement of gic and giic in carbon/epoxy composites. *Composites Science and Technology*, 39(3):193–205, 1990.
- [18] P. Davies. Review of standard procedures for delamination resistance testing. In Srinivasan Sridharan, editor, *Delamination Behaviour of Composites*, Woodhead Publishing Series in Composites Science and Engineering, page 65–86. Woodhead Publishing, 2008.
- [19] Donald Adams, Leif Carlsson, and Byron Pipes. *Experimental Characterization of Advanced Composite Material*. CRC Press, 01 1987.
- [20] G. Hug, P. Thévenet, Joseph Fitoussi, and D. Baptiste. Effect of the loading rate on mode I interlaminar fracture toughness of laminated composites. *Engineering Fracture Mechanics*, 73:2456–2462, 11 2006.
- [21] A.J. Brunner, Bamber Blackman, and Peter Davies. A status report on delamination resistance testing of polymer–matrix composites. *Engineering Fracture Mechanics (0013-7944) (Elsevier), 2008-06 , Vol. 75 , N. 9, 75:2779–2794*, 06 2008.
- [22] Wenlong Zhang and Ala Tabiei. Composite laminate delamination simulation and experiment: a review of recent development. *Applied Mechanics Reviews*, 05 2018.
- [23] Bamber Blackman, J. Dear, Anthony Kinloch, H. MacGillivray, Y. Wang, J.G. Williams, and P. Yayla. The failure of fibre composites and adhesively bonded fibre composites under high rates of test. part i. *Journal of Materials Science*, 30:5885, 01 1995.
- [24] M. Colin de Verdiere, Alex Skordos, Michael May, and A.C. Walton. Influence of loading rate on the delamination response of untufted and tufted carbon epoxy non crimp fabric composites: Mode i. *Engineering Fracture Mechanics*, 96:11–25, 12 2012.
- [25] Takayuki Kusaka, Masaki Hojo, Y.-W Mai, Tomoaki Kurokawa, Taketoshi Nojima, and Ochiai Shojiro. Rate dependence of mode i fracture behaviour in carbon-fibre/epoxy composite laminates. *Composites Science and Technology*, 58:591–602, 03 1998.
- [26] M. Isakov, Michael May, Philipp Hahn, Hanna Paul, and Masato Nishi. Fracture toughness measurement without force data—application to high rate dcb on cfrp. *Composites Part A: Applied Science and Manufacturing*, 119, 04 2019.
- [27] Huifang Liu, Hailiang Nie, Chao Zhang, and Yulong Li. Loading rate dependency of Mode I interlaminar fracture toughness for unidirectional composite laminates. *Composites Science and Technology*, 167, 07 2018.
- [28] ISO 25217:2009. Adhesives — Determination of the mode 1 adhesive fracture energy of structural adhesive joints using double cantilever beam and tapered double cantilever beam specimens. Standard, International Organization for Standardization, Geneva, CH, 2009.
- [29] Haritz Zabala, Laurentzi Aretxabaleta, G. Castillo, and J. Aurrekoetxea. Loading rate dependency on mode I interlaminar fracture toughness of unidirectional and woven carbon fibre epoxy composites. *Composite Structures*, 01 2014.
- [30] Solver Thorsson, Anthony Waas, Joseph Schaefer, Brian Justusson, and Salvatore Liguore. Effects of elevated loading rates on mode I fracture of composite laminates

- using a modified wedge-insert fracture method. *Composites Science and Technology*, 156, 12 2017.
- [31] C. T. Sun and C Han. A method for testing interlaminar dynamic fracture toughness of polymeric composites. *Composites Part B: Engineering*, 35:647–655, 09 2004.
- [32] A. Aliyu and I. M. Daniel. *Effects of strain rate on delamination fracture toughness of graphite/epoxy*. Delamination and debonding of materials. ASTM International, West Conshohocken, PA, 01 1985.
- [33] R. Krueger. The virtual crack closure technique for modeling interlaminar failure and delamination in advanced composite materials. In Pedro P. Camanho and Stephen R. Hallett, editors, *Numerical Modelling of Failure in Advanced Composite Materials*, Woodhead Publishing Series in Composites Science and Engineering, page 3–53. Woodhead Publishing, 2015.
- [34] George R. Irwin. *Fracture*, page 551–590. Springer Berlin Heidelberg, Berlin, Heidelberg, 1958.
- [35] Graziano Curti and maria Grazia Curà. *Fondamenti di meccanica strutturale*. CLUT, 2006.
- [36] *Abaqus/CAE 2019 User's Manual*. Dassault Systèmes, Vélizy-Villacoublay, FR, 2019.
- [37] S.R. Hallett and P.W. Harper. Modelling delamination with cohesive interface elements. In Pedro P. Camanho and Stephen R. Hallett, editors, *Numerical Modelling of Failure in Advanced Composite Materials*, Woodhead Publishing Series in Composites Science and Engineering, page 55–72. Woodhead Publishing, 2015.
- [38] F.A.M. Pereira, M.F.S.F. de Moura, N. Dourado, J.J.L. Morais, J. Xavier, and M.I.R. Dias. Direct and inverse methods applied to the determination of mode I cohesive law of bovine cortical bone using the dcb test. *International Journal of Solids and Structures*, 128:210–220, 2017.
- [39] Alexander Bardelcik, Michael Worswick, and Mary Wells. The influence of martensite, bainite and ferrite on the as-quenched constitutive response of simultaneously quenched and deformed boron steel—experiments and model. *Materials & Design*, 55:509–525, 03 2014.
- [40] Brendan Murray, Sander Fonteyn, Delphine Carrella-Payan, Kalliopi-Artemi Kalteremidou, Anghel Cernescu, Danny Hemelrijck, and Lincy Pyl. Crack tip monitoring of Mode I and Mode II delamination in CF/epoxies under static and dynamic loading conditions using digital image correlation. 05 2018.

Acknowledgements

I developed this work at the University of Waterloo, Ontario, Canada, thanks to a scholarship provided by Politecnico di Torino and Fiat Chrysler Automobiles, under a project supervised by professor Giovanni Belingardi. On the Italian side, I would like to thank everyone that made this precious and enriching exchange possible.

On the Canadian side, I would like to thank my Canadian supervisor, professor John Montesano, head of the Composite Research Group at the University of Waterloo in which I worked, for his hospitality and mentoring. Last but not least, I would like to thank Ph. D. candidate Khizar Rouf for his help, guidance and inclination for working long hours together.

Chapter 4

Appendix

4.1 Crack tracking script

```
1 clear; clc;
2 close all;
3 cd 'C:\Users\Andrea\Documents\MATLAB\Waterloo DIC MATLAB'
4 disp('==== Welcome to ...the DCB DIC crack tip tracking utility =====')
5
6 % Select specimen
7 specimen_no = 10;
8
9 % Options
10 options.suppress_plots = 0;
11 options.save_plots = 1;
12 options.enhanced_search = 0;
13
14 % Preliminary functions
15 % Prepare filenames
16 [specimen_no,path,filename,datafile,resultfile,a.handcrafted,...
17     imgfiletype] = Prepare_filenames(specimen_no);
18 % Import specimen data (all specimens)
19 [Spec_data] = Import_all_specimen_data();
20 disp(['Processing specimen ',num2str(specimen_no),' (',filename,')'])
21
22 % Data
23 first_frame = Spec_data.First_frame_c1(Spec_data.Test==specimen_no);
24 last_frame = Spec_data.Last_frame_c1(Spec_data.Test==specimen_no);
25 crack_ref.mm = 110;
26
27 % Prepare save files
28 if $\sim$sisfile(datafile)
29     save(datafile,'specimen_no')
30 else
31     save(datafile,'specimen_no','-append')
32 end
33
34 %% NEW C R O P
```

```

35 % User is prompted to identify the area of crack propagation. Search is
36 % narrowed down to that area.
37
38 [S0,S_crop_fields] = Frame_loader(specimen_no,path,filename,first_frame);
39
40 % Pixel to mm scale factor
41 px_to_mm = (S0.x_c(end)-S0.x_c(1))/(S0.x(end)-S0.x(1));
42
43 % Determine if specimen data file already exists
44 if isfile(datafile)
45     tmpvar = load(datafile);
46     if ~isempty(find(contains(fields(tmpvar),'crop_template'),1))
47         answer = questdlg(['A cropping template data file for',...
48             'this specimen exists already'],'Dialog box',...
49             'Use existing template','Start new template',...
50             'Use existing template');
51         % Handle response
52         switch answer
53             case 'Use existing template'
54                 choice = 1;
55                 disp('Template loaded.')
56                 crop_roi = tmpvar.crop_roi;
57                 crop_template = tmpvar.crop_template;
58             case 'Start new template'
59                 choice = 2;
60         end
61     else
62         choice = 2;
63     end
64     clearvars tmpvar
65 else
66     choice = 2;
67 end
68
69 f1 = figure('Name','ROI selection','NumberTitle','off');
70 % f1.WindowState = 'maximized';
71 f1.Position = [450.0 100.0 960.0 640.0];
72 if specimen_no<=10
73     img = imread([path,'\Camera 1',filename,'-',...
74         num2str(first_frame,'%04.f'),imgfiletype]);
75     image('CData',img,'XData',[0 1024],'YData',[0 -1024])
76     xlim([0 1024]); ylim([-1024*3/5 -1024*1/5]);
77 elseif specimen_no>10
78     img = imread([path,'\Camera 1',filename,'-',...
79         num2str(first_frame,'%05.f'),imgfiletype]);
80     image('CData',img,'XData',[0 -1920],'YData',[0 -1080])
81     xlim([-1920 0]); ylim([-1080*3/5 -1080*1/5]);
82 end
83 colormap('gray'); box on; axis equal; axis off;
84 % set(gcf,'units','normalized','position',[0 0 1 1])
85
86 if choice==2
87     c = uicontrol('Style','pushbutton','String','Ok',...
88         'Callback','uiresume');
89     crop_roi = images.roi.Polygon('Color','r');

```

```

90     title(strcat('Zoom in on the beam'))
91     uiwait
92     title(['Draw a rectangle around the area of crack propagation'])
93     draw(crop_roi); drawnow;
94     uiwait
95     crop_roi.InteractionsAllowed = 'none';
96     delete(c)
97
98     crop_template = $\sim$\inROI(crop_roi,S0.x,-S0.y);
99 end
100
101 hold on;
102 title('Data points')
103 pX = reshape(S0.x,numel(S0.x),1); pY = -reshape(S0.y,numel(S0.y),1);
104 scatter(pX,pY, '.', 'MarkerEdgeColor',[0.8 0.8 0.8],...
105         'DisplayName','All data points')
106 pX(crop_template) = NaN; pY = -reshape(S0.y,numel(S0.y),1);
107 scatter(pX,pY, '.r', 'DisplayName','Cropped data points')
108 legend('Position',[0.65 0.25 0.1 0.05])
109
110 if isfile(resultfile)
111     tmpvar = load(resultfile);
112     crack = tmpvar.crack_tip;
113     clearvars tmpvar
114     results_flag = 1;
115 else
116     results_flag = 0;
117 end
118
119 f2 = figure('Name','Selected data points','NumberTitle','off');
120 f2.WindowState = 'maximized';
121 set(gcf,'units','normalized','position',[0 0 1 1])
122 subplot(1,2,1)
123 title('Data points, initial frame')
124 if specimen_no<=10
125     img = imread(strcat(path,'\Camera 1',filename,'-',...
126                       num2str(first_frame,'%04.f'),imgfiletype));
127     image('CData',img,'XData',[0 1024],'YData',[0 -1024])
128     colormap('gray'); hold on; box on; axis equal; axis off;
129     xlim([0 1024]); ylim([-1024 0]);
130 elseif specimen_no>10
131     img = imread(strcat(path,'\Camera 1',filename,'-',...
132                       num2str(first_frame,'%05.f'),imgfiletype));
133     image('CData',img,'XData',[0 -1920],'YData',[0 -1080])
134     colormap('gray'); hold on; box on; axis equal; axis off;
135     xlim([-1920 0]); ylim([-1080 0]);
136 end
137 pX(crop_template) = NaN; pY = -reshape(S0.y,numel(S0.y),1);
138 scatter(pX,pY, '.r')
139 if results_flag==1
140     pX = [crack.x]; pY = -[crack.y];
141     scatter(pX([crack.index]$\sim$=0),pY([crack.index]$\sim$=0),...
142           'ow','filled','MarkerEdgeColor',[0 0 0],...
143           'DisplayName','Crack tip position');
144 end

```

```

145 subplot(1,2,2)
146 title('Data points, tenth to last frame')
147 if specimen_no<=10
148     img = imread(strcat(path, '\Camera 1', filename, '-', ...
149         num2str(last_frame-10, '%04.f'), imgfiletype));
150     image('CData', img, 'XData', [0 1024], 'YData', [0 -1024])
151     colormap('gray'); box on; axis equal; axis off; hold on;
152     xlim([0 1024]); ylim([-1024 0]);
153 elseif specimen_no>10
154     img = imread(strcat(path, '\Camera 1', filename, '-', ...
155         num2str(last_frame-10, '%05.f'), imgfiletype));
156     image('CData', img, 'XData', [0 -1920], 'YData', [0 -1080])
157     colormap('gray'); hold on; box on; axis equal; axis off;
158     xlim([-1920 0]); ylim([-1080 0]);
159 end
160
161 [S_tmp, $\sim$] = Frame_loader(specimen_no, path, filename, last_frame-10);
162 pX = reshape(S_tmp.x+S_tmp.u, numel(S_tmp.x), 1);
163 pY = -reshape(S_tmp.y+S_tmp.v, numel(S_tmp.y), 1);
164 pX(S_tmp.sigma==-1) = NaN; pX(crop_template) = NaN;
165 scatter(pX, pY, 'r')
166 if results_flag==1
167     pX = reshape(S_tmp.x+S_tmp.u, numel(S_tmp.x), 1);
168     pY = -reshape(S_tmp.y+S_tmp.v, numel(S_tmp.y), 1);
169     plot_vec = [crack.index(2:end)];
170     scatter(pX(plot_vec([crack.log] $\sim$=0)), ...
171         pY(plot_vec([crack.log] $\sim$=0)), 'ow', 'filled', ...
172         'MarkerEdgeColor', [0 0 0], ...
173         'DisplayName', 'Crack tip position');
174 end
175
176 save(datafile, 'crop_roi', 'crop_template', '-append')
177
178 %% User picks crack reference point
179 %% The user is prompted to pick a line
180 %% across the beam at the marked 110 mm.
181 %% The midpoint of the line, whose coordinates are known,
182 %% is then used as a reference point for crack position.
183
184 if isfile(datafile)
185     tmpvar = load(datafile);
186     if $\sim$isempty(find(contains(fields(tmpvar), 'crack_ref'), 1))
187         answer = questdlg(['A calibration data file for', ...
188             'this specimen exists already'], 'Dialog box', ...
189             'Use existing data', 'Start new calibration', ...
190             'Use existing data');
191         % Handle response
192         switch answer
193             case 'Use existing data'
194                 disp('Data loaded.')
195                 crack_ref = tmpvar.crack_ref;
196                 choice = 1;
197             case 'Start new calibration'
198                 choice = 2;
199         end

```

```

200     else
201         choice = 2;
202     end
203     clearvars tmpvar
204 else
205     choice = 2;
206 end
207
208 figure('Name','ROI selection','NumberTitle','off')
209 if specimen.no<=10
210     img = imread(strcat(path,'\Camera 1',filename,'-',...
211         num2str(first_frame,'%04.f'),imgfiletype));
212     image('CData',img,'XData',[0 1024],'YData',[0 -1024])
213 elseif specimen.no>10
214     img = imread(strcat(path,'\Camera 1',filename,'-',...
215         num2str(first_frame,'%05.f'),imgfiletype));
216     image('CData',img,'XData',[0 -1920],'YData',[0 -1080])
217 end
218 colormap('gray'); box on; axis equal; axis off;
219 % Resize image to approximately zoom in on beam free end
220 xlim(sort([S0.x(1,1) S0.x(1,round(end/7))]));
221 ylim([-S0.y(end,1) -S0.y(1,1)+50]);
222 options.b = 0.8; options.a = 3/4*options.b;
223 set(gcf,'units','normalized','position',...
224     [(1-options.a)/2,(1-options.b)/2,options.a,options.b])
225
226 if choice==2
227     disp('Calibration')
228     title(strcat('Zoom in on at beam at', {' '},...
229         num2str(crack_ref.mm), {' '}, 'mm'))
230
231     roi = images.roi.Line('Color','r');
232     h = 0;
233     c = uicontrol('Style','pushbutton','String','Ok',...
234         'Callback','uiresume');
235     drawnow
236     uiwait
237     title(strcat('Draw a line across the beam at the marked', {' '},...
238         num2str(crack_ref.mm), {' '}, 'mm'))
239     draw(roi);
240     uiwait
241
242     roi.InteractionsAllowed = 'none';
243     delete(c)
244     % Calculate the crack position reference point
245     crack_ref.picked_x = sum(roi.Position(:,1))/2;
246     crack_ref.picked_y = sum(roi.Position(:,2))/2;
247     % Find the closest data point
248     pX = reshape(S0.x,numel(S0.x),1); pY = -reshape(S0.y,numel(S0.y),1);
249     crack_ref.index = dsearchn([pX, pY],...
250         [crack_ref.picked_x crack_ref.picked_y]);
251     for j = 1:length(S_crop_fields)
252         crack_ref.(S_crop_fields{j}) =...
253             S0.(S_crop_fields{j})(crack_ref.index);
254     end

```

```

255 end
256
257 hold on
258 pX = reshape(S0.x,numel(S0.x),1); pY = -reshape(S0.y,numel(S0.y),1);
259 scatter(pX,pY, '.', 'MarkerEdgeColor',[0.8 0.8 0.8],...
260         'DisplayName','Data points')
261 plot(crack_ref.picked_x,crack_ref.picked_y, '*r', 'MarkerSize',10,...
262       'DisplayName','Picked position')
263 text(crack_ref.picked_x+2,crack_ref.picked_y+2, '[110,0]', 'Color','r')
264 plot(crack_ref.x,-crack_ref.y, 'og', 'MarkerSize',10,...
265       'DisplayName','Closest data point')
266 text(crack_ref.x-2,-crack_ref.y-2,num2str(crack_ref.index), 'Color','g')
267 legend
268 title('Crack position reference point')
269 drawnow
270
271 save(datafile,'crack_ref','-append')
272
273 %% Main loop over the frames
274
275 % Build the frame list
276 % This allows the script to work even if frames are missing or deleted
277 file_list = dir([path '\Camera 1']);
278 file_list = {file_list($\sim${file_list.isdir}).name};
279 frame_no = 0;
280 for j=1:length(file_list)
281     frame_temp = file_list{j};
282     if strcmp(frame_temp(end-3:end),'.out')
283         frame_no = frame_no+1;
284         if specimen_no<=10
285             crack(frame_no).frame = str2num(frame_temp(:,end-7:end-4));
286         elseif specimen_no>10
287             crack(frame_no).frame = str2num(frame_temp(:,end-8:end-4));
288         end
289     end
290 end
291 clearvars file_list frame_temp
292
293 % Run frame processing function
294 crack = Frame_processor_struct(specimen_no,crack,crop_template,...
295     S_crop_fields,path,filename,options,imgfiletype);
296
297 %% Calculate full crack length
298
299 ex = '';
300 [crack] = Calculate_crack_length(last_frame,px_to_mm,crack_ref,crack,...
301     a_handcrafted,resultfile,ex);
302
303 %% Secondary loop over decimated frames
304 % Run another processing loop on a decimated amount of frames, if
305 % the number of crack propagation points is low
306
307 if length(nonzeros([crack.log] == 1))<30
308     disp('The number of crack propagation points is low')
309     subfolder_path = fullfile(path,'\Camera 1','Decimated images');

```

```

310     mkdir(subfolder_path);
311
312     crack_growth_frames = [crack([crack.log]==1).frame];
313     crack_growth_frames = [0,crack_growth_frames,last_frame];
314
315     % Frame decimation loop: keeps one in five frames
316     % between successive crack propagation frames,
317     % plus all crack propagation frames and the ones immediately before
318     frame_list = 0; length_frame_list = 1;
319     for j=1:length(crack_growth_frames)-1
320         for k=[crack_growth_frames(j):5:crack_growth_frames(j+1),...
321             crack_growth_frames(j+1)-1]
322             frame_list(length_frame_list) = k;
323             length_frame_list = length_frame_list+1;
324         end
325     end
326
327     frame_list = unique(frame_list);
328
329     % Copy the decimated frames to new folder
330     for j=frame_list
331         if specimen_no<=10
332             filename_1=[path,'\Camera ...
333                 1',filename,'-',num2str(j,'%04.f')];
334             filename_2=[subfolder_path,filename,'-',num2str(j,'%04.f')];
335         elseif specimen_no>10
336             filename_1=[path,'\Camera ...
337                 1',filename,'-',num2str(j,'%05.f')];
338             filename_2=[subfolder_path,filename,'-',num2str(j,'%05.f')];
339         end
340         copyfile(strcat(filename_1,imgfiletype),...
341             strcat(filename_2,imgfiletype),'f');
342     end
343
344     figure()
345     grid on; box on; hold on;
346     plot(frame_list,frame_list,'b','DisplayName','Decimated frame list')
347     plot(crack_growth_frames,crack_growth_frames,'or',...
348         'DisplayName','Crack growth frame')
349     legend
350     disp(['The new number of frames is ',num2str(length_frame_list)])
351     pause
352
353     % New crop template
354     if specimen_no<=10
355         S0 = load(strcat(subfolder_path,filename,'-',...
356             num2str(first_frame,'%04.f'),'mat'));
357     elseif specimen_no>10
358         S0 = load(strcat(subfolder_path,filename,'-',...
359             num2str(first_frame,'%05.f'),'mat'));
360     end
361     tmpvar = load(datafile); crop_roi = tmpvar.crop_roi; clearvars tmpvar
362     crop_template = $\sim$\inROI(crop_roi,S0.x,-S0.y);
363     % Run frame processing function

```

```

363     crack = Frame_processor_struct(specimen_no,crack,crop_template,...
364         S_crop_fields,[path,'\Camera 1'],filename,options,imgfiletype);
365
366 end
367
368 %% Calculate decimated crack length
369
370 ex = '_decimated';
371 [crack_tip] = Calculate_crack_length(last_frame,px_to_mm,crack_ref,...
372     crack_tip,a_handcrafted,resultfile,ex);
373
374 %% Final plot
375
376 disp('Specimen.10-VIC-sigma ran successfully')
377
378 for j=max_frame-[0:5:60]
379     clearvars S_tmp pX pY
380
381     figure()
382     img = imread([path,filename,'-',num2str(j,'%04.f'),imgfiletype]);
383     image('CData',img,'XData',[0 1024],'YData',[0 -1024])
384     colormap('gray'); box on; axis equal; axis off; hold on;
385     xlim([0 1024]); ylim([-1024 0]);
386     S_tmp = load(strcat(path,filename,'-',num2str(j,'%04.f'),'mat'));
387     pX = reshape(S_tmp.x+S_tmp.u,numel(S_tmp.x),1);
388     pY = -reshape(S_tmp.y+S_tmp.v,numel(S_tmp.y),1);
389     scatter(pX,pY,'r');
390     pX(S_tmp.sigma==-1) = NaN; scatter(pX,pY,'y');
391     pX(crop_template) = NaN; scatter(pX,pY,'g')
392     title(strcat('Frame',num2str(j)))
393 end
394
395 return
396 %%
397
398 if specimen_no<=10
399     S0 = load(strcat(subfolder_path,filename,'-',...
400         num2str(first_frame,'%04.f'),'mat'));
401 elseif specimen_no>10
402     S0 = load(strcat(subfolder_path,filename,'-',...
403         num2str(first_frame,'%05.f'),'mat'));
404 end
405 crop_template = $\sim$inROI(crop_roi,S0.x,-S0.y);
406 crack_tip = Frame_processor_struct(specimen_no,crack,crop_template,...
407     S_crop_fields,strcat(path,'\Camera 1'),filename,options,imgfiletype);
408
409 %% Function to calculate crack length
410
411 function [crack] = Calculate_crack_length(max_frame,px_to_mm,...
412     crack_ref,crack,a_handcrafted,resultfile,ex)
413     crack_ref.mm = 110;
414
415     for j=1:length([crack.x])
416         crack(j).length_pix = sqrt((crack(j).x-crack_ref.x).^2+...
417             (crack(j).y-crack_ref.y).^2);

```

```
418     crack(j).length_mm = crack_ref.mm-crack(j).length_pix*px_to_mm;
419 end
420
421 figure()
422 hold on; grid on; box on;
423 plot(a_handcrafted.frame,a_handcrafted.a,...
424     'displayName','Manually measured crack length')
425 plot([crack.frame],interp1([crack.frame],[crack.length_mm],...
426     [crack.frame]),...
427     'displayName','Automatically measured crack length')
428 legend('Location','northwest')
429 xlabel('Frame'); ylabel('Crack length {\it a} [mm]')
430 xlim([0 max_frame]); ylim([0 110])
431
432 if isempty(ex)
433     saveas(gcf,resultfile(1:end-4),'fig')
434     save(resultfile,'crack')
435 else
436     saveas(gcf,strcat(resultfile(1:end-4),ex),'fig')
437     save(strcat(resultfile(1:end-4),ex,'.mat'),'crack')
438 end
439 end
```

4.2 Frame processing function

```

1  %% Frame processing loop function
2  function [crack] = Frame_processor_struct(specimen_no,crack,...
3      crop_template,S_crop_fields,path,filename,options,imgfiletype)
4
5      disp('Beginning frame processing')
6      max_frame = crack(end).frame;
7      discard_flag = 0;    % 0: not detected; 1: accepted; -1: discarded
8      discarded_values = 0;
9      if $\sim$exist(fullfile(path,'Crack diagrams'),'dir')
10         mkdir(path,'Crack diagrams');
11         mkdir(path,'Discarded crack diagrams');
12     end
13
14     % Initialise "crack_tip" structure
15     crack(1).index = 0;
16     for j=1:length(S_crop_fields)
17         crack(1).(S_crop_fields{j}) = 0;
18     end
19
20     for j=2:length(crack) % begin with frame "0001", compare with prev.
21         frame = crack(j).frame;
22
23         if $\sim$mod(j,50)
24             disp(['Processing frame ',num2str(frame)])
25         end
26
27         [S,$\sim$] = Frame_loader(specimen_no,path,filename,frame);
28
29         % Loop to eliminate non-working points
30         S_NaN = S;
31         for k = 1:length(S_crop_fields)
32             S_NaN.(S_crop_fields{k})(S.sigma== -1 | isnan(S.sigma)) = NaN;
33         end
34
35         % Loop to crop area from initial template
36         S_NaN_crop = S_NaN;
37         for k = 1:length(S_crop_fields)
38             S_NaN_crop.(S_crop_fields{k})(crop_template) = NaN;
39         end
40
41         % Loop to crop area from previous crack tip position
42         S_NaN_crop2 = S_NaN_crop;
43         if j>2 && crack(j-1).index==0
44             crack_tip_guess = max(max(S_NaN_crop.x));
45             for k = 1:length(S_crop_fields)
46                 S_NaN_crop2.(S_crop_fields{k})...
47                     (S_NaN_crop.x<crack_tip_guess-120) = NaN; % sx
48             end
49         elseif j>2 && crack(j-1).index$\sim$=0
50             [$\sim$,col] = ind2sub(size(S_NaN_crop2.x),crack(j-1).index);
51             for k = 1:length(S_crop_fields)

```

```

52         S_NaN_crop2.(S_crop_fields{k})(:,col:end) = NaN; % dx
53         S_NaN_crop2.(S_crop_fields{k})...
54             (S_NaN_crop.x<crack(j-1).x-200) = NaN; % sx
55     end
56 end
57
58 % Find the crack tip and store properties
59 crack_tip_candidate = find(S_NaN_crop2.sigma>=0.01,1,'first');
60
61 % Check on the points adjacent to the crack tip candidate
62 % At least a fraction of them must also pass the check on sigma
63 if ~isempty(crack_tip_candidate)
64     if crack(j-1).index==0 ...
65         && S_NaN_crop.x(crack_tip_candidate)<crack(j-1).x-40
66         tolerance = 0.9;
67     else
68         tolerance = 0.4;
69     end
70     crack_tip_tmp_adjacent = intersect(intersect(find...
71         (S_NaN_crop.x>S_NaN_crop.x(crack_tip_candidate)),...
72         find(S_NaN_crop.x<...
73             S_NaN_crop.x(crack_tip_candidate)+50)),intersect(find(...
74         S_NaN_crop.y<S_NaN_crop.y(crack_tip_candidate)+2),...
75         find(S_NaN_crop.y>S_NaN_crop.y(crack_tip_candidate)-2)));
76     checkvar1 = numel(nonzeros(S_NaN_crop.sigma...
77         (crack_tip_tmp_adjacent)>=0.01));
78     if checkvar1/numel(crack_tip_tmp_adjacent)<tolerance
79         discard_flag = -1; % discard the value
80         discarded_values = discarded_values+1;
81     else
82         discard_flag = 1; % accept the value
83     end
84     discovery_type = 1; % conventional search
85 end
86
87 % Check that sigma isn't above threshold on the whole beam
88 if ~isempty(crack_tip_candidate)
89     checkvar1 = numel(intersect(find(S_NaN_crop.sigma>=0.01),...
90         find(S_NaN_crop.x<S_NaN_crop.x(crack_tip_candidate))));...
91     % No. of points with sigma over threshold
92     checkvar2 = numel(intersect(...
93         find(~isnan(S_NaN_crop.sigma)),...
94         find(S_NaN_crop.x<S_NaN_crop.x(crack_tip_candidate))));...
95     % No. of valid points
96     if checkvar1/checkvar2>0.4
97         discard_flag = -1; % discard the value
98     end
99 end
100
101 % Candidate crack position is accepted
102 if discard_flag==1
103     crack(j).index = crack_tip_candidate;
104     for k = 1:length(S_crop_fields)
105         crack(j).(S_crop_fields{k}) = ...
106             S_NaN_crop2.(S_crop_fields{k})(crack(j).index);

```

```

107         end
108         crack(j).log = 1; % 1: crack growth
109     else
110         crack(j).index = crack(j-1).index;
111         for k = 1:length(S_crop_fields)
112             crack(j).(S_crop_fields{k}) = ...
113                 crack(j-1).(S_crop_fields{k});
114         end
115         crack(j).log = 0; % 0: crack arrest
116     end
117
118     if options.suppress_plots\sim$=1 && discard_flag\sim$=0
119         % Crack tip growth figure
120         figure(100)
121         f.WindowState = 'minimized';
122         ax1 = gca; ax1p = get(ax1,'pos');
123         if strcmp(imgfiletype, '.tif')
124             img = imread(strcat([path, '\Camera 1'], filename, '-', ...
125                                 num2str(frame, '%04.f'), imgfiletype));
126         elseif strcmp(imgfiletype, '.png')
127             img = imread(strcat([path, '\Camera 1'], filename, '-', ...
128                                 num2str(frame, '%05.f'), imgfiletype));
129         end
130         image('CData', img, 'XData', [0 1024], 'YData', [0 -1024])
131         axis equal; xlim([0 1024]); ylim([-1024 0]); axis off;
132         set(gcf, 'units', 'normalized', 'position', ...
133             [(1-options.a)/2, -options.b, options.a, options.b])
134         colormap(gca, 'gray');
135         ax2 = axes; set(ax2, 'pos', ax1p); % axis off;
136         linkaxes([ax1, ax2], 'xy')
137         set(ax1, 'pos', get(ax2, 'pos'))
138         axes(ax2)
139         hold on
140         colormap(gca, 'jet')
141         pX=reshape(S_NaN_crop.x+S_NaN_crop.u, numel(S_NaN_crop.x), 1);
142         pY=-reshape(S_NaN_crop.y+S_NaN_crop.v, numel(S_NaN_crop.y), 1);
143         psigma = reshape(S_NaN_crop.sigma, numel(S_NaN_crop.sigma), 1);
144         scatter(pX, pY, [], psigma, '.', ...
145             'DisplayName', 'Sigma data points');
146         caxis([0.001 0.011]);
147         if discovery_type==1 % conventional search
148             scatter(pX(crack_tip_tmp_adjacent), ...
149                 pY(crack_tip_tmp_adjacent), ...
150                 'ok', 'DisplayName', 'Crack tip adjacent points')
151         if discard_flag<0 % value has been discarded
152             scatter(pX(crack_tip_candidate), ...
153                 pY(crack_tip_candidate), 'ob', 'filled', ...
154                 'MarkerEdgeColor', [0 0 0], 'DisplayName', ...
155                 'Discarded candidate crack tip position');
156         end
157     end
158     if discovery_type==2 % short range search
159         scatter(pX(crack_tip_tmp_adjacent), ...
160             pY(crack_tip_tmp_adjacent), 'ok', ...
161             'DisplayName', 'Short range search adjacent points')

```

```

162         if discard_flag<0 % value has been discarded
163             scatter(pX(temp_value),pY(temp_value),...
164                 'ob','filled',...
165                 'MarkerEdgeColor',[0 0 0],'DisplayName',...
166                 'Discarded candidate crack tip position');
167         end
168     end
169     if frame>0 && crack(j-1).index$\sim$=0
170         scatter(pX(crack(j-1).index),pY(crack(j-1).index),...
171             'ow','filled','MarkerEdgeColor',[0 0 0],...
172             'DisplayName','Previous crack tip position');
173     end
174     if crack(j).index$\sim$=0
175         scatter(pX(crack(j).index),pY(crack(j).index),...
176             'ow','filled','MarkerEdgeColor',[0 0 0],...
177             'DisplayName','Current crack tip position');
178     end
179     xlim([0 1050]); ylim([-1050 0]); axis equal; axis off;
180     text(0.15,0.98,datestr(now,'dd mmmm yyyy HH:MM:SS.FFF'),...
181         'Color','w','Units','normalized',...
182         'HorizontalAlignment','left')
183     title(['Crack growth diagram, frame ' num2str(frame)])
184     legend('Location','northeast')
185     if options.save_plots==1 && discard_flag>0
186         saveas(gcf, strcat([path, '\Camera 1'],...
187             '\Crack diagrams\','Frame_',...
188             num2str(frame, '%05.f')), 'fig')
189         saveas(gcf, [path, '\Camera 1', '\Crack diagrams\'],...
190             'Frame_', num2str(frame, '%05.f'), '.png'], 'png')
191     end
192     if options.save_plots==1 && discard_flag<0
193         saveas(gcf, [path, '\Camera 1'],...
194             '\Discarded crack diagrams\','Discarded-frame_',...
195             num2str(frame, '%05.f')], 'fig')
196         saveas(gcf, strcat([path, '\Camera 1'],...
197             '\Discarded crack diagrams\','Discarded-frame_',...
198             num2str(frame, '%05.f'), '.png'], 'png')
199     end
200     close(gcf)
201 end
202
203 % Reset values for next step
204 if discard_flag== -1
205     discarded_values = discarded_values+1;
206 end
207 discard_flag = 0;
208 crack_tip_candidate = double.empty;
209 end
210
211 disp('Frame processing complete')
212 disp(strcat(num2str(discarded_values),{' '},'values were discarded'))
213 end

```